Analysis and design of numerical methods for problems arising in plasma physics

Martin Campos Pinto

Analysis and design of numerical methods for problems arising in plasma physics

Martin Campos Pinto

Habilitation Thesis

(applied mathematics)

defended on March 8, 2017

Composition of the Jury

Reviewers :	**Annalisa Buffa**	*EPFL, Lausanne*
	Patrick Ciarlet	*POEMS, ENSTA ParisTech*
	Ralf Hiptmair	*ETH Zürich*
Jury :	**Patrick Ciarlet**	*POEMS, ENSTA ParisTech*
	Albert Cohen	*LJLL, Université Pierre et Marie Curie*
	Bruno Després	*LJLL, Université Pierre et Marie Curie*
	Frédéric Hecht	*LJLL, Université Pierre et Marie Curie*
	Ralf Hiptmair	*ETH Zürich*
	Benoît Perthame	*LJLL, Université Pierre et Marie Curie*
	Eric Sonnendrücker	*IPP, Max-Planck Garching*
	Chantal Stehlé	*LERMA, Université Pierre et Marie Curie*

Mis en page avec la classe thloria.

Remerciements

Par bien des aspects, la recherche en mathématiques ressemble à la marche en montagne. Qu'il s'agisse de trouver une voie accessible vers un col aperçu dans la brume ou de gravir des pentes parfois raides pour atteindre de nouveaux espaces, l'effort y est souvent solitaire mais les plaisirs se partagent comme de bons repas, lorsque la vue est dégagée et que les esprits se libèrent pour prendre de la hauteur.

Le plaisir de la marche est également celui des nouvelles rencontres et des échanges, et je voudrais remercier Annalisa Buffa, Patrick Ciarlet et Ralf Hiptmair d'avoir accepté de relire mon mémoire et de m'avoir fait part de leurs commentaires. Un grand merci également à Chantal Stehlé, Frédéric Hecht et Benoît Perthame pour avoir bien voulu faire part de mon jury. Quant à Albert Cohen, dont l'énergie ne m'a jamais quitté depuis mes années de thèse, il sait ce que je lui dois et je profite avec plaisir de cette nouvelle occasion pour lui redire ma gratitude.

Au cours de ces dernières années j'ai eu la chance de travailler avec des chercheurs enthousiastes, et ma propre progression doit beaucoup à la finesse de leur vue et à la portée de leur regard. Je voudrais ainsi remercier Bruno Després pour m'avoir accueilli avec beaucoup de générosité au sein du groupe de travail qu'il avait constitué au LJLL pour étudier la modélisation mathématique et numérique des plasmas avec Frédérique Charles et Lise-Marie Imbert-Gérard, puis Mehdi Badsi et maintenant Anouk Nicolopoulos et Teddy Pichard. Qu'ils soient ici remerciés pour les très beaux problèmes que nous avons étudiés ensemble depuis quelques années.

Lors de mon séjour à Strasbourg, Eric Sonnendrücker et Stéphanie Salmon m'ont fait découvrir de nouveaux horizons grâce aux questions passionnantes qu'ils se posaient sur les discrétisations des équations de Maxwell, et ils en sont également remerciés ici. Nos nombreuses tentatives d'exploration sur ces problèmes se sont parfois heurtées à des impasses et si elles ont parfois débouché sur de jolies solutions, ce fut le plus souvent grâce à leur curiosité et à leur motivation. Au LBNL, Alex Friedman, Steve Lund et leurs collègues du groupe Heavy Ion Fusion m'ont fait le plaisir de partager avec moi leur expertise physique et numérique des plasmas cinétiques, et de m'accompagner dans la poursuite de nouvelles méthodes particulaires. En remontant un peu plus loin dans le temps je voudrais également remercier Wolfgang Dahmen pour les beaux problèmes de préconditionnement multi-échelles que nous avons attaqués ensemble, rejoints dans cet effort par Kolja Brix, Ralf Massjung et Claudio Canuto.

Au delà de ces collaborations, de nouveaux liens ont pu se nouer au sein de projets tels que CHROME, où les échanges avec Stéphane Heuraux, Filipe da Silva et les membres du groupe POEMS m'ont permis de mieux comprendre certaines propriétés de la propagation des ondes dans les plasmas magnétisés. Le projet SELALIB est également le lieu de nombreuses interactions agréables et fructueuses avec les collègues de l'institut Max-Planck à Garching (Katharina Kormann, Yaman Güçlü, Ahmed Ratnani, Jakob Ameres, Eric Sonnendrücker encore, et par connexité, Florian Hindelang et Céline Caldini-Queiros), ceux de Strasbourg (Michel Mehrenberger, Sever Hirstoaga, et par

connexité Philippe Helluy, Emmanuel Franck, Michael Gutnic) et les anciens (Pierre Navaro et Nicolas Crouseilles notamment), et maintenant à Paris (Antoine Le Hyaric et Pierre-Henri Tournier).

En élargissant le cercle, j'ai conscience que mon travail se nourrit d'échanges réguliers avec de nombreux chercheurs, mathématiciens ou physiciens. La communauté mobilisée sur les questions de modélisation des plasmas est large et relativement cohérente, ce qui permet d'agréables rencontres et retrouvailles, à des rythmes plus ou moins réguliers, avec des collègues de divers horizons. Je pense ainsi à Blanca Ayuso, Alessandro Biancalani, Alain Bossavit, José-Antonio Carrillo, Young-Pil Choi, Stéphane Colombi, Fabrice Deluzet, François Dubois, Alexandre Ern, Francis Filbet, Virginie Grandgirard, Mohammed Lemou, Mathieu Lutz, Omar Maj, Marie Mounier, Claudia Negulescu, Simon Labrunie, Thomas Rey, Rémi Sentis... et la liste est loin d'être exhaustive.

Surtout, je sais que la beauté des chemins reflète souvent la qualité des compagnons de voyage. En ce qui me concerne j'ai toujours eu la chance d'être entouré de collègues chaleureux, que ce soit à Paris, Berkeley, Aachen ou Strasbourg. A défaut de pouvoir tous les citer, qu'ils sachent que je les remercie d'être ce qu'ils sont, et de faire des laboratoires de recherche des lieux de vie et de pensée.

Je garde enfin mes derniers remerciements pour ma famille. En plus du goût pour la science, elle m'a fait découvrir et aimer la marche, les thèses, et la montagne.

To Prosper, Gaston, Hector, and to Clémentine

Table of contents

Remerciements **i**

Introduction **1**

1 Lagrangian and semi-lagrangian methods for transport problems **5**

1.1 An adaptive semi-lagrangian method with interpolatory wavelets 6

1.2 Smooth particles with polynomial transformations 11

1.3 A forward-backward semi-lagrangian method 15

2 Compatible nonconforming approximation of the Maxwell equations **19**

2.1 The time-dependent Maxwell system 20

2.2 Conforming approximation with mixed finite elements 21

2.3 Conga (conforming/nonconforming Galerkin) discretization 24

2.4 Abstract criteria for the compatible approximation of the sources 27

2.5 Application to the conforming and Conga discretizations 32

2.6 Application to the coupling with a particle method 33

2.7 Link with a standard DG discretization 35

3 Theoretical and numerical study of some reduced models **37**

3.1 Kinetic sheaths in an electrostatic plasma 37

3.2 FDTD wave propagation in a magnetized plasma 42

3.3 Hybrid resonances in magnetized plasmas 45

Some prospects **51**

Bibliography **53**

What I cannot create, I do not understand. (Richard Feynman)

Introduction

For the applied mathematician, plasma physics represents a vast field of exciting problems. As ionized gases have only been isolated at the end of the nineteenth century (the word "plasma" being suggested by Irving Langmuir in 1928) it is a rather young field but has become an important one during the twentieth century, most notably for its applications in nuclear fusion and astrophysics. Indeed, visible matter in our universe essentially exists in a plasma state. Since the fifties, these progresses have been fueled by the rapid expansion of scientific computing. Many numerical schemes have been designed for the simulation of real plasmas, and they have played an important role both as scientific tools in the study of matter, and as a research topic for themselves.

For the Vlasov-Maxwell system, which can be regarded as an accurate model for magnetic confinement fusion plasmas, a variety of numerical methods have been developped since the sixties, and their properties have been validated by the joint works of mathematicians and physicists. Nevertheless, because of the complex interactions between the fields and the particles one may say that the number of computations required to simulate an actual tokamak confinement experiment with such methods is far too large to use them on a regular basis.

Based on these observations, we have devoted most of our work to the improvement of existing methods, with a special care for the designing process and the mathematical analysis of their properties. For the Vlasov equation

$$\partial_t f(t,x,v) + v \cdot \nabla_x f(t,x,v) + F(t,x) \cdot \nabla_v f(t,x,v) = 0$$

which models the transport of charged particles, represented by their density f in the phase space (x,v), under the action of electromagnetic forces F, we have developped numerical methods that aim at improving the accuracy of existing codes, at a moderate cost. In the framework of semi-lagrangian methods, which combine a lagrangian transport step and a projection step of the transported densities on given discretization grids, we have studied new algorithms to predict adaptive grids in such a way that the accuracy of the approximated densities is guaranteed in the scheme. We have next considered particle (i.e., lagrangian) methods, due to their high popularity in the plasma physics community. A weakness of these methods is the presence of a numerical "noise" in the transported densities that is characterized by strong oscillations of probabilistic or deterministic nature. To address this issue we have proposed several techniques to reconstruct accurate approximations of the density, based on the position of the particles as computed by an existing solver.

Our interest for the Maxwell equations

$$\begin{cases} \partial_t B + \operatorname{curl} E = 0 \\ \partial_t E - \operatorname{curl} B = -J \end{cases}$$

which model the evolution of an electromagnetic field E, B in the presence of a current density J, was first motivated by the compatible coupling between finite element solvers and particle discretizations for the current sources. In the framework of finite difference schemes developped for the Maxwell equations since the sixties, several techniques were known indeed to approximate the current carried by the numerical particles in such a way that the divergence constraints expressed by the Gauss laws

$$\begin{cases} \operatorname{div} B = 0 \\ \operatorname{div} E = \rho \end{cases}$$

would be well preserved over long simulation times, without having to solve additional equations as in the case of *divergence cleaning* methods. In a collaboration with Eric Sonnendrücker and his team, we have then extended these charge-conserving current deposition techniques to finite element solvers on general meshes. Our works to further extend these methods to the framework of discontinuous Galerkin schemes, which involve fully discontinuous functions to improve the locality of the computations and the handling of nonconforming meshes, led us next to clarify two important points. First, that long-time stability properties can be guaranteed for solvers which reproduce at the discrete level some well-known structure relations satisfied by the exact differential operators and their associated function spaces, and that this discrete structure provides a natural criterion for the compatible approximation of the current sources. Second, that it is easy to design numerical schemes of discontinuous Galerkin type which preserve this fundamental structure, by using the important works already done by the mathematical community on structure-preserving conforming methods. These studies let us to propose a new class of nonconforming discretizations (called "Conga" for *Conforming/Nonconforming Galerkin*), which seem to extend in a natural way most of the stability and accuracy properties established for conforming finite element methods (including the spectral correctness) to the setting of fully discontinuous function spaces, without having to introduce penalization terms as it is usually done for existing nonconforming methods. Their implementation in actual codes allowed us to verify that these theoretical properties would translate into good numerical qualities, and it also highlighted some similarities with standard discontinuous Galerkin methods.

Since a few years I have also joined the endeavor of Bruno Després in the study of several reduced models for specific plasma problems. Together with our PhD student Mehdi Badsi, we have designed a mathematical model for plasma sheaths, which are thin layers of charged plasma close to an absorbing wall which potential adjusts itself to preserve the neutrality of the plasma. As their behavior had not been described in fully satisfactory mathematical terms, we have proposed a first self-consistent model corresponding to a simple one-dimensional configuration, which we have shown to be well-posed under certain conditions that include some of the classical criteria used by physicists to describe key features of plasma sheaths. In the "cold plasma" reduced model we have also studied several problems of electromagnetic wave propagation in the presence of a strong magnetic field imposed by external devices, as in the case of a tokamak. After solving some discretization issues that would cause numerical instabilities in standard codes used by plasma physicists, we have proposed a new formulation of the

cold plasma system in the presence of hybrid resonances, which correspond to an energy transfer from the wave to the background ion bath, in the limit of a vanishing ion-electron collisionality. The limit equations being ill-posed (lack of unicity), we have proposed a new formulation to recover a well-posed problem by adding integral constraints involving manufactured solutions that contain singularities of the same nature than the exact solutions.

This memoir provides a summary of these works and is organized in three chapters. The first one describes the semi-lagrangian and lagrangian methods developped for the approximation of transport problems to which the above Vlasov equation is a particular case. The main ingredients of their analysis are presented, as well as some a priori error estimates. The approximation of the Maxwell equations by compatible methods is presented in the second chapter. After a reminder on conforming mixed finite element discretizations and their structure, we introduce the nonconforming Conga discretization and describe its main properties, in particular for the compatible approximation of the source terms. These results are then applied to the case of particle approximations for the current, and a connection is drawn with some discontinuous Galerkin methods. The third chapter finally presents the works done in the study of electrostatic plasma sheaths and in the modeling of electromagnetic wave propagation in magnetized plasmas.

Chapter 1

Lagrangian and semi-lagrangian methods for transport problems

This chapter addresses the approximation of a transport equation

$$\partial_t f(t,x) + u(t,x)\cdot\nabla f(t,x) = 0, \qquad t\in[0,T], \quad x\in\mathbb{R}^d \tag{1.1}$$

associated with an initial data $f^0 : \mathbb{R}^d \to \mathbb{R}$, a final time T and a velocity field $u : [0,T]\times\mathbb{R}^d \to \mathbb{R}^d$. In most cases u is itself a function of the density f and the problem is non-linear. To simplify the presentation we will assume here that u is given, and smooth enough so that there exist characteristic trajectories $X(t) = X(t;s,x)$, solutions to the ODE

$$X'(t) = u(t,X(t)), \qquad X(s) = x, \qquad t\in[0,T] \tag{1.2}$$

with $x\in\mathbb{R}^d$ and $s\in[0,T]$. The flow $F_{s,t} : x \mapsto X(t)$ is then invertible and satisfies $(F_{s,t})^{-1} = F_{t,s}$. In particular, the solution to (1.1) takes the form

$$f(t,x) = f^0((F_{0,t})^{-1}(x)) \qquad \text{for } \ t\in[0,T],\ x\in\mathbb{R}^d. \tag{1.3}$$

We then consider the following question: if we are given a reliable numerical scheme for the characteristic flow between two time steps $t_n = n\Delta t$, be it the *forward* flow

$$F^{n,n+1} = F_{t_n,t_{n+1}} \tag{1.4}$$

as in the classical approach of particle methods [99, 95], or the *backward* flow

$$B^{n,n+1} = (F_{t_n,t_{n+1}})^{-1} \tag{1.5}$$

as in the backward semi-lagrangian approach [122, 127, 125], which method can we use to efficiently – and accurately – approximate the transported density $f^n = f(t_n)$?

Publication list

The material in this chapter is based on the following works:

[39] M. Campos Pinto, Adaptive semi-Lagrangian schemes for Vlasov equations, in *Analytical and Numerical Aspects of Partial Differential Equations*, E. Emmrich and P. Wittbold (Eds.) de Gruyter, Berlin, 2009

⟦40⟧ M. Campos Pinto, How to predict accurate wavelet grids in adaptive semi-Lagrangian schemes? *ESAIM: Proc.* 29, 2009

⟦55⟧ M. Campos Pinto, E. Sonnendrücker, A. Friedman, D.P. Grote and S.M. Lund, Noiseless Vlasov–Poisson simulations with linearly transformed particles, *Journal of Computational Physics* 275, 2014

⟦41⟧ M. Campos Pinto, Towards smooth particle methods without smoothing, *Journal of Scientific Computing* 65, 2015

⟦44⟧ M. Campos Pinto, J.A. Carrillo, F. Charles and Y.P. Choi, Convergence of a linearly transformed particle method for aggregation equations, ⟨arXiv:1507.07405⟩, 2015

⟦46⟧ M. Campos Pinto and F. Charles, Uniform Convergence of a Linearly Transformed Particle Method for the Vlasov–Poisson System, *SIAM Journal on Numerical Analysis* 54, 2016

⟦45⟧ M. Campos Pinto and F. Charles, From particle methods to hybrid semi-Lagrangian schemes, ⟨hal-01385676⟩, submitted, 2016

1.1 An adaptive semi-lagrangian method with interpolatory wavelets

During my PhD ⟦38, 50⟧ and together with Michel Mehrenberger we have developed an adaptive semi-lagrangian scheme based on hierarchical $\mathbb{P}_1$ finite element interpolations on dynamically adapted meshes. Pursuing in the same direction I have studied an extension of that method to interpolatory wavelet bases.

The resulting method is inspired by a similar scheme proposed in [14] but differs in the fact that it is mostly driven by the notion of good adaptation of a wavelet tree to a given function. This tool allows us to design a prediction method for adaptive grids, which comes with an a priori error estimate for the resulting transported and projected densities.

Semi-lagrangian methods [122, 121, 127, 125] compute discrete solutions f_h^n that approximate the exact $f(t_n)$ on the times $t_n = n\Delta t$, $n = 0, 1, \ldots, N = T/\Delta t$, following two principles:

- the approximate solutions f_h^n are determined by its point values on a grid Γ_h;
- the point values of f_h^{n+1} are computed from those of f_h^n by using the method of characteristics, with a formula of the form

$$f_h^{n+1}(x_i) = f_h^n(B_h^{n,n+1}(x_i)), \qquad x_i \in \Gamma_h$$

  where $B_h^{n,n+1}$ is an approximation to the backward flow (1.5) that is computed from f_h^n.

It is of course necessary to specify the different steps to define a numerical scheme. For instance, in the simplest case where a regular grid $\Gamma_h = h\mathbb{Z}$ is used in dimension 1 for an equation with given velocity u, we can use a Runge-Kutta scheme for the approximated backward scheme.

Computing the values of f_h^{n+1} on the grid then amounts to evaluating f_h^n on the points $B_h^{n,n+1}(x_i)$, $i \in \mathbb{Z}$. This may be done with local interpolations of order $2R$, letting

$$L_{k,j}(x) = \prod_{\substack{j'=-R+1 \\ j' \neq j}}^{R} \frac{x - x_{k+j'}}{x_{k+j} - x_{k+j'}}, \qquad j = -R+1, \dots, R$$

the $2R$ Lagrange polynomials associated to the nodes $x_{k-R+1}, \cdots, x_{k+R}$, with $k \in \mathbb{Z}$, and then setting

$$f_h^n(x) = \sum_{l=-R+1}^{R} L_{k,l}(x) f_h^n(x_{k+l}) \qquad \text{where } k \text{ is such that } x \in [x_k, x_{k+1}]. \tag{1.6}$$

The interpolation method thus defines how the approximated solution f_h^n is determined by its values on the grid Γ_h.

In the articles [39, 40], I have developed a method where (in dimension $d = 2$, for simplicity) the transported densities are approximated by means of interpolatory wavelets,

$$f_h^n(x) = \sum_{\lambda \in \Lambda^n} d_\lambda^n \varphi_\lambda(x), \qquad \Lambda^n \subset \Gamma_\infty := \{2^{-\ell} k : \ell \in \mathbb{N}, k \in \mathbb{Z}^2\}.$$

Here Λ^n is a non-uniform dyadic grid, φ_λ is the interpolatory wavelet associated to the dyadic node λ, and $d_\lambda^n \in \mathbb{R}$ is the corresponding wavelet coefficient sometimes called *detail*. Based on a hierarchical representation of continuous functions, interpolatory wavelets provide both a high order interpolation tool on non-uniform grids and a practical refinement criterion for the grid. Their construction derives from an iterative process that we may recall. By partitioning the set of dyadic nodes in successive levels,

$$\Gamma_\infty = \Gamma_0 \cup \Big(\cup_{\ell \geq 1} \nabla_\ell \Big) \quad \text{with} \quad \nabla_\ell = \Gamma_\ell \setminus \Gamma_{\ell-1} \quad \text{and} \quad \Gamma_\ell = 2^{-\ell}\mathbb{Z}^2,$$

we let $|\lambda|$ denote the level of a node λ, characterized by the relation $\lambda \in \nabla_{|\lambda|}$. On the corresponding uniform grid we then set

$$\varphi_\lambda(\gamma) = \delta_{\lambda,\gamma}, \qquad \gamma \in \Gamma_{|\lambda|} \tag{1.7}$$

and the construction proceeds by increasing levels. From the values on Γ_ℓ with $\ell \geq |\lambda|$, those of level $\ell + 1$ are given by an interpolation formula of the form (1.6): for $\gamma \in \nabla_{\ell+1}$ this amounts to defining a local stencil $S_\gamma \subset \Gamma_\ell$, as

$$S_\gamma = \begin{cases} \gamma + 2^{-\ell}\big(\{-R+1, \dots, R\} - \frac{1}{2} \times \{0\}\big) & \text{if } \gamma \in 2^{-(\ell+1)}\big((2\mathbb{Z}+1) \times 2\mathbb{Z}\big) \\ \gamma + 2^{-\ell}\big(\{0\} \times \{-R+1, \dots, R\} - \frac{1}{2}\big) & \text{if } \gamma \in 2^{-(\ell+1)}\big(2\mathbb{Z} \times (2\mathbb{Z}+1)\big) \\ \gamma + 2^{-\ell}\big(\{-R+1, \dots, R\} - \frac{1}{2}\big)^2 & \text{otherwise, i.e. if } \gamma \in 2^{-(\ell+1)}(2\mathbb{Z}+1)^2 \end{cases} \tag{1.8}$$

as illustrated on Figure 1.1, and to setting

$$\varphi_\lambda(\gamma) = \sum_{\mu \in S_\gamma} \pi_{\gamma,\mu} \varphi_\lambda(\mu) \qquad \text{for } \gamma \in \nabla_{\ell+1}, \quad \ell \geq |\lambda| \tag{1.9}$$

where $\pi_{\gamma,\mu}$ is the value at γ of the Lagrange polynomial associated with a node μ in the stencil S_γ.

It is known (see, e.g. [71, 62]) that this process converges towards a basis of $\mathcal{C}^0(\mathbb{R}^2)$, which is hierarchical as a result of the multi-scale construction: we have

$$g = \sum_{\gamma \in \Gamma_0} g(\gamma)\varphi_\gamma + \sum_{\ell \geq 1} \sum_{\gamma \in \nabla_\ell} d_\gamma(g)\varphi_\gamma \qquad \text{with} \qquad d_\gamma(g) = g(\gamma) - \sum_{\mu \in S_\gamma} \pi_{\gamma,\mu} g(\mu)$$

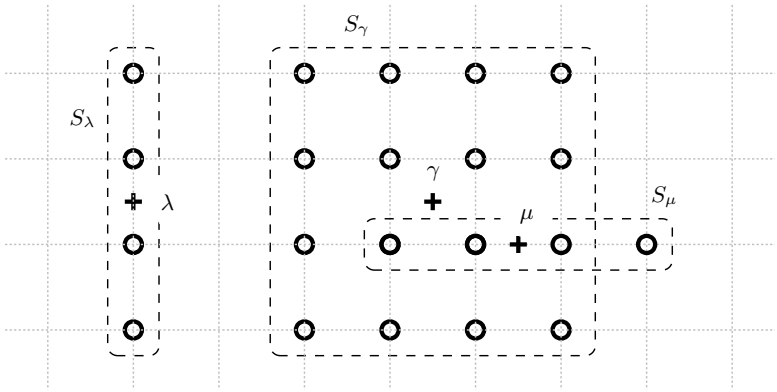

Figure 1.1: Interpolation stencils in the dyadic grid $\Gamma_\ell = 2^{-\ell}\mathbb{Z}^2$ for the 3 types of level $\ell+1$ nodes listed in (1.8), with $R = 2$.

for an arbitrary $g \in \mathcal{C}^0(\mathbb{R}^2)$, the infinite sum being convergent in L^∞. Thus, the successive coefficients of g correspond to interpolation errors which are small where g is smooth. In our method this property is exploited by introducing (i) *admissible* grids of dyadic nodes $\Lambda \subset \Gamma_\infty$ that must satisfy

$$\gamma \in \Lambda \quad \Longrightarrow \quad S_\gamma \subset \Lambda \tag{1.10}$$

and (ii) a wavelet interpolation operator on these grids,

$$P_\Lambda g := \sum_{\gamma \in \Lambda \cap \Gamma_0} g(\gamma)\varphi_\gamma + \sum_{\gamma \in \Lambda \setminus \Gamma_0} d_\gamma(g)\varphi_\gamma, \qquad g \in \mathcal{C}^0(\mathbb{R}^2).$$

Using (1.10) one verifies that g and $P_\Lambda g$ coincide on Λ, so that P_Λ is indeed an interpolation. We thus have a convenient framework for a semi-lagrangian method.

Given an approximation f_h^n to $f(t_n)$ on a grid Λ^n, the objective is then to predict a grid Λ^{n+1} that is well adapted to the approximation $f(t_{n+1})$ to be computed. For this purpose we have designed an algorithm of *dyadic grid transport*, which analysis relies on the notion of good adaptation to a given function. To describe it and deduce a constructive criterion we introduce some notations. The *children* of a node γ of level ℓ are the nodes of level $\ell+1$

$$\mathcal{C}(\gamma) = \begin{cases} \gamma + 2^{-\ell}\big(\{-\frac{1}{2},\frac{1}{2}\}\times\{0\}\big) & \text{if } \gamma \in 2^{-\ell}\big((2\mathbb{Z}+1)\times 2\mathbb{Z}\big) \\ \gamma + 2^{-\ell}\big(\{0\}\times\{-\frac{1}{2},\frac{1}{2}\}\big) & \text{if } \gamma \in 2^{-\ell}\big(2\mathbb{Z}\times(2\mathbb{Z}+1)\big) \\ \gamma + 2^{-\ell}\big(\{-\frac{1}{2},0,\frac{1}{2}\}^2 \setminus (0,0)\big) & \text{otherwise, i.e. if } \gamma \in 2^{-\ell}(2\mathbb{Z}+1)^2 \end{cases} \tag{1.11}$$

as pictured in Figure 1.2. The *parent* $\mathcal{P}(\lambda)$ of a node λ is then characterized by the relation $\lambda \in \mathcal{C}(\mathcal{P}(\lambda))$. An admissible grid (1.10) is clearly a wavelet tree in the sense where $\lambda \in \Lambda$ implies $\mathcal{P}(\lambda) \in \Lambda$.

The *outer leaves* of a tree are defined as the set

$$\mathcal{L}_{\rm out}(\Lambda) = \{\lambda \in \Gamma_\infty \setminus \Lambda : \mathcal{P}(\lambda) \in \Lambda\}$$

and the *star-nodes* of level ℓ are the nodes in $\nabla_\ell^* = 2^{-\ell}(2\mathbb{Z}+1)^2 \subset \nabla_\ell$, which correspond to a refinement in both dimensions as in the third line of (1.8) or (1.11). The set of all the star-nodes is

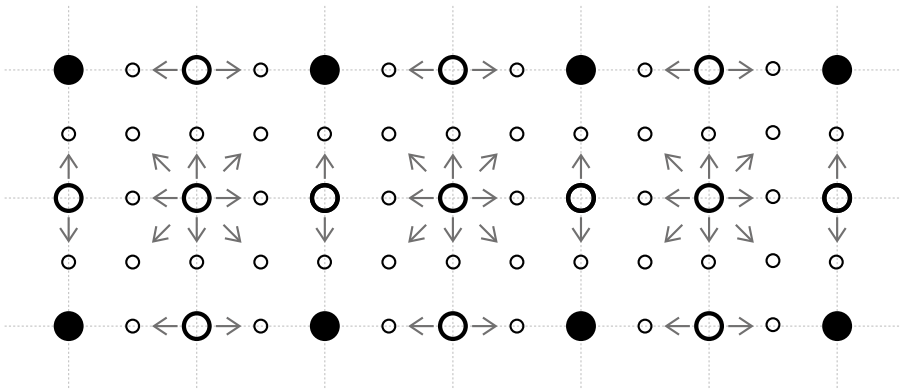

Figure 1.2: Tree structure of wavelet grids. Here the black nodes are on the uniform grid $\Gamma_{\ell-1} = 2^{1-\ell}\mathbb{Z}^2$, the big white nodes are in $\nabla_\ell = \Gamma_\ell \setminus \Gamma_{\ell-1}$ and the small white nodes are in $\nabla_{\ell+1}$. The arrows indicate the parent $\to$ child relations.

$\Gamma^*_\infty = \cup_{\ell\in\mathbb{Z}}\nabla^*_\ell$, and one verifies that if Λ is an admissible grid, then the outer star-leaves allows to form a mesh associated with Λ. Specifically, the set

$$M(\Lambda) := \{\Omega_\lambda : \lambda \in \mathcal{L}_{\rm out}(\Lambda) \cap \Gamma^*_\infty\} \tag{1.12}$$

composed of cells of the form

$$\Omega_\lambda := \lambda + 2^{-|\lambda|}]-1,1[^2$$

is a partition of $\mathbb{R}^2$ which local resolution corresponds to the maximal level of the star-nodes of Λ. Lastly, the *neighbors* of a star-node $\gamma \in \Gamma^*_\infty$ are the nodes which influence domain $\Sigma_\lambda = \lambda + 2^{-|\lambda|}(2R-1)[-1,1]^2$ (corresponding to the convex hull of the stencil S_λ) intersect its cell Ω_γ: their set is denoted

$$\mathcal{N}(\gamma) = \{\lambda \in \Gamma_\infty : \Sigma_\lambda \cap \Omega_\gamma \neq \emptyset\}, \qquad \gamma \in \Gamma^*_\infty.$$

It is then possible to specify the notion of good adaptation to a given function. More precisely we shall define two versions of that notion: a weak one and a strong one.

Definition 1.1 *Let $0 < \kappa < 1$ be a fixed constant. Given $\varepsilon > 0$ and $g \in \mathcal{C}^0(\mathbb{R}^2)$, a dyadic grid Λ is said* weakly ε-adapted *to g if*

$$\sup_{\gamma\in\mathcal{L}_{\rm out}(\Lambda)\cap\Gamma^*_\infty} \sup_{\lambda\in\mathcal{N}(\gamma)\setminus\Lambda} 2^{\kappa(|\lambda|-|\gamma|)}|d_\lambda(g)| \le \varepsilon.$$

If the second supremum can be taken over the entire set $\mathcal{N}(\gamma)$, including the neighbors in the grid Λ, then the latter is said strongly ε*-adapted to g.*

These criteria provide a practical tool to construct wavelet trees well adapted to a given function, by refining the dyadic mesh (1.12) associated with the star-nodes in such a way that on every mesh cell Ω_γ, it holds $2^{\kappa|\lambda|}|d_\lambda(g)| \le \varepsilon 2^{\kappa|\gamma|}$ for all the nodes λ which domain Σ_λ intersects Ω_γ. In the weak version we see that nodes belonging to the tree are excluded from the criterion, for the reason that only the details outside the tree contribute to the interpolation error. Indeed we have the following estimate.

Lemma 1.2 *If Λ is a grid weakly ε-adapted to $g \in \mathcal{C}^0(\mathbb{R}^2)$ and graded in the sense that $\mathcal{N}(\gamma) \cap \Gamma_{|\gamma|-1} \subset \Lambda$ holds for all $\gamma \in \Lambda$, then the associated interpolation error satisfies*

$$\|g - P_\Lambda g\|_{L^\infty(\mathbb{R}^2)} \lesssim \varepsilon$$

with a constant independent of g.

Thus, the weak adaptation is sufficient for the accurate approximation to a given function.

The principle of the strong adaptation (which requires to refine the tree in the vicinity of large details, even when their nodes are already present in the grid) is that it is robust enough to be preserved by a simple algorithm of dyadic grid transport. Such an algorithm can be obtained by refining the nodes which image by the backward flow touches a cell of essentially higher level. The specific form involves a fixed integer $\delta \geq 1$ corresponding to a number of additional refinement levels.

Algorithm 1.3 ($\mathbb{T}_B(\Lambda)$: dyadic grid transport) *Let $\delta \in \mathbb{N} \setminus \{0\}$. Given a backward flow B, and starting from $\Lambda_0^* := \Gamma_0^*$, we build*

$$\Lambda_{\ell+1}^* := \Lambda_\ell^* \cup \big\{\gamma \in \mathcal{L}_{\rm out}(\Lambda_\ell^*) \cap \Gamma_\infty^* : \min\{|\lambda| : \lambda \in \mathcal{L}_{\rm out}(\Lambda) \cap \Gamma_\infty^*, B(\gamma) \in \overline{\Omega}_\lambda\} > |\gamma| - \delta\big\}$$

until $\Lambda_{L+1}^* = \Lambda_L^*$, and we let $\mathbb{T}_B(\Lambda) := \Lambda_L^*$ be the resulting dyadic grid.

The following theorem states that this process indeed allows to build grids that are well adapted to the functions transported by the flow B.

Theorem 1.1 (see [39], Th. 6.9) *If the flow B and its inverse are Lipschitz of respective constants L and L', and if $\delta \geq 1 + \ln_2\big(L(8R + 2LL' - 3)\big)$, the Algorithm 1.3 preserves the grid adaptation in the sense where*

$$\text{if } \Lambda \text{ is strongly } \varepsilon\text{-adapted to } g, \text{ then } \mathbb{T}_B(\Lambda) \text{ is weakly } C\varepsilon\text{-adapted to } \mathcal{T}_B g = g \circ B$$

with a constant C that does not depend on B. Moreover the size of the predicted tree is stable,

$$\#\big(\mathbb{T}_B(\Lambda)\big) \lesssim \#(\Lambda). \tag{1.13}$$

Our adaptive scheme is then as follows. Using an algorithm $\mathbb{A}_\varepsilon$ that builds a grid strongly adapted to a given function according to the above criterion, and a refinement algorithm $\mathbb{G}$ to build graded trees (see [39], Sec. 6.1), we begin by interpolating the initial density on its associated tree,

$$f_\varepsilon^0 := P_{\Lambda_\varepsilon^0} f^0 \quad \text{with} \quad \Lambda_\varepsilon^0 := \mathbb{G}(\mathbb{A}_\varepsilon(f^0)). \tag{1.14}$$

For $n + 1 \leq N = T/\Delta t$, we then proceed in two steps.

(i) We first transport the approximated density with a semi-lagrangian method based on the predicted tree

$$\tilde{f}_\varepsilon^{n+1} := P_{\tilde{\Lambda}_\varepsilon^{n+1}} \mathcal{T} f_\varepsilon^n \quad \text{with} \quad \tilde{\Lambda}_\varepsilon^{n+1} := \mathbb{G}\big(\mathbb{T}_{B_h^{n,n+1}}(\Lambda_\varepsilon^n)\big). \tag{1.15}$$

Here, $\mathcal{T} f_\varepsilon^n = f_\varepsilon^n \circ B_h^{n,n+1}$ denotes the density transported along an approximated flow computed from f_ε^n, as given by some reference semi-lagrangian method.

(ii) We then correct the grid in such a way that it stays strongly adapted to the approximated density,

$$f_\varepsilon^{n+1} := P_{\Lambda_\varepsilon^{n+1}} \tilde{f}_\varepsilon^n \quad \text{with} \quad \Lambda_\varepsilon^{n+1} := \mathbb{G}\big(\mathbb{A}_\varepsilon(\tilde{f}_\varepsilon^{n+1})\big). \tag{1.16}$$

Since the approximated flow is computed from f_ε^n, we may assume that is satisfies

$$\left\|B^{n,n+1} - B_h^{n,n+1}\right\|_{L^\infty(\Omega)} \lesssim \Delta t^r + \Delta t \|f(t^n) - f_\varepsilon^n\|_{L^\infty(\Omega)} \tag{1.17}$$

for some integer r corresponding to the order of the time scheme. It is then possible to prove the following estimate.

Theorem 1.2 *We assume that the approximated flow satisfies an estimate of the form* (1.17)*. If the initial data f^0 is Lipschitz, as well as the forward and backward flows* (1.4)*,* (1.5)*, then the approximated solution computed by the scheme* (1.14)-(1.16) *satisfies*

$$\|f(t_n) - f_\varepsilon^n\|_{L^\infty(\Omega)} \lesssim (\Delta t)^{r-1} + \varepsilon/\Delta t \tag{1.18}$$

for $n\Delta t \leq T$, with a constant independent of ε and Δt.

1.2 Smooth particles with polynomial transformations

In spite of their accuracy, semi-lagrangian methods are not the standard approach in plasma physics. Apart from the Gysela code [86, 87] a majority of the large kinetic codes developed for plasma problems is indeed based on purely eulerian or lagrangian approaches (see e.g., [82, Sec. 3.1] for a review in the area of gyrokinetic fusion plasmas). Essentially, lagrangian solvers rely on a particle representation of the densities in the phase space. Used in plasma physics as early as in the 1950s [78, 72, 37] (and in fluid dynamics, c.f. [59, 68]), the main advantages of this approach are its relative low cost (no phase space mesh like semi-lagrangian methods, and a natural adaptation of the computing resources to the areas where the plasma actually is), its simplicity and its robustness over long simulation times, mainly due to its ability to preserve several fundamental physical quantities [99, 95].

However, particle methods also have their flaws. In particular, numerical results are often affected by non-physical oscillations (of probabilistic or deterministic nature) which hamper their interpretation when the number of particles is not significantly increased as the resolution of the method is improved. Several techniques do exist to reduce these oscillations (for instance by periodically remapping the density on new particle grids [73, 98, 113, 101], or by adequately averaging the weights of neighboring particles [10, 66], or even by using local formulas to reconstruct the density [131, 63], to quote only a few) however their mathematical analysis is usually not sufficient for an accurate assessment of their performances.

Based on this observation, my objective has been to study numerical schemes that allow an accurate representation of the densities and which implementation would be as easy as possible in the framework of an existing particle code. By simplicity I have essentially worked in a deterministic setting (i.e. with particles initially located on a given grid), but keeping in mind an application of my works to the probabilistic setting of Monte Carlo methods used in many particle codes, see e.g., [28].

In its deterministic version, the standard particle method [100, 118] approximates the density f by a collection of numerical particles of the form

$$f_{h,\epsilon}^n(x) = \sum_{k\in\mathbb{Z}^d} w_k \varphi_\epsilon(x - x_k^n). \tag{1.19}$$

Here w_k is the weight of the particle centered in x_k^n, and φ_ϵ denotes a smoothed Dirac mass with scale $\epsilon > 0$, typically of the form $\varphi_\epsilon(x) = \epsilon^{-d}\varphi(\epsilon^{-1}x)$ with φ a smooth and compactly supported shape function such as a B-spline or some smoothing kernel with vanishing moments, see e.g. [68, 98]. As

for h it represents the average inter-particle distance. To simplify our presentation we may consider that the particles are initially located on a cartesian grid,

$$x_k^0 = hk, \qquad k \in \mathbb{Z}^d, \tag{1.20}$$

and we will assume that their trajectories follow the exact flow (1.4),

$$x_k^{n+1} = F^{n,n+1}(x_k^n).$$

The weights are then usually given by an initial approximation of the local masses, e.g., $w_k = h^d f^0(x_k^0)$. In the classical analysis this process is seen as (i) an approximation (in a distributions sense) of f^0 by a weighted sum of Dirac measures, (ii) the exact transport of that distribution, and (iii) the smoothing of the resulting measure approximation by the convolution kernel φ_ϵ. Provided that the latter satisfies a moment condition of order $r \geq 1$, the standard error estimate [11, 118] takes the form

$$\|f(t^n) - f_{h,\epsilon}^n\|_{L^p} \leq C\Big(\epsilon^r \|f^0\|_{W^{r,p}} + (h/\epsilon)^m \|f^0\|_{W^{m,p}}\Big), \quad 1 \leq p \leq \infty. \tag{1.21}$$

It is possible to improve this estimate by using more different initial quadratures [63], but in any case this kind of results highlights one weakness of the reconstruction (1.19), that is the need to choose $\epsilon \gg h$ as $\epsilon, h \to 0$ to guarantee the strong convergence of the densities, which translates into a growing particle overlapping which is has an expensive cost in actual computations. In practice most particle codes run with a moderate particle overlapping, that is sufficient for the weak convergence of the densities and, in the general case where the flow itself depends on the transported densities, for the an accurate approximation of the particle trajectories.

The lack of strong convergence generally leads to oscillations in the approximated densities. To reduce them while keeping a bounded particle overlapping ($\epsilon \sim h$), many authors have proposed methods of *forward semi-lagrangian* (FSL) type, which consist of periodically remapping the density (1.19) on the grid [73, 98, 113, 65, 69, 101]. These projections have a smoothing effect which tend to solve the oscillations due to the distortion of the particle cloud, but they also introduce a numerical diffusion which may spoil the accuracy over long time ranges, so that several authors have investigated advanced remapping techniques, see [101] or [12, 13, 133] for multi-scale methods.

In order to reduce the oscillations with a limited use of remappings and a bounded particle overlapping, I have studied in a series of articles [[41, 55, 46]] a class of methods where the particles are transformed so to better follow the characteristic transport flow. Again, the initial density is approximated by a collection of weighted particles,

$$f_h^0(x) = \sum_{k \in \mathbb{Z}^d} w_k \varphi_h(x - x_k^0) \tag{1.22}$$

but unlike (1.19) where the particles shapes were simply translated along the trajectories, they are now transformed using local approximations of the backward flow $B^{0,n} = (F_{0,t_n})^{-1}$. At the first order the method uses linear expansions of the flow around each trajectory

$$B_{(1),k}^{0,n} : x \mapsto x_k^0 + D_k^n (x - x_k^n) \tag{1.23}$$

where D_k^n is a deformation matrix that corresponds to the jacobian matrix $J_{B^{0,n}}(x_k^n)$, and it transports the shape functions according to

$$\varphi_h(x - x_k^0) \;\mapsto\; \varphi_h(B_{(1),k}^{0,n}(x) - x_k^0) = \varphi_h(D_k^n(x - x_k^n)).$$

The linearly-transformed particle (LTP) approximation then takes the form

$$f_h^n(x) = \sum_{k\in\mathbb{Z}^d} w_k \varphi_h(D_k^n(x - x_k^n)) \tag{1.24}$$

and we have the following result (see ⟦41⟧, Th. 1).

Theorem 1.3 *The LTP approximation* (1.24) *satisfies*

$$\|f(t_n) - f_h^n\|_{L^\infty} \leq \|f^0 - f_h^0\|_{L^\infty} + Ch\|f^0\|_{L^\infty} \tag{1.25}$$

with a constant C that depends on the smoothness of the flow $F^{0,n}$ and that of its inverse.

At the second order the local expansion of the backward flow reads

$$B_{(2),k}^{0,n} : x \mapsto x_k^0 + D_k^n(x - x_k^n) + \frac{1}{2}\big((x - x_k^n)^t (Q_k^n)_i (x - x_k^n)\big)_{1\leq i\leq d}\Big)$$

with a quadratic term $(Q_k^n)_i$ that corresponds to the hessian matrix $H_{(B^{0,n})_i}(x_k^n)$ of the flow component i. The method is generalized to an arbitrary order r by setting

$$B_{(r),k}^{0,n}(x) := (x - x_k^n) + x_k^0 + \phi_k'(0) + \cdots + \frac{1}{r!}\phi_k^{(r)}(0) \quad \text{where} \quad \phi_k(s) = (B^{0,n} - I)(x_k^n + s(x - x_k^n)).$$

However, as the mapping $B_{(r),k}^{0,n}$ is not injective in general, the support of $\varphi_h(B_{(r),k}^{0,n}(x) - x_k^0)$ has no reason to be contained in a neighborhood of x_k^n. To define the polynomial transformation of the particle shape it is then necessary to introduce an a priori restriction of the supports. In ⟦41⟧ the proposed method consists of transporting (using the linearized flow $F_{(1),k}^{0,n} = (B_{(1),k}^{0,n})^{-1}$) an extension of the initial particle support. If the latter is included in a ball $\Sigma_{h,k}^0 = B_{\ell^\infty}(x_k^0, h\rho^0)$, we set

$$\Sigma_{h,k}^n := F_{(1),k}^{0,n}\big(B_{\ell^\infty}(x_k^0, h\rho_{h,k}^n)\big) \quad \text{with} \quad \rho_{h,k}^n := \rho^0 + \frac{1}{h}\|B_{(1),k}^{0,n} - B^{0,n}\|_{L^\infty(F^{0,n}(\Sigma_{h,k}^0))} \tag{1.26}$$

and we define the polynomial transformation of the smooth particles by

$$\varphi_h(x - x_k^0) \;\mapsto\; \mathbb{1}_{\Sigma_{h,k}^n}(x)\varphi_h\big(B_{(r),k}^{0,n}(x) - x_k^0\big).$$

The following result (see ⟦41⟧, Th. 2) establishes the order r convergence of the resulting reconstruction.

Theorem 1.4 *The approximation based on order r polynomial transformations of the particle shapes, defined as*

$$f_h^n(x) = \sum_{k\in\mathbb{Z}^d} w_k \mathbb{1}_{\Sigma_{h,k}^n}(x)\varphi_h\big(B_{(r),k}^{0,n}(x) - x_k^0\big) \tag{1.27}$$

satisfies

$$\|f(t_n) - f_h^n\|_{L^\infty} \leq \|f^0 - f_h^0\|_{L^\infty} + Ch^r\|f^0\|_{L^\infty} \tag{1.28}$$

with a constant C that depends on the smoothness of the flow $F^{0,n}$ and that of its inverse.

The explicit form of the constants C that appear in the above theorems (given in ⟦41⟧) indicates a rapid deterioration of the accuracy when the flow becomes less regular. For this reason it is beneficial to occasionally remap the density, as this allows to restart the above process with a reinitialized characteristic flow. One may observe that periodic remappings on the grid formally turn the method into a semi-lagrangian one. The polynomial shape transformations can then be seen as a way to reduce

the number of remappings needed, as our estimates show that the approximated densities converge as $h \to 0$ even if no remappings are performed.

Since the matrices D_k^n and $(Q_k^n)_i$ involved in the linear and quadratic flows (for the first orders) approximate the jacobian and hessian matrices of the backward flow, namely $J_{B^{0,n}}(x_k^n)$ and $H_{(B^{0,n})_i}(x_k^n)$, it is possible in practice to compute them from the position of the neighboring markers. A finite difference approximation on the initial grid of the derivatives of the forward flow $F^{0,n} = F_{0,t_n}$ indeed leads to

$$J_k^n := \left(\frac{(x_{k+e_j}^n - x_{k-e_j}^n)_i}{2h} \right)_{1 \le i,j \le d} \approx J_{F^{0,n}}(x_k^0) \tag{1.29}$$

and from the identity $J_{F^{0,n}}(x_k^0) J_{B^{0,n}}(x_k^n) = I_d$, we may set

$$D_k^n := (J_k^n)^{-1}. \tag{1.30}$$

For the quadratic terms we approximate the hessian matrices of the forward flow by

$$(H_k^n)_i := \Big((h)^{-2} \sum_{\alpha_1,\alpha_2=0}^{1} (-1)^{\alpha_1+\alpha_2} \big(x_{k+\alpha_1 e_{j_1} + \alpha_2 e_{j_2}}^n \big)_i \Big)_{1 \le j_1, j_2 \le d} \approx H_{(F^{0,n})_i}(x_k^0). \tag{1.31}$$

By differentiating twice (at x_k^0) the identity $I = B^{0,n} F^{0,n}$ we obtain

$$0 = \big(J_{\bar{F}^n}(x_k^0) \big)^t H_{(B^{0,n})_i}(x_k^n) J_{F^{0,n}}(x_k^0) + \sum_{j=1}^{d} \big(J_{B^{0,n}}(x_k^n) \big)_{i,j} H_{(F^{0,n})_j}(x_k^0),$$

so that we set

$$(Q_k^n)_i := -(D_k^n)^t \Big(\sum_{j=1}^{d} (D_k^n)_{i,j} (H_k^n)_j \Big) D_k^n. \tag{1.32}$$

One can assess the accuracy of these approximations. Specifically, there exists a threshold $h^*(F^{0,n})$ under which the matrices J_k^n are invertible and we have, for all $k \in \mathbb{Z}^d$,

$$h \le h^*(F^{0,n}) \quad \Longrightarrow \quad \|D_k^n - J_{B^{0,n}}(x_k^n)\| \le Ch^2 \quad \text{and} \quad \|(Q_k^n)_i - H_{(B^{0,n})_i}(x_k^n)\| \le Ch \tag{1.33}$$

with constants C that depend on the exact flow $F^{0,n}$, see e.g. the Appendix in ⟦45⟧.

Several numerical tests have demonstrated the convergence properties of this approach. Thus Figure 1.3 shows the error curves corresponding to the transport of a smooth density in a velocity field $u(t,x) = \cos\left(\frac{\pi t}{T}\right) \operatorname{curl} \phi(x)$ with $\phi(x) := -\frac{1}{\pi} \sin^2(\pi x_1) \sin^2(\pi x_2)$, such that the solution reverts to its initial state at $t = T$ after a maximal stretching reached at $t = T/2$. There we verify that the traditional smooth particle approximation (1.19), represented (under the acronym TSP) for several values of the exponent q determining the size $\epsilon = h^q$ of the particle supports, only converges for values $q < 1$ which correspond to a growing particle overlapping, moreover the subsequent convergence is rather slow. The convergence of the FSL method (with remappings but no shape transformations) is faster but requires to decrease the remapping period Δt_r with the inter-particle distance h, which in practice is similar to imposing a CFL condition. The main strength of the LTP and QTP methods (involving linear and quadratic transformations) is that the convergence holds for constant values of the period Δt_r, and that the optimal values of this period, which correspond to the best compromise between the remapping errors and the flow distortion, are significantly larger with the QTP method.

During my collaboration with physicists from the "Heavy Ion Fusion" group at Lawrence Berkeley Laboratory, I have described and numerically validated a *Linearly-Transformed Particle-In-Cell*

(LTPIC) scheme for the 1d1v Vlasov-Poisson system, involving particles transformed using the LTP method and an electric field solved by a standard finite difference scheme. The numerical results [55] have then shown to be comparable to that of high order grid based solvers (e.g. semi-lagrangian ones), renowned for their accuracy.

Together with Frédérique Charles of the LJLL we have extended the analysis to this non-linear 1d1v Vlasov-Poisson problem. In the article [46] we have proven the a priori convergence of the approximated density in the L^∞ norm (at order 1) and that of the particle trajectories (at order 2). In comparison with the standard estimates of Cottet and Raviart [67] applied to the case of particle shapes with bounded overlapping ($\varepsilon \sim h$), our approach allows to gain one order of convergence at the price of linearly transforming the shape of each particle.

With Frédérique Charles (LJLL), Young-Pil Choi and José Antonio Carrillo (Imperial College) we have also applied the LTP method to a class of aggregation equations, for which we have shown (both theoretically and numerically) strong convergence results for the density, that seem to be out of reach for particle methods with fixed scale. These results have been presented in the submitted article [44].

1.3 A forward-backward semi-lagrangian method

Although the previous method improves the accuracy of the smooth particle reconstructions, it has the downside that it produces particle shapes which support may extend a lot along some directions, which makes it hard (and expensive) to localize them in the phase space. In particular, it is not easy to rapidly determine which particles are involved in the evaluation of the densities (1.24) or (1.27) at a given point x, moreover their distance to x may grow indefinitely between two remappings, so that their inventory quickly becomes very costly in several space dimensions.

To avoid such a phenomenon, the simplest option is to stop representing f^n as a collection of smooth particles. However we still wish to preserve the main ingredient of the LTP and QTP methods, that is the local approximation of the backward flow $B^{0,n}$ close to the markers x_k^n using the formulas (1.29)-(1.32). Indeed the latter seem to provide accurate results (as seen in the numerical simulations displayed in Figure 1.3 for instance) and only involves the exact position of the neighboring markers.

To reach this objective a natural solution consists of implementing in the framework of particle methods the improved locality principle proposed by Colombi and Alard in [64] to design highly accurate semi-lagrangian schemes. Indeed, to the point particles (markers) transported *forward* we can associate a representation based on the local approximation of the *backward flow* by the techniques described above. Specifically, the method proposed in [45] approximates the density $f(t^n, x) = f^0(B^{0,n}(x))$ using the following steps :

(i) To every marker x_k^n one associates a local approximation $B_{h,k}^{0,n}$ of the backward flow, computed just as in the LTP or QTP methods, using finite differences. We remind that at the first order this approximated flow takes the form

$$B_{h,k}^{0,n}(x) = x_k^0 + D_k^n(x - x_k^n) \tag{1.34}$$

with a matrix D_k^n computed by the formulas (1.29)-(1.30), and at the second order it reads

$$B_{h,k}^{0,n}(x) = x_k^0 + D_k^n(x - x_k^n) + \frac{1}{2}\big((x - x_k^n)^t (Q_k^n)_i (x - x_k^n)\big)_{1\le i\le d} \tag{1.35}$$

with matrices $(Q_k^n)_i$ computed with the formulas (1.31)-(1.32).

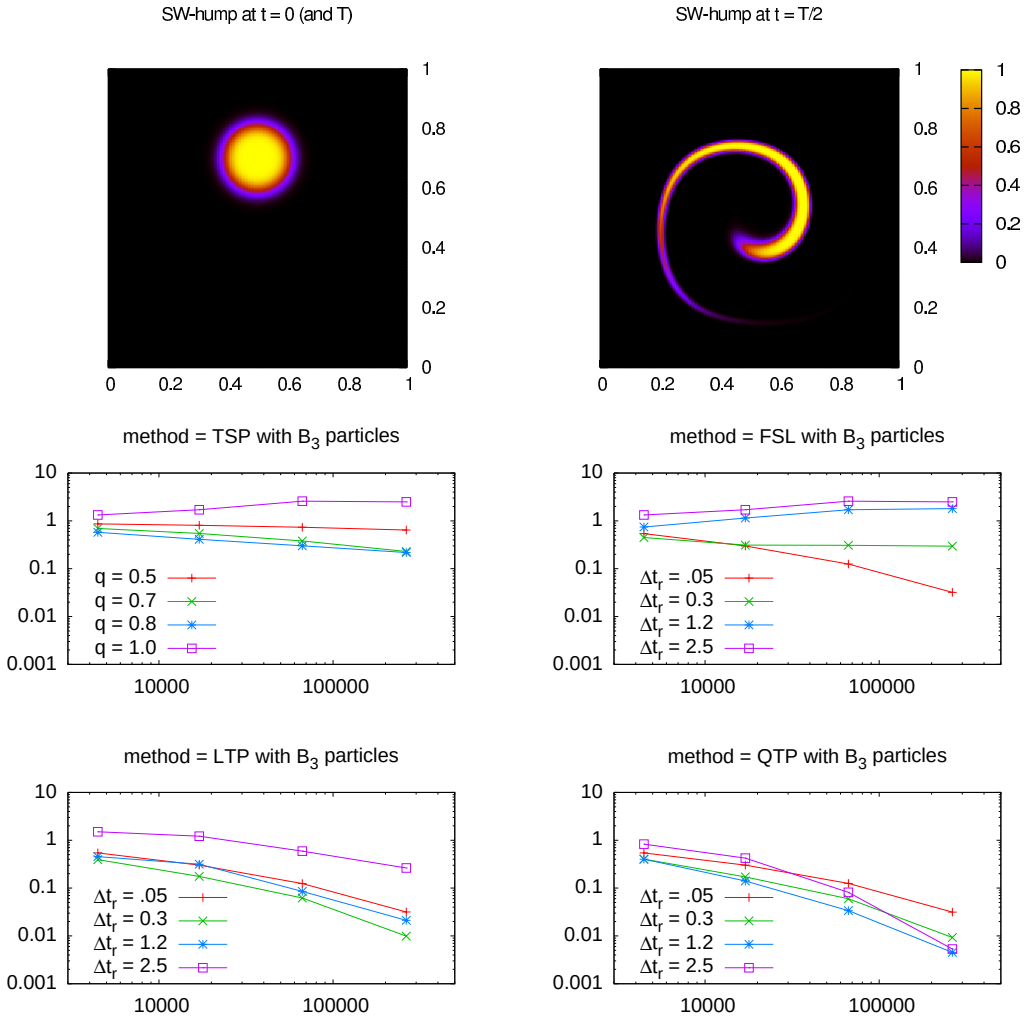

Figure 1.3: Convergence curves (L^∞ errors vs. particle numbers $N \sim h^{-2}$) for a passive transport problem with reversible flow, approximated using several methods as described in Section 1.2: the TSP (traditional smooth particle) method uses smooth particles with radius $\epsilon = h^q$ without remappings, the FSL (forward semi-lagrangian) method remaps the particules $\epsilon = h$ with different periods Δt_r, like the LTP and QTP methods which in addition impose a transformation (linear or quadratic) of the smooth particle shapes. The above figures show the exact solution at $t = 0$ and T on the left, and at $t = T/2$ the time of maximal stretching, on the right.

(ii) In order to smoothly patch together these local approximations of the backward flow, we then consider a partition of unity

$$\sum_{i \in \mathbb{Z}^d} S(x - i) = 1, \qquad x \in \mathbb{R}^d \tag{1.36}$$

that involves a compactly supported shape function $S \geq 0$, such as a B-spline. Using again a grid of step-size h, which nodes will be denoted $\xi_i = ih$ to avoid a confusion with the markers, we let $S_{h,i}(x) = S\big((x - \xi_i)/h\big)$ the averaging shape function associated with node ξ_i. A global

approximation of the backward flow is then given by

$$B_h^{0,n}(x) := \sum_{i\in\mathbb{Z}^d} B_{h,k^*(n,i)}^{0,n}(x) S_{h,i}(x) \tag{1.37}$$

where the marker of index $k^*(n,i)$ is defined as the closest one to the node ξ_i at time t_n, i.e.,

$$k^*(n,i) := \operatorname*{argmin}_{k\in\mathbb{Z}^d} \|x_k^n - \xi_i\|_\infty.$$

(iii) The approximated density is then given by a standard lagrangian representation, i.e.,

$$f_h^n(x) := f^0\big(B_h^{0,n}(x)\big) \tag{1.38}$$

that we may call a forward-backward lagrangian scheme, possibly specifying L-FBL or Q-FBL depending whether the local flows are given by linear (1.34) or quadratic (1.35) expansions.

Again, it is important to reinitialize the characteristic flows when they become too irregular to be accurately approximated by the local expansions, and as in the previous section this may be done using remappings, i.e., particle reinitialization based on the density transported thus far.

We can verify that with the new process the evaluation of the density on a given point is more local than with the LTP or QTP methods, where the polynomial transformation of the particle shapes may trigger a rapid (and indefinite) extension of their support. In the numerical simulations, this enhanced locality is evidenced by a significant gain in cpu time, already visible in $d = 2$ dimensions on second-order methods illustrated in Fig. 1.4, because of the rapid growth of the particle support in the QTP method, see (1.26). This gain will be more dramatic with higher space dimension, especially in the case of Vlasov equations in $d = 2+2$ or $d = 3+3$ dimensions. Such configurations are currently under implementation within the Selalib platform [124] developed in collaboration with teams at IPP in Garching (Germany), at IRMA in Strasbourg and at IRMAR in Rennes.

We also have the following estimates, where the threshold $h^*(F^{0,n})$ corresponds to the ability to invert the jacobian matrix approximated by finite differences, see (1.33).

Theorem 1.5 *Let $h \le h^*(F^{0,n})$. If the exact flow $F^{0,n}$ and its inverse $B^{0,n}$ are in $W^{2,\infty}(\mathbb{R}^d)$, then the approximation* (1.38) *of first order (L-FBL) satisfies*

$$\|f(t^n) - f_h^n\| \le Ch^2$$

with a constant independent of h. If in addition $F^{0,n}$ and $B^{0,n}$ are in $W^{3,\infty}(\mathbb{R}^d)$, then the approximation (1.38) *of second order (Q-FBL) satisfies*

$$\|f(t^n) - f_h^n\| \le Ch^3$$

with a constant independent of h.

In comparison with particle methods using polynomial transformations, these estimates allow to gain one order of convergence. The main reason for this being that, in the approximated density, the decomposition in terms of scale h is now performed on the backward flow rather than on the density itself, which avoids a loss of h in the Lipschitz constant of the numerical density. This convergence gain is not only visible in the a priori estimates : it is also observed in some numerical simulations when the transport (without remappings) is realized on long enough periods, as illustrated on Figure 1.5.

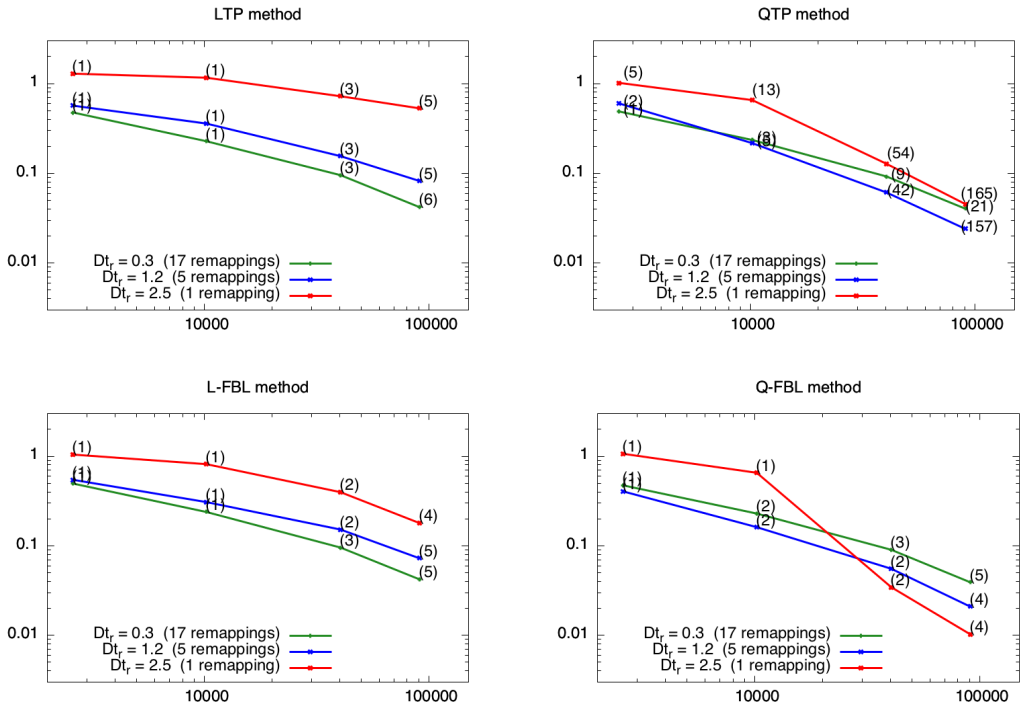

Figure 1.4: Convergence curves (L^∞ errors vs. particle numbers $N \sim h^{-2}$) for the passive transport problem illustrated on Figure 1.3. The upper curves serve as a reminder of the convergence properties of the methods with polynomial shape transformation (LTP and QTP), whereas the lower curves indicate that of the forward backward lagrangian (fbl) approximations (1.38). The number in parenthesis indicate the cpu times (in seconds) of each run.

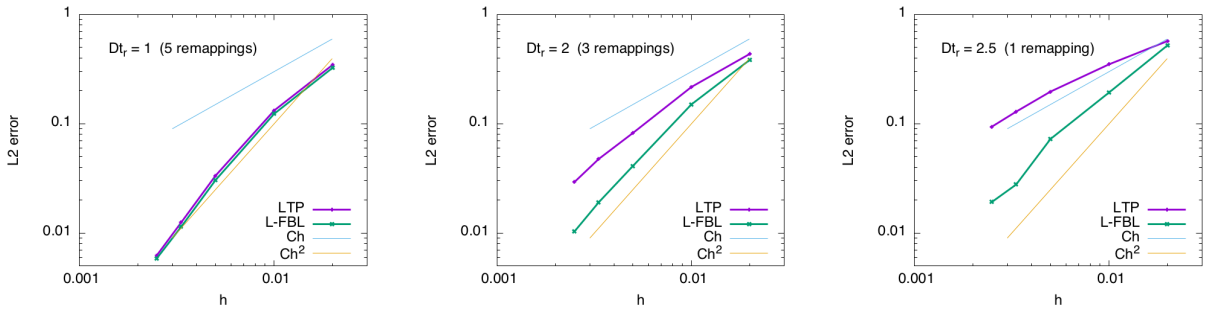

Figure 1.5: Convergence curves (L^2 relative errors vs. h) for the passive transport problem illustrated on figure 1.3, approximated by the LTP and L-FBL methods. The gain of one order appears clearly on these L^2 curves when the remapping period is increased.

Chapter 2

Compatible nonconforming approximation of the Maxwell equations

Publication list

The material in this chapter is based on the following works:

⟦48⟧ M. Campos Pinto, S. Jund, S. Salmon and E. Sonnendrücker, Charge conserving FEM-PIC schemes on general grids, *Comptes Rendus Mecanique* 342, 2014

⟦54⟧ M. Campos Pinto and E. Sonnendrücker, Gauss-compatible Galerkin schemes for time-dependent Maxwell equations, *Mathematics of Computation* 85, 2016

⟦42⟧ M. Campos Pinto, Constructing exact sequences on non-conforming discrete spaces, *Comptes Rendus Mathematique* 354, 2016

⟦51⟧ M. Campos Pinto, M. Mounier and E. Sonnendrücker, Handling the divergence constraints in Maxwell and Vlasov–Maxwell simulations, *Applied Mathematics and Computation* 272, 2016

⟦49⟧ M. Campos Pinto, M. Lutz and M. Mounier, Electromagnetic PIC simulations with smooth particles: a numerical study, *ESAIM: Proc.* 53, 2016

⟦52⟧ M. Campos Pinto and E. Sonnendrücker, Compatible Maxwell solvers with particles I: conforming and non-conforming 2D schemes with a strong Ampere law, ⟨hal-01303852⟩, under revision for SMAI-JCM, 2016

⟦53⟧ M. Campos Pinto and E. Sonnendrücker, Compatible Maxwell solvers with particles II: conforming and non-conforming 2D schemes with a strong Faraday law, ⟨hal-01303861⟩, under revision for SMAI-JCM, 2016

⟦43⟧ M. Campos Pinto, Structure-preserving conforming and nonconforming discretizations of mixed problems, ⟨hal-01471295⟩, submitted, 2017

2.1 The time-dependent Maxwell system

For the approximation of the Maxwell equations (written here in 2D for clarity, as the presence of two curl operators, one scalar and one vector-valued in bold font, will help us better visualize some key features of the analysis)

$$\begin{cases} \partial_t B + \operatorname{curl} \boldsymbol{E} = 0 \\ \partial_t \boldsymbol{E} - c^2 \,\mathbf{curl}\, B = -\dfrac{1}{\varepsilon_0}\boldsymbol{J}, \end{cases} \tag{2.1}$$

mixed finite elements are a reference method [85, 18]. Compared to the historical FDTD (finite difference time domain) approach [138] they are designed to reach high order accuracy in complex geometries, and when the discrete spaces involved can be endowed with compatibility relations reproducing the geometric structure of the functional spaces where some fundamental properties of the equations are naturally expressed, they have indeed important stability and approximation properties, be it for the time-dependent system (2.1) or the eigenvalue problem

$$\mathbf{curl} \operatorname{curl} \boldsymbol{E} = \lambda \boldsymbol{E}$$

as it has been evidenced by several authors, see e.g. [106, 27, 93, 16, 135, 17].

To describe this structure we will borrow some notations to the finite element exterior calculus, see [25, 27, 93, 2, 3, 94]. Letting

$$W^0 = L^2(\Omega), \qquad W^1 = L^2(\Omega)^2, \qquad W^2 = L^2(\Omega), \qquad W^3 = \mathbb{R}, \tag{2.2}$$

we introduce operators d^l, $l \in \{0,1,2\}$, with domains $V^l \subset W^l$ and values in W^{l+1}, as follows

$$V^0 = H_0^1(\Omega) \xrightarrow{d^0 = -\mathbf{grad}} V^1 = H_0(\operatorname{curl};\Omega) \xrightarrow{d^1 = \operatorname{curl}} V^2 = L^2(\Omega) \xrightarrow{d^2 = \fint_\Omega} V^3 = \mathbb{R} \tag{2.3}$$

where $\fint_\Omega = |\Omega|^{-1}\int_\Omega$. Here we assume that Ω is a bounded and simply-connected Lipschitz domain, so that the sequence is exact, in the sense that the image of each operator coincides with the kernel of the next operator in the sequence, see e.g. [140, Rem. 3.17]. The adjoint operators $(d^l)^*$ have domains denoted $V^*_{l+1} \subset W^{l+1}$ and values in W^l, they read

$$V_3^* = \mathbb{R} \xrightarrow{(d^2)^* = \iota} V_2^* = H(\mathbf{curl};\Omega) \xrightarrow{(d^1)^* = \mathbf{curl}} V_1^* = H(\operatorname{div};\Omega) \xrightarrow{(d^0)^* = \operatorname{div}} V_0^* = L^2(\Omega) \tag{2.4}$$

where ι is the canonical injection $\mathbb{R} \to L^2(\Omega)$. This sequence is also exact [140, Cor. 3.16]. Following [1, 57] we may use a "composite" operator to represent the combined action of the two curls,

$$\mathcal{A} := c\begin{pmatrix} 0 & -d^1 \\ (d^1)^* & 0 \end{pmatrix} = c\begin{pmatrix} 0 & -\operatorname{curl} \\ \mathbf{curl} & 0 \end{pmatrix}. \tag{2.5}$$

It is an unbounded operator from $\mathcal{W} := W^2 \times W^1$ into itself, defined on $\mathcal{V} := D(\mathcal{A}) = V_2^* \times V^1$, i.e., $\mathcal{V} = H(\mathbf{curl};\Omega) \times H_0(\operatorname{curl};\Omega)$. Equipped with metallic boundary conditions $\boldsymbol{E} \times \boldsymbol{n} = 0$ on $\partial\Omega$, the Maxwell system (2.1) then rewrites as

$$\partial_t U - \mathcal{A}U = -F \tag{2.6}$$

with $U = (cB, \boldsymbol{E})^T$ and $F = (0, \varepsilon_0^{-1}\boldsymbol{J})^T$. The well-posedness of this equation follows from standard arguments: $\mathcal{A}$ being skew-symmetric in the sense where $\mathcal{A}^* = -\mathcal{A}$, it generates a contraction semi-group of class $\mathcal{C}_0$ [139, section IX.8] and the Cauchy problem (2.6) is studied using classical tools

[117]. For instance if $F \in \mathcal{C}^1([0,T];\mathcal{W})$, then (2.6) equipped with an initial data $U^0 \in \mathcal{V}$ has a unique solution $U \in \mathcal{C}^0([0,T[;\mathcal{V})$.

The full Maxwell system also involves Gauss laws, which follow by formally taking the divergence of the Ampère and Faraday equations (2.1) and can be seen as an admissibility criterion for the general solutions to (2.6). Thus, the electric Gauss law

$$\operatorname{div} \boldsymbol{E} = \frac{1}{\varepsilon_0}\rho \tag{2.7}$$

represents a condition to be satisfied between the $\boldsymbol{E}$ field and the charge density ρ. It actually is a condition on the initial data, since it holds at any time t if it holds at $t = 0$, and if the sources satisfy the "continuity" equation

$$\partial_t \rho + \operatorname{div} \boldsymbol{J} = 0$$

which expresses the fact that the current density $\boldsymbol{J}$ is the flux of the charge density ρ. A similar reasoning applies for the magnetic Gauss law, for which the sources are always zero in principle. In 3D the latter reads $\operatorname{div} \boldsymbol{B} = 0$, and in the 2D model considered here this relation degenerates into $⨍_\Omega B = \text{cst}$, according to the restricted sequence (2.3). Again we may write these laws in a "composite" form,

$$\mathcal{D}U = R \quad \text{with} \quad \mathcal{D} = \begin{pmatrix} d^2 & 0 \\ 0 & (d^0)^* \end{pmatrix} = \begin{pmatrix} ⨍_\Omega & 0 \\ 0 & \operatorname{div} \end{pmatrix} \tag{2.8}$$

and writing $R = (⨍_\Omega cB^0, \epsilon_0^{-1}\rho)^T$ the generalized charge density in this 2D model.

2.2 Conforming approximation with mixed finite elements

In the standard approach one chooses a conforming discretization $V_h^l \subset V^l$ of the primal sequence (2.3), on which discrete operators can be defined by a simple restriction $d_h^l = d^l|_{V_h^l}$. Several choices are possible with systematic constructions described in [92, 2]. A usual choice [106, 108] consists of taking, on a (geometrically) conforming triangulation $\mathcal{T}_h$ of Ω,

$$V_h^0 = \mathcal{L}_{p,0}(\Omega,\mathcal{T}_h) \xrightarrow{d_h^0 = -\,\mathbf{grad}\,|_{V_h^0}} V_h^1 = \mathcal{N}_{p-1,0}(\Omega,\mathcal{T}_h) \xrightarrow{d_h^1 = \operatorname{curl}|_{V_h^1}} V_h^2 = \mathbb{P}_{p-1}(\mathcal{T}_h) \tag{2.9}$$

where we have denoted

$$\mathbb{P}_{p-1}(\mathcal{T}_h) = \{v \in L^2(\Omega) : v|_T \in \mathbb{P}_{p-1}(T),\ T \in \mathcal{T}_h\} \tag{2.10}$$

the space of piecewise polynomials of maximal degree $p-1$ on $\mathcal{T}_h$,

$$\mathcal{N}_{p-1,0}(\Omega,\mathcal{T}_h) = \mathcal{N}_{p-1}(\mathcal{T}_h) \cap H_0(\operatorname{curl};\Omega) \quad \text{with} \quad \mathcal{N}_{p-1}(T) = \mathbb{P}_{p-1}(T)^2 + \binom{-y}{x}\mathbb{P}_{p-1}(T) \tag{2.11}$$

the (first-kind) Nédélec space equipped with homogeneous boundary conditions, and

$$\mathcal{L}_{p,0}(\Omega,\mathcal{T}_h) = \mathbb{P}_p(\mathcal{T}_h) \cap \mathcal{C}_0(\Omega) \tag{2.12}$$

the space of continuous ("Lagrange") finite elements with homogeneous Dirichlet boundary conditions.

The space (2.11) is associated with edge-based curl-conforming degrees of freedom which we shall not remind here (for this we refer to [18] or ⟦52⟧ for instance) but are designed to enforce the continuity of the tangential components of the discrete fields across the edges of the mesh. In two dimensions

these elements can be obtained by rotating the div-conforming Raviart-Thomas elements [119] by an angle of $\pi/2$, and their 3D extension has been proposed in [114]. These elements have been extensively studied, see e.g. [85, 18]. In particular, it is well known that the discrete sequence (2.9) is again exact, which is easily verified by a direct argument (⟦52⟧, Lemma 3.2) or derived from the fact that these spaces are a particular case of the general construction described in [2]. We may note that this framework has been extended to other conforming spaces such as spline finite elements in [36].

The mixed finite element approximation to (2.1) based on these conforming spaces then consists of computing $(B_h, \boldsymbol{E}_h) \in \mathcal{C}^0([0,T[; V_h^2 \times V_h^1)$, solution to

$$\begin{cases} \langle \partial_t B_h, \varphi\rangle + \langle \operatorname{curl} \boldsymbol{E}_h, \varphi\rangle = 0 & \varphi \in V_h^2 \subset L^2(\Omega) \\ \langle \partial_t \boldsymbol{E}_h, \boldsymbol{\varphi}\rangle - c^2 \langle B_h, \operatorname{curl} \boldsymbol{\varphi}\rangle = -\frac{1}{\varepsilon_0}\langle \boldsymbol{J}_h, \boldsymbol{\varphi}\rangle & \boldsymbol{\varphi} \in V_h^1 \subset H_0(\operatorname{curl};\Omega) \end{cases} \tag{2.13}$$

where $\langle\cdot,\cdot\rangle$ is the usual scalar product of $L^2(\Omega)$ and $\boldsymbol{J}_h \in \mathcal{C}^0([0,T]; V_h^1)$ represents an approximation of the source term $\boldsymbol{J}$. A common choice [106, 108, 103], ⟦48⟧ is to define this term by a simple L^2 projection in the discrete space V_h^1, i.e.

$$\langle \boldsymbol{J}_h, \boldsymbol{\varphi}\rangle = \langle \boldsymbol{J}, \boldsymbol{\varphi}\rangle, \qquad \boldsymbol{\varphi} \in V_h^1. \tag{2.14}$$

In Section 2.4 we will show that for the elements considered here, this choice satisfies a commuting diagram leading to a long time stability property, but this is not always the case.

By using the embedding $\operatorname{curl} V_h^1 \subset V_h^2$, we observe that the first equation holds in a strong sense,

$$\partial_t B_h + \operatorname{curl} \boldsymbol{E}_h = 0 \qquad (\text{in } V_h^2). \tag{2.15}$$

In particular, we see that in 3D this approach computes a B_h field which divergence remains zero as long as it is at initial time, with no need to compute it in a subspace of $H(\operatorname{div};\Omega)$.

We observe that equality (2.15) implies, by formal differentiation of the second equation in (2.13), that the approximate field satisfies

$$\langle \partial_t^2 \boldsymbol{E}_h, \boldsymbol{\varphi}\rangle + c^2 \langle \operatorname{curl} \boldsymbol{E}_h, \operatorname{curl} \boldsymbol{\varphi}\rangle = -\tfrac{1}{\varepsilon_0}\langle \partial_t \boldsymbol{J}_h, \boldsymbol{\varphi}\rangle \tag{2.16}$$

a formulation studied in the classical article [107].

Following the same principle it is possible to design a discrete model based on the dual sequence (2.4). This route is taken in several works [1, 106, 130] and we also have studied it in ⟦52⟧ for the 2D case and in ⟦54⟧ in the 3D setting. The boundary conditions are then discretized in a natural way (through the equations instead of the discrete spaces), and it is the Ampère equation (with an approximate current) that is satisfied in a strong sense by the discrete solutions.

An important quality of the mixed discretization is that, under some conditions on the involved spaces the evolution operator defined in (2.13),

$$\mathcal{A}_h := c \begin{pmatrix} 0 & -d_h^1 \\ (d_h^1)^* & 0 \end{pmatrix} = c \begin{pmatrix} 0 & -\operatorname{curl}|_{V_h^1} \\ (\operatorname{curl}|_{V_h^1})^* & 0 \end{pmatrix} : \ (V_h^2 \times V_h^1) \ \to \ (V_h^2 \times V_h^1), \tag{2.17}$$

is *spectrally correct* in the sense that its eigenmodes provide a correct approximation of those of the exact operator $\mathcal{A}$ in the domain Ω. This type of properties has been studied for a long time by many authors, see for instance [26, 19, 22, 15, 110, 56], and we can remind a synthetic version presented in [3] under the assumptions that

- (H1) the intersection $V^1 \cap V_1^*$ is dense and compact in W^1,

- (H2) there exists a sequence of projections $\pi_h^l : W^l \to V_h^l$ that are uniformly bounded in W^l and in V^l with respect to h, and for which the following diagram commutes

$$\begin{array}{ccccccc} V^0 & \xrightarrow{d^0} & V^1 & \xrightarrow{d^1} & V^2 & \xrightarrow{d^2} & V^3 \\ \downarrow{\scriptstyle \pi_h^0} & & \downarrow{\scriptstyle \pi_h^1} & & \downarrow{\scriptstyle \pi_h^2} & & \downarrow{\scriptstyle \pi_h^3} \\ V_h^0 & \xrightarrow{d^0} & V_h^1 & \xrightarrow{d^1} & V_h^2 & \xrightarrow{d^2} & V_h^3 \end{array} \tag{2.18}$$

  in the sense that $d^l \pi_h^l = \pi_h^{l+1} d^l$ for $l \in \{0, 1, 2\}$. Here we obviously set $V_h^3 = \mathbb{R}$.

We verify that these assumptions indeed hold: (H1) corresponds to the compact inclusion of $H_0(\mathrm{curl}; \Omega) \cap H(\mathrm{div}; \Omega)$ in $L^2(\Omega)^2$ which is inferred from [109, cor. 3.49] that establishes its 3D analog. Property (H2) can be derived from the general construction proposed in [60, cor. 6.3] for a family of discrete exact sequences described in [2], to which (2.9) belongs. We can then specify the approximation property by considering an operator G which represents the inverse of $\mathbf{curl}\,\mathrm{curl}$ on the space

$$X^1 := (\ker d^1)^\perp \cap V^1 = \{\boldsymbol{u} \in H_0(\mathrm{curl}; \Omega) : \mathrm{div}\, \boldsymbol{u} = 0\} \tag{2.19}$$

where the $\perp$ exponent denotes the L^2 orthogonal complement. Specifically, $G : L^2(\Omega)^2 \to X^1$ is defined by

$$\langle \mathrm{curl}\, G\boldsymbol{u}, \mathrm{curl}\, \boldsymbol{v} \rangle = \langle \boldsymbol{u}, \boldsymbol{v} \rangle, \qquad \boldsymbol{v} \in X^1. \tag{2.20}$$

It is a compact and self-adjoint operator from $L^2(\Omega)^2$ into itself, and as such it has a countable set of nonnegative eigenvalues which only accumulate at 0: thus we may write

$$0 < \lambda_1 \leq \lambda_2 \leq \cdots$$

the inverse of the positive eigenvalues, writing several times multiples eigenvalues. We denote by $(\boldsymbol{u}_i)_{i \geq 1}$ an orthonormal sequence of associated eigenvectors, and we call $\mathfrak{E}_i$ the space spanned by $\boldsymbol{u}_i$. Following [20] we then write $m(N)$ the dimension of the space generated by the first N *distinct* eigenvalues: this space, $\mathfrak{E}_1 + \cdots + \mathfrak{E}_{m(N)}$, does not depend on the choice of the $\boldsymbol{u}_i$'s. We then show that the nonzero eigenmodes of $\mathcal{A}$, of the form $-i\omega$ given its skew-symmetric nature, are in bijection with those of G: we have

$$\mathcal{A} \begin{pmatrix} cb \\ \boldsymbol{e} \end{pmatrix} = -i\omega \begin{pmatrix} cb \\ \boldsymbol{e} \end{pmatrix} \quad \Longleftrightarrow \quad \begin{cases} G\boldsymbol{e} = \left(\dfrac{\omega}{c}\right)^{-2} \boldsymbol{e} \\ b = \dfrac{1}{i\omega} \mathrm{curl}\, \boldsymbol{e}. \end{cases} \tag{2.21}$$

To characterize the eigenmodes of the conforming discretization (2.13), (2.17), we then approximate X^1 by the discrete space

$$X_h^1 := (\ker d_h^1)^\perp \cap V_h^1 = \{\boldsymbol{u} \in V_h^1 : \langle \boldsymbol{u}, \mathbf{grad}\, \varphi \rangle = 0, \varphi \in V_h^0\}, \tag{2.22}$$

and we consider $G_h : L^2(\Omega)^2 \to X_h^1$ defined by

$$\langle \mathrm{curl}\, G_h \boldsymbol{u}, \mathrm{curl}\, \boldsymbol{v} \rangle = \langle \boldsymbol{u}, \boldsymbol{v} \rangle, \qquad \boldsymbol{v} \in X_h^1. \tag{2.23}$$

Again it is a compact and self-adjoint operator from $L^2(\Omega)^2$ into itself, and we can order the inverse of the nonzero eigenvalues as

$$0 < \lambda_{1,h} \leq \lambda_{2,h} \leq \cdots$$

by writing again several times the multiple eigenvalues. As above, we denote by $(\boldsymbol{u}_{i,h})_{i\geq 1}$ an orthonormal sequence of associated eigenvectors, and we let $\mathfrak{E}_{i,h}$ be the space spanned by $\boldsymbol{u}_{i,h}$. Again these eigenmodes can be associated one-to-one with those of $\mathcal{A}_h$, via an equivalence identical to (2.21).

The analysis developed in [3] then allows to establish the convergence

$$\|G - G_h\|_{\mathcal{L}(L^2(\Omega)^2, L^2(\Omega)^2)} \to 0,$$

and the perturbation theory of linear operators guarantees that the approximate eigenmodes $(\lambda_{i,h}, \boldsymbol{u}_{i,h})_{i\geq 1}$ converge towards the exact ones $(\lambda_i, \boldsymbol{u}_i)_{i\geq 1}$ in the sense of Definition 2.1 in [16]: for all $\varepsilon > 0$ and all $N \geq 1$, there exists $h_0 > 0$ such that for all $h \leq h_0$ we have

$$\max_{1\leq i\leq m(N)} |\lambda_i - \lambda_{i,h}| \leq \varepsilon \qquad \text{and} \qquad \operatorname{gap}\left(\sum_{1=i}^{m(N)} \mathfrak{E}_i, \sum_{1=i}^{m(N)} \mathfrak{E}_{i,h}\right) \leq \varepsilon, \tag{2.24}$$

the gap between the two spaces being classically defined as

$$\operatorname{gap}(\mathfrak{E}, \mathfrak{F}) := \max\left(\sup_{\substack{u\in\mathfrak{E}\\ \|u\|\leq 1}} \inf_{v\in\mathfrak{F}} \|u - v\|, \sup_{\substack{v\in\mathfrak{F}\\ \|v\|\leq 1}} \inf_{u\in\mathfrak{E}} \|u - v\|\right). \tag{2.25}$$

2.3 Conga (conforming/nonconforming Galerkin) discretization

An objective that we had set for ourselves was to extend approximations of the form (2.13) to *fully discontinuous* finite element spaces while preserving most of the above properties, namely:

(i) in the 3D version, the ability to compute an exactly divergence-free B_h field, without computing it in a div-conforming discrete space,
(ii) the spectral correctness of the discrete evolution operator $\mathcal{A}_h$ without adding dissipative terms,
(iii) high order error estimates that are stable over long time ranges.

(2.26)

Because it may double the number of degrees of freedom on the mesh interfaces, the use of fully discontinuous spaces increases the size of the discrete problems (and often makes the preconditioning more difficult, see e.g. [31, 32]) but it also has several advantages. First, it can provide better (non-oscillating) approximations when the exact solutions themselves are known to be discontinuous across some given interface. Second, it improves the locality of the computations which is a need in parallel codes to reduce the time-consuming interprocessor communications. When a time-dependent problem such as (2.1) is solved with an explicit time scheme, the mass matrices must be inverted at each time step. In a conforming method like (2.13), the basis functions of V_h^1 are generally supported in more than one cell and the inversion is thus a nonlocal operation, which may induce costly computations (e.g. on 3D unstructured meshes). Several authors have investigated mass lumping techniques to alleviate this burden, however no clear solution has been offered yet for general meshes. With fully discontinuous spaces the mass matrices are block diagonal which makes the inversion purely local, if not trivial.

The common approach with such spaces consists of using discontinuous Galerkin methods (see e.g. [80, 96]) which unfortunately, do not possess the desired properties: to be spectrally correct they seem to require dissipative terms [89, 134, 35, 29] and the long time stability of the problem with sources requires to correct the fields using *divergence cleaning* techniques, which amount to solve additional parabolic or hyperbolic equations, see for instance [112, 97, 129].

For this reason we have proposed a discretization in which the nonconforming spaces are incorporated in such a way that the geometric structure of the conforming approximation (2.13) is preserved. The resulting method has been named Conga in [[54]], for "COnforming/Nonconforming GAlerkin".

The basic idea is to start from a reference conforming formulation and relax the interelement continuity constraints of the discrete spaces to use only fully discontinuous elements. Since V_h^2 is already discontinuous, we only need one new space $\tilde{V}_h^1 \not\subset H_0(\mathrm{curl};\Omega)$, and it will be convenient to assume that it satisfies

$$V_h^1 \subset \tilde{V}_h^1 \not\subset V^1.$$

In the framework of (2.9), it appears in our analysis that the natural choice is to consider a broken Nédélec space

$$\tilde{V}_h^1 := \mathcal{N}_{p-1}(\mathcal{T}_h) = \{\boldsymbol{u} \in L^2(\Omega)^2 : \boldsymbol{u}|_T \in \mathcal{N}_{p-1}(T),\ T \in \mathcal{T}_h\}. \tag{2.27}$$

We note that it is also possible to use for $\tilde{V}_h^1$ a space of standard piecewise polynomials such as $\mathbb{P}_{p-1}(\mathcal{T}_h)^2$, and in this case the reference conforming sequence should involve the second-kind Nédélec space [115] for V_h^1, see [[53]], Rem. 4.5.

The second ingredient is a bounded projection on the conforming space,

$$\mathcal{P}_h^1 : L^2(\Omega)^2 \to V_h^1 \subset \tilde{V}_h^1, \qquad (\mathcal{P}_h^1)^2 = \mathcal{P}_h^1, \tag{2.28}$$

which will allow a natural extension of the method to discontinuous spaces. We ask that this projection preserves the first $m \geq 1$ moments on each cell,

$$\langle (\mathcal{P}_h^1 - I)\boldsymbol{u}, \boldsymbol{v}\rangle = 0, \qquad \boldsymbol{u} \in L^2(\Omega)^2, \quad \boldsymbol{v} \in \mathbb{P}_{m-1}(\mathcal{T}_h)^2,$$

so that the adjoint operator approximates the identity

$$(\mathcal{P}_h^1)^* \boldsymbol{u} \to \boldsymbol{u}, \qquad h \to 0, \tag{2.29}$$

for all $\boldsymbol{u} \in L^2(\Omega)^2$. Since the discontinuous space $\tilde{V}_h^1$ is obtained by restricting the conforming basis functions of V_h^1 on the cells of $\mathcal{T}_h$, it is natural to define its degrees of freedom the same way, as the restriction of the conforming ones to the individual cells. A convenient projector is then obtained by averaging the broken degrees of freedom coming from adjacent cells, and it will be stable in L^2 if the conforming degrees in V_h^1 are designed by integration against local polynomials, inferred from the local conforming basis by duality, as described in [77]. Applying $\mathcal{P}_h^1$ on $\tilde{V}_h^1$ is then a local procedure, and an almost trivial one. We refer to [[53]] for a detailed presentation.

The Conga approximation associated to (2.13) then consists of computing $(B_h, \boldsymbol{E}_h) \in \mathcal{C}^0([0,T]; V_h^2 \times \tilde{V}_h^1)$ solutions to

$$\begin{cases} \langle \partial_t B_h, \varphi\rangle + \langle \mathrm{curl}\, \mathcal{P}_h^1 \boldsymbol{E}_h, \varphi\rangle = 0 & \varphi \in V_h^2 \subset L^2(\Omega) \\ \langle \partial_t \boldsymbol{E}_h, \tilde{\boldsymbol{\varphi}}\rangle - c^2 \langle B_h, \mathrm{curl}\, \mathcal{P}_h^1 \tilde{\boldsymbol{\varphi}}\rangle = -\frac{1}{\varepsilon_0}\langle \boldsymbol{J}_h, \tilde{\boldsymbol{\varphi}}\rangle & \tilde{\boldsymbol{\varphi}} \in \tilde{V}_h^1 \not\subset H_0(\mathrm{curl};\Omega) \end{cases} \tag{2.30}$$

where $\boldsymbol{J}_h$ again denotes a discrete version (now in $\tilde{V}_h^1$) of the source term $\boldsymbol{J}$. By contrast to the conforming case, we will see that an L^2 projection *is not* a proper option to define $\boldsymbol{J}_h$ here, and should be replaced by an approximation operator involving the conforming projection $\mathcal{P}_h^1$.

The first objective listed in (2.26) readily follows from (2.30): using the embedding $\mathrm{curl}\, \mathcal{P}_h^1 \tilde{V}_h^1 \subset V_h^2$, we indeed see that the first equation holds again in strong sense in V_h^2,

$$\partial_t B_h + \mathrm{curl}\, \mathcal{P}_h^1 \boldsymbol{E}_h = 0. \tag{2.31}$$

In particular (and when it makes sense, e.g. in 3D), the discrete B_h field will be exactly divergence free as long as it is initially.

And as in the conforming case, we observe that by differentiating in time the second equation in (2.30) and using (2.31) we find

$$\langle \partial_t^2 \boldsymbol{E}_h, \tilde{\boldsymbol{\varphi}} \rangle + c^2 \langle \operatorname{curl} \mathcal{P}_h^1 \boldsymbol{E}_h, \operatorname{curl} \mathcal{P}_h^1 \tilde{\boldsymbol{\varphi}} \rangle = -\tfrac{1}{\varepsilon_0} \langle \partial_t \boldsymbol{J}_h, \tilde{\boldsymbol{\varphi}} \rangle \tag{2.32}$$

a new formulation that we can compare with (2.16).

Following the same path than for the conforming discretization, it is also possible to establish the second property listed in (2.26), namely that the Conga evolution operator

$$\tilde{\mathcal{A}}_h := c \begin{pmatrix} 0 & -d_h^1 \mathcal{P}_h^1 \\ (d_h^1 \mathcal{P}_h^1)^* & 0 \end{pmatrix} = c \begin{pmatrix} 0 & -\operatorname{curl} \mathcal{P}_h^1|_{\tilde{V}_h^1} \\ (\operatorname{curl} \mathcal{P}_h^1|_{\tilde{V}_h^1})^* & 0 \end{pmatrix} : \ (V_h^2 \times \tilde{V}_h^1) \ \to \ (V_h^2 \times \tilde{V}_h^1) \tag{2.33}$$

is spectrally correct. As before we begin by specifying an appropriate discretization of the space X^1, (2.19), which relies on the identification of a new exact sequence involving the nonconforming space $\tilde{V}_h^1$. By using the properties of the conforming exact sequence (2.9) and those of the conforming projection (2.28), we easily verify the key identity

$$\ker(d_h^1 \mathcal{P}_h^1|_{\tilde{V}_h^1}) = \ker d_h^1 \oplus \ker(\mathcal{P}_h^1|_{\tilde{V}_h^1}) = d_h^0 V_h^0 \oplus (I - \mathcal{P}_h^1) \tilde{V}_h^1, \tag{2.34}$$

from which we infer that the following sequence, although *nonconforming*, is again exact ⟦42⟧

$$\tilde{V}_h^0 := V_h^0 \times \tilde{V}_h^1 \ \xrightarrow{\tilde{d}_h^0} \ \tilde{V}_h^1 \ \xrightarrow{\tilde{d}_h^1 = d_h^1 \mathcal{P}_h^1|_{V_h^1}} \ V_h^2. \tag{2.35}$$

Here $\tilde{V}_h^0$ plays the role of a new discretization for the space V^0 (here H_0^1), that can be said nonconforming in the sense that $\tilde{V}_h^0 \not\subset V^0$. We note that it involves continuous finite elements, however none of them will appear in the resulting computations. The corresponding discretization for the operator d^0 (here the gradient), induced by (2.34), is defined as

$$\tilde{d}_h^0 : \tilde{V}_h^0 \ni (\varphi, \tilde{\boldsymbol{v}}) \mapsto d_h^0 \varphi + (I - \mathcal{P}_h^1) \tilde{\boldsymbol{v}}. \tag{2.36}$$

i.e., $\tilde{d}_h^0(\varphi, \tilde{\boldsymbol{v}}) = \mathbf{grad}\, \varphi + (I - \mathcal{P}_h^1) \tilde{\boldsymbol{v}}$. We then approximate the space $X^1 = (\ker d^1)^\perp \cap V^1$ with

$$\tilde{X}_h^1 := (\ker d_h^1 \mathcal{P}_h^1)^\perp \cap \tilde{V}_h^1 = \{ \tilde{\boldsymbol{u}} \in \tilde{V}_h^1 : \langle \tilde{\boldsymbol{u}}, \mathbf{grad}\, \varphi \rangle + \langle \tilde{\boldsymbol{u}}, (I - \mathcal{P}_h^1) \tilde{\boldsymbol{v}} \rangle = 0, \, \varphi \in V_h^0, \, \tilde{\boldsymbol{v}} \in \tilde{V}_h^1 \}, \tag{2.37}$$

and the nonconforming discretization of the eigenvalue problem (2.20) takes the form of an operator $\tilde{G}_h : L^2(\Omega)^2 \to \tilde{X}_h^1$, defined by

$$\langle \operatorname{curl} \mathcal{P}_h^1 \tilde{G}_h \boldsymbol{u}, \operatorname{curl} \mathcal{P}_h^1 \boldsymbol{v} \rangle = \langle \boldsymbol{u}, \boldsymbol{v} \rangle, \qquad \boldsymbol{v} \in \tilde{X}_h^1. \tag{2.38}$$

Again this is a compact and self-adjoint operator from $L^2(\Omega)^2$ in itself, and we denote the inverse of its nonzero eigenvalues by

$$0 < \tilde{\lambda}_{1,h} \leq \tilde{\lambda}_{2,h} \leq \cdots$$

with a repetition of the multiple eigenvalues. We let $(\tilde{\boldsymbol{u}}_{i,h})_{i \geq 1}$ denote an orthonormal sequence of associated eigenvectors, and $\tilde{\mathfrak{E}}_{i,h}$ the space spanned by $\tilde{\boldsymbol{u}}_{i,h}$. These eigenmodes can be put in bijection with those of $\tilde{\mathcal{A}}_h$ using a characterization similar to (2.21). By using the properties (2.28)-(2.29) of the projection $\mathcal{P}_h^1$ and the relations of the discrete exact sequences, we then prove the following result.

Theorem 2.1 ([54]) *The nonconforming (Conga) approximation $\tilde{G}_h$ of the inverse of* **curl** curl *defined by* (2.38) *can be expressed as a function of its conforming analog* (2.23)*, as*

$$\tilde{G}_h = P_{\tilde{X}_h^1} G_h P_{\tilde{X}_h^1}$$

where $P_{\tilde{X}_h^1}$ is the L^2 projection in the discontinuous space (2.37)*. Moreover this operator converges towards the exact inverse* (2.20)*,*

$$\|G - \tilde{G}_h\|_{\mathcal{L}(L^2(\Omega)^2, L^2(\Omega)^2)} \to 0, \qquad h \to 0.$$

In particular, the discrete eigenmodes $(\tilde{\lambda}_{i,h}, \tilde{\boldsymbol{u}}_{i,h})_{i\geq 1}$ of the Conga operators $\tilde{G}_h$ and $\tilde{\mathcal{A}}_h$ converge towards the exact modes $(\lambda_i, \boldsymbol{u}_i)_{i\geq 1}$ in the sense of (2.24)*.*

In $\mathbb{R}^2$, we have shown [53] that the Conga operator (2.33) coincides with the standard DG discretization with centered fluxes (without penalty terms), which spectral correctness has been studied and numerically verified in [89] but not formally proven, up to our knowledge. In the 3D case the Conga discretization differs from the DG ones, which are known to be not spectrally correct [89, 134] unless penalty terms are introduced for the jumps (as demonstrated in [35, 34]) or interface conditions are imposed in the solutions [29], which would forbid the use of fully discontinuous functions. In this direction we can cite the work [91] where it is proven that such interface conditions are necessary for the approximation of an elliptic problem (a Poisson equation) in mixed form, when the scheme does involve ant coupling of the adjacent cells through its discrete operators. In a sense, the Conga discretization thus allows to realize such a coupling without penalization.

We note that spectral correctness is an essential ingredient for the performances of the associated evolution problem. This is rather clear since some spurious (resp. correct) modes could (resp. could not) propagate with a spectrally incorrect operator, and this has been specified with a priori uniform error estimates in [21]. The absence of penalty terms is an advantage in the treatment of evolution problems, where it amounts to an absence of numerical dissipation which in turn offers better conservation properties.

2.4 Abstract criteria for the compatible approximation of the sources

The long time stability of the numerical methods for the Maxwell system (2.1) is connected to their conservation properties regarding the divergence constraints. Indeed we have seen that at the continuous level, the Gauss laws were preserved by the Ampère and Faraday equations, which is easily verified by taking the divergence of the latter. When the numerical methods do not preserve this principle, which is often the case with DG schemes, they are likely to develop long time instabilities by accumulation of small errors [129] *even when their convergence as $h \to 0$ is established with high order*. To avoid such instabilities, the usual approach is to introduce dissipative terms [88, 89] or to correct the fields using approximate resolutions of the Gauss laws first introduced for finite difference schemes [24, 105, 104] and then generalized to other methods under the form of elliptic, parabolic or hyperbolic correction schemes [111, 96, 9, 61], see also [51] for a recent review on such techniques.

Here we propose to specify some compatibility relations that the numerical sources should satisfy in order to remove these instabilities, without resorting to numerical dissipation or field correction techniques. As we will see, these compatibility criteria are naturally verified by conforming mixed formulations, and for nonconforming Conga discretizations they can implemented using simple and local operations.

The principle of compatible discretizations is to preserve the relations that guarantee the exact conservation of the Gauss laws. Here we have in mind the fundamental identity div **curl** $= 0$, but we

will see that the latter first needs to be properly expressed in a given discrete setting, since it only makes sense as one ingredient in a whole system. To specify this we consider a space discretization of the Maxwell equations (2.1), of the form

$$\begin{cases} \partial_t B_h + \operatorname{curl}_h \boldsymbol{E}_h = 0 \\ \partial_t \boldsymbol{E}_h - c^2 \, \mathbf{curl}_h \, B_h = -\dfrac{1}{\varepsilon_0} \boldsymbol{J}_h. \end{cases} \tag{2.39}$$

To reproduce the identity $\operatorname{div} \mathbf{curl} = 0$ in this setting consists of identifying a discrete divergence operator div_h such that

$$\operatorname{div}_h \mathbf{curl}_h = 0. \tag{2.40}$$

It is then clear that system (2.39) will preserve a discrete Gauss law of the form

$$\operatorname{div}_h \boldsymbol{E}_h = \frac{1}{\varepsilon_0} \rho_h \tag{2.41}$$

as long as the discrete sources satisfy the associated continuity equation

$$\partial_t \rho_h + \operatorname{div}_h \boldsymbol{J}_h = 0, \tag{2.42}$$

and a similar reasoning applies to the magnetic Gauss law. It is not clear, however, whether (2.41) is strong enough to guarantee the long time stability of the discrete solutions. For that purpose it is necessary that (2.41) allows to characterize the "discrete irrotational" part of the electric field, i.e., the fields in $\ker \operatorname{curl}_h$, indeed their temporal growth is not controlled by the evolution equation (2.39). Equation (2.42) may then be used as a practical criterion to identify the source approximation operators that are *compatible* with the discretization (2.39). We then decompose the last objective in our list (2.26) as follows.

(iii-a) in an abstract setting, identify which properties of the discrete differential operators and of the source approximation operators guarantee a long time stability,

(iii-b) for several schemes (conforming or not), identify source approximation operators that meet these criteria,

(iii-c) study the numerical implementation of the resulting schemes in the case where the sources are provided by a particle solver.

(2.43)

In the particular case where the exact sources are given, it is possible to realize a simplified version of this program which does not involve a discrete divergence. To this end, one uses the exact sequence (2.4) and a standard property of adjoint operators, see [30, Cor. 2.18], to write that $\ker(d^0)^* = (\operatorname{Im} d^0)^\perp = (d^0 V^0)^\perp = (\ker d^1)^\perp$, where the $\perp$ exponent denotes the orthogonal complement in the natural L^2 space W^l. It follows that

$$\ker \mathcal{D} = \mathbb{R}^\perp \times \ker(d^0)^* = (\ker(d^1)^*)^\perp \times (\ker d^1)^\perp = (\ker \mathcal{A})^\perp. \tag{2.44}$$

Thus, in the absence of sources we see that the Gauss law (2.8) constrains the general solutions to the evolution equation (2.6) to be orthogonal to the irrotational fields, which corresponds to the genuinely oscillating modes of the operator $\mathcal{A}$. According to its skew-symmetric nature we can indeed decompose the full L^2 space $\mathcal{W} = W^2 \times W^1$ as

$$\mathcal{W} = \ker \mathcal{A} \ \oplus \ (\ker \mathcal{A})^\perp \quad \text{with} \quad \begin{cases} \ker \mathcal{A} = \{U \in \mathcal{S} : \partial_t U = 0\} \\ (\ker \mathcal{A})^\perp = \operatorname{Span}(\{U \in \mathcal{S} : \partial_t U = -i\omega U, \omega \neq 0\}) \end{cases} \tag{2.45}$$

where $\mathcal{S}$ denotes the set of solutions to the homogeneous Ampère-Faraday system (2.6).

If the exact source is given we may then consider semi-discrete schemes for (2.6) of the form

$$\partial_t U_h - \mathcal{A}_h U_h = -\Pi_h F \tag{2.46}$$

where $\mathcal{A}_h : \mathcal{V}_h \to \mathcal{V}_h$ is a skew-symmetric operator that approximates $\mathcal{A}$ on a discrete space $\mathcal{V}_h \subset \mathcal{W}$, which may correspond to either (2.17) or (2.33), and Π_h is an approximation operator on $\mathcal{V}_h$ that converges to the identity as $h \to 0$.

In ⟦54⟧ we have proposed a criterion to identify schemes of the form (2.46) that are compatible with the orthogonal constraint expressed by the Gauss laws, without explicitly involving the discrete version of those laws. In the absence of sources, this constraint reads $U \in (\ker \mathcal{A})^\perp$ and a discrete analog is $U_h \in (\ker \mathcal{A}_h)^\perp$, which again can be interpreted as the absence of stationary modes relative to $\mathcal{A}_h$, following a decomposition similar to (2.45) for this skew-symmetric operator. In the presence of sources, a natural extension of that constraint is to ask that, when the exact solution contains no stationary modes for $\mathcal{A}$, then the approximate solution contains no stationary modes for $\mathcal{A}_h$. We observe that such a requirement will be met as long as the operator Π_h satisfies

$$Z \in (\ker \mathcal{A})^\perp \quad \Longrightarrow \quad \Pi_h Z \in (\ker \mathcal{A}_h)^\perp$$

or equivalently, $\mathcal{A}$ being skew-symmetric, closed and with dense domain, as long as $\Pi_h(\operatorname{Im} \mathcal{A}) \subset \operatorname{Im} \mathcal{A}_h$. This property essentially amounts to a commuting diagram.

Definition 2.1 (⟦54⟧) *The semi-discrete scheme* (2.46) *is called* **Gauss-compatible** *on a space* $\hat{\mathcal{V}} \subset \mathcal{V}$ *if there exists an auxiliary approximation operator* $\hat{\Pi}_h : \hat{\mathcal{V}} \to \mathcal{V}_h$ *which converges pointwise to the identity as* $h \to 0$*, and such that*

$$\Pi_h \mathcal{A} = \mathcal{A}_h \hat{\Pi}_h \qquad \text{on} \quad \hat{\mathcal{V}}, \tag{2.47}$$

where $\mathcal{A}$ *is the exact evolution operator* (2.5)*.*

Here $\hat{\mathcal{V}}$ typically represents the regularity required for the definition of the approximation operators. Relation (2.47) indeed corresponds to a commuting diagram,

$$\begin{array}{ccc} \hat{\mathcal{V}} & \xrightarrow{\quad\mathcal{A}\quad} & \mathcal{A}\hat{\mathcal{V}} \\ {\scriptstyle \hat{\Pi}_h}\downarrow & & \downarrow{\scriptstyle \Pi_h} \\ \mathcal{V}_h & \xrightarrow{\quad\mathcal{A}_h\quad} & \mathcal{V}_h \end{array} \tag{2.48}$$

and it easily leads to a priori error and long time stability estimates.

Theorem 2.2 (⟦54⟧, Th. 3.2) *If the semi-discrete scheme* (2.46) *is Gauss-compatible on some space* $\hat{\mathcal{V}}$*, then the approximate solution satisfies*

$$\|(U_h - \hat{\Pi}_h U)(t)\| \le \|(U_h - \hat{\Pi}_h U)(0)\| + \int_0^t \|(\Pi_h - \hat{\Pi}_h)\partial_t U(s)\| \, \mathrm{d}s \tag{2.49}$$

for any exact solution $U \in \mathcal{C}^0([0,T];\hat{\mathcal{V}})$ *of the time-dependent Maxwell equations* (2.6)*.*

Proof. The argument is only a few lines and can be given here. By applying Π_h to the Maxwell system (2.6) and using the commuting diagram (2.47), we obtain

$$\partial_t \Pi_h U - \mathcal{A}_h \hat{\Pi}_h U = \Pi_h(\partial_t U - \mathcal{A}U) = -\Pi_h F = \partial_t U_h - \mathcal{A}_h U_h,$$

so that $\hat{\Pi}_h U - U_h$ is the solution of an evolution equation with source term $(\hat{\Pi}_h - \Pi_h)\partial_t U$,

$$\partial_t(\hat{\Pi}_h U - U_h) - \mathcal{A}_h(\hat{\Pi}_h U - U_h) = (\hat{\Pi}_h - \Pi_h)\partial_t U.$$

The estimate (2.49) is then inferred from the contraction properties of the semi-group generated by $\mathcal{A}_h$. ∎

The following long time stability result is a straightforward consequence of the above estimate.

Corollary 2.2 (long time stability) *If $\bar{U} = \bar{U}(0) \in \hat{\mathcal{V}}$ is a steady state solution to* (2.6)*, then $U_h := \hat{\Pi}_h \bar{U}$ is a steady state solution to* (2.46)*. Moreover, the estimate*

$$\|(U_h - \hat{\Pi}_h \bar{U})(t)\| \leq \|(U_h - \hat{\Pi}_h \bar{U})(0)\|, \qquad t \geq 0$$

is valid for any *initial data $U_h(0) \in \mathcal{V}_h$.*

In the general case where we are only given an approximate source F_h we must consider semi-discrete schemes of the form

$$\partial_t U_h - \mathcal{A}_h U_h = -F_h. \tag{2.50}$$

Since the previous approach no longer applies we must go back to the announced program, which consists of identifying sufficient conditions under which a discrete Gauss law (2.41) allows to control the temporal growth of the field E_h. For this we introduce the following definition, in which the discrete spaces V_h^l are not necessarily those from the sequence (2.9), nor even subspaces of the V^ls in (2.3).

Definition 2.3 ([52], Def. 2.7 and 2.9) *We say that a space discretization of the Maxwell equations* (2.1) *of the form*

$$\begin{cases} \partial_t B_h + \operatorname{curl}_h \boldsymbol{E}_h = 0 \\ \partial_t \boldsymbol{E}_h - c^2 \operatorname{\mathbf{curl}}_h B_h = -\dfrac{1}{\varepsilon_0} \boldsymbol{J}_h \end{cases} \quad \textit{with} \quad \begin{cases} \operatorname{curl}_h : V_h^1 \to V_h^2 \\ \operatorname{\mathbf{curl}}_h = (\operatorname{curl}_h)^* : V_h^2 \to V_h^1 \end{cases} \tag{2.51}$$

(and with general spaces V_h^l that are not necessarily conforming) completed by discrete Gauss laws

$$\begin{cases} \operatorname{div}_h \boldsymbol{E}_h = \dfrac{1}{\varepsilon_0}\rho_h \\ \int_\Omega B_h = \int_\Omega B_h^0 \end{cases} \quad \textit{with} \quad \begin{cases} \operatorname{div}_h : V_h^1 \to V_h^0 \\ \int_\Omega : V_h^2 \to \mathbb{R} \end{cases} \tag{2.52}$$

is **structure-preserving** *if, letting $\operatorname{\mathbf{grad}}_h := -(\operatorname{div}_h)^* : V_h^0 \to V_h^1$, we have the following properties.*

- Exact sequence*: the sequence*

$$V_h^0 \xrightarrow{\operatorname{\mathbf{grad}}_h} V_h^1 \xrightarrow{\operatorname{curl}_h} V_h^2 \xrightarrow{\int_\Omega} \mathbb{R} \tag{2.53}$$

  is exact in the sense that $\operatorname{\mathbf{grad}}_h V_h^0 = \ker \operatorname{curl}_h$ and $\operatorname{curl}_h V_h^1 = \ker(\int_\Omega|_{V_h^2})$.

- Stability*: the operators involved in* (2.53) *satisfy Poincaré-Friedrichs inequalities*

$$\begin{aligned} &\|u\| \le c_P \|\mathbf{grad}_h\, u\|, && u \in V_h^0 \cap (\ker \mathbf{grad}_h)^\perp \\ &\|\boldsymbol{u}\| \le c_P \|\mathrm{curl}_h\, \boldsymbol{u}\|, && \boldsymbol{u} \in V_h^1 \cap (\ker \mathrm{curl}_h)^\perp \\ &\|u\| \le c_P \|⨍_\Omega u\|, && u \in V_h^2 \cap (\ker ⨍_\Omega)^\perp \end{aligned} \tag{2.54}$$

with a constant c_P independent of h.

Again we note that the presence of the canonical injection $\iota : \mathbb{R} \to L^2(\Omega)$ and its adjoint $⨍_\Omega$ is due to the degenerate form of the magnetic Gauss law in this 2D model. In 3D these operators should be replaced by a discrete gradient and a discrete divergence defined as its adjoint, differing a priori from those already involved in the above definition.

We also observe that properties (2.53)-(2.54) are equivalently expressed on the dual sequence

$$\mathbb{R} \xrightarrow{\ \iota\ } V_h^2 \xrightarrow{\ \mathbf{curl}_h\ } V_h^1 \xrightarrow{\ \mathrm{div}_h\ } V_h^0.$$

As for the structure underlying Definition 2.3, it may be clearer when these properties are formulated on the composite operators

$$\mathcal{A}_h = c \begin{pmatrix} 0 & -\mathrm{curl}_h \\ \mathbf{curl}_h & 0 \end{pmatrix} \qquad \text{and} \qquad \mathcal{D}_h = \begin{pmatrix} ⨍_\Omega & 0 \\ 0 & \mathrm{div}_h \end{pmatrix}.$$

Then the exact sequence property (2.53) amounts to the orthogonality of the kernels, $\ker \mathcal{D}_h = (\ker \mathcal{A}_h)^\perp$, and the uniform estimates (2.54) amount to the stability of the composite operators,

$$\|Z\| \le c_P \|\mathcal{D}_h Z\|, \quad Z \in (\ker \mathcal{D}_h)^\perp \qquad \text{and} \qquad \|Z\| \le c_P \|\mathcal{A}_h Z\|, \quad Z \in (\ker \mathcal{A}_h)^\perp.$$

As will be verified soon (and may be clear already from the latter form) the above definition provides a convenient framework for long-time stability estimates. The corresponding discrete continuity equation (2.42) can then be used as a practical criterion for the approximate source. Following the usual terminology [132], we introduce another definition.

Definition 2.4 (⟦52⟧, Def. 2.12) *We say that a space discretization of the Maxwell equations* (2.1) *of the form* (2.51)-(2.52) *is* **charge-conserving** *if it is structure-preserving in the sense of Definition 2.3 and if the approximate source verifies the associated continuity equation,*

$$\partial_t \rho_h + \mathrm{div}_h\, \boldsymbol{J}_h = 0. \tag{2.55}$$

We are then in position to state two estimates: under the sole assumption that a scheme is charge-conserving, which corresponds to Definition 2.4 (which includes the structure-preserving property), we have a *long time stability result*, see ⟦52⟧, Th. 2.14. Under an additional commuting diagram assumption, we also have an error estimate involving the accuracy of the approximate source.

Theorem 2.3 (⟦52⟧, Th. 2.15) *If the semi-discrete scheme* (2.51)-(2.52) *is charge-conserving in the sense of Definition 2.4 and if the associated evolution operator $\mathcal{A}_h$ satisfies a commuting diagram relation* (2.47) *for approximation operators Π_h and $\hat{\Pi}_h$, then the solution $U_h = (cB_h, \boldsymbol{E}_h)^T$ of* (2.51) *satisfies the discrete Gauss laws* (2.52) *and the a priori estimate*

$$\begin{aligned} \|(U_h - \Pi_h U)(t)\| \le c_P \Big(&\|\mathcal{A}_h(U_h^0 - \hat{\Pi}_h U^0)\| + \|F_h^0 - \Pi_h F^0\| + \|(R_h - \mathcal{D}_h \Pi_h U)(t)\| + \|(F_h - \Pi_h F)(t)\| \\ &+ \|\big(\mathcal{A}_h(\Pi_h - \hat{\Pi}_h)U(t)\| + \int_0^t \|\partial_t \big(\mathcal{A}_h(\Pi_h - \hat{\Pi}_h)U + (F_h - \Pi_h F)\big)(s)\|\, \mathrm{d}s \Big) \end{aligned}$$

with $R_h = (c⨍_\Omega B_h^0, \varepsilon_0^{-1}\rho_h)^T$ and $F_h = (0, \varepsilon_0^{-1}\boldsymbol{J}_h)^T$. Here c_P is the constant from (2.54).

2.5 Application to the conforming and Conga discretizations

The following results show that the abstract framework developed in the previous section applies naturally to the mixed conforming and Conga formulations presented in the sections 2.2 and 2.3, up to a proper choice of the source approximation operator. Consistent with the above choice, we present some results in 2D, which mostly corresponds to those of the article ⟦53⟧. The 3D case is addressed in the article ⟦54⟧. We finally assume that the domain Ω has no reentrant corners, so that the exact solutions can be assumed smooth, at least in a first stage, see e.g. [4, 5].

Theorem 2.4 *The conforming discretization* (2.13) *associated with an orthogonal projection for the current source* $\boldsymbol{J}_h = P_{V_h^1}\boldsymbol{J}$*, characterized by* (2.14)*, is Gauss-compatible on the product space* $\hat{\mathcal{V}} = V_2^* \times (H^1(\Omega)^2 \cap V^1)$.

The complete statement of this theorem, given in ⟦53⟧, specifies the approximation operators involved in Definition 2.1. They write

$$\Pi_h = \begin{pmatrix} P_{V_h^2} & 0 \\ 0 & P_{V_h^1} \end{pmatrix} \qquad \text{and} \qquad \hat{\Pi}_h = \begin{pmatrix} P_{V_h^2} & 0 \\ 0 & \pi_h^{\mathrm{curl}} \end{pmatrix}$$

where π_h^{curl} denotes the canonical interpolation for the edge elements. The approximation properties of these operators allow us to derive an explicit form for the a priori error estimate (2.49), as

$$\begin{aligned}\|(B-B_h)(t)\| + \|(\boldsymbol{E}-\boldsymbol{E}_h)(t)\| \lesssim \|B_h(0) - P_{V_h^2}B(0)\| + \|\boldsymbol{E}_h(0) - \pi_h^{\mathrm{curl}}\boldsymbol{E}(0)\| \\ + h^m\Big(|B(0)|_m + \int_0^t |\partial_t B(s)|_m \,\mathrm{d}s\Big) + h^{m'}\Big(|\boldsymbol{E}(0)|_{m'} + \int_0^t |\partial_t \boldsymbol{E}(s)|_{m'} \,\mathrm{d}s\Big)\end{aligned}$$

for $0 \le m \le p$, $1 \le m' \le p$, and with a constant independent of h and t.

Theorem 2.5 *The Conga discretization* (2.30) *associated with a discontinuous approximate current* $\boldsymbol{J}_h \in \tilde{V}_h^1$ *defined by the relations*

$$\langle \boldsymbol{J}_h, \boldsymbol{\varphi}\rangle = \langle \boldsymbol{J}, \mathcal{P}_h^1\boldsymbol{\varphi}\rangle, \qquad \boldsymbol{\varphi} \in \tilde{V}_h^1, \tag{2.56}$$

i.e., $\boldsymbol{J}_h = (\mathcal{P}_h^1)^*\boldsymbol{J}$*, is Gauss-compatible on the product space* $\hat{\mathcal{V}} := V_2^* \times (H^1(\Omega)^2 \cap V^1)$.

We observe that computing the approximate current is *local* with the latter formula, as is the projection $\mathcal{P}_h^1$ and the inversion of the mass matrix in the space $\tilde{V}_h^1$. Again the complete statement of this theorem, given in ⟦53⟧, specifies the approximation operators involved in Definition 2.1. They write

$$\Pi_h = \begin{pmatrix} P_{V_h^2} & 0 \\ 0 & (\mathcal{P}_h^1)^* \end{pmatrix} \qquad \text{and} \qquad \hat{\Pi}_h = \begin{pmatrix} P_{V_h^2} & 0 \\ 0 & \pi_h^{\mathrm{curl}} \end{pmatrix}$$

where π_h^{curl} denotes again the canonical interpolation of the edge elements. Again the approximation properties of these operators allow us to derive an explicit form for the a priori error estimate (2.49), as

$$\begin{aligned}\|(B-B_h)(t)\| + \|(\boldsymbol{E}-\boldsymbol{E}_h)(t)\| \lesssim \|B_h(0) - P_{V_h^2}B(0)\| + \|\boldsymbol{E}_h(0) - \pi_h^{\mathrm{curl}}\boldsymbol{E}(0)\| \\ + h^m\Big(|B(0)|_m + \int_0^t |\partial_t B(s)|_m \,\mathrm{d}s\Big) + h^{m'}\Big(|\boldsymbol{E}(0)|_{m'} + \int_0^t (|\partial_t \boldsymbol{E}(s)|_{m'}) \,\mathrm{d}s\Big)\end{aligned}$$

for $0 \le m \le p$, $1 \le m' \le p-1$, and with a constant independent of h and t.

Our unified analysis allows us to recover known convergence orders for the conforming finite element schemes (see, e.g. [107]) and nonconforming as well ([80]). As for the long time stability results, they seem to be new for unpenalized nonconforming methods.

Lemma 2.5 *The conforming discretization* (2.13) *associated to the discrete Gauss laws* (2.52) *defined by*

$$(\mathrm{div}_h)^* := -\,\mathbf{grad} : V_h^0 \to V_h^1 \tag{2.57}$$

see (2.9)*, is structure-preserving in the sense of Definition 2.3.*

Lemma 2.6 *The Conga discretization* (2.30) *associated to the discrete Gauss laws* (2.52) *defined by*

$$\begin{cases} \mathbf{grad}_h : (V_h^0 \times \tilde{V}_h^1) \ni (\phi, \tilde{\boldsymbol{u}}) \mapsto \mathbf{grad}\,\phi + (I - \mathcal{P}_h^1)\tilde{\boldsymbol{u}} \in \tilde{V}_h^1 \\ \mathrm{div}_h := -(\mathbf{grad}_h)^* : \tilde{V}_h^1 \to (V_h^0 \times \tilde{V}_h^1) \end{cases} \tag{2.58}$$

see (2.9)*, is structure-preserving in the sense of Definition 2.3.*

We observe that with the operator (2.57) involved in the conforming case, the proper discrete Gauss law (2.52) takes a standard weak form in finite elements,

$$-\langle \boldsymbol{E}_h(t), \mathbf{grad}\,\phi\rangle = \frac{1}{\varepsilon_0}\langle \rho_h(t), \phi\rangle, \qquad \phi \in V_h^0. \tag{2.59}$$

It is less standard in the case of the Conga discretization: with (2.58), it takes the form

$$-\langle \boldsymbol{E}_h(t), \mathbf{grad}\,\phi + (I - \mathcal{P}_h^1)\tilde{\boldsymbol{u}}\rangle = \frac{1}{\varepsilon_0}\langle \rho_h(t), \phi\rangle \qquad (\phi, \tilde{\boldsymbol{u}}) \in V_h^0 \times \tilde{V}_h^1. \tag{2.60}$$

2.6 Application to the coupling with a particle method

We now consider the case where the sources are given by a particle method under the form of N (macro) particles with positions $\mathbf{x}_\kappa(t)$ and velocities $\mathbf{v}_\kappa(t) = \mathbf{x}'_\kappa(t)$, $\kappa = 1, \dots N$, pushed forward along some characteristic trajectories. By associating to each particle a charge q_κ and a shape function ζ_ε of scale $\varepsilon \ge 0$ (either the Dirac measure if $\varepsilon = 0$, or a smoothed version if $\varepsilon > 0$, see e.g. [96]), we define the corresponding charge and current densities as

$$\rho_N(t, \mathbf{x}) := \sum_{\kappa=1}^{N} q_\kappa \zeta_\varepsilon(\mathbf{x} - \mathbf{x}_\kappa(t)) \qquad \text{and} \qquad \boldsymbol{J}_N(t, \mathbf{x}) := \sum_{\kappa=1}^{N} q_\kappa \mathbf{v}_\kappa(t) \zeta_\varepsilon(\mathbf{x} - \mathbf{x}_\kappa(t)). \tag{2.61}$$

Since $\mathbf{v}_\kappa(t) = \mathbf{x}'_\kappa(t)$, we verify that these sources satisfy an exact continuity equation $\partial_t \rho_N + \mathrm{div}\,\boldsymbol{J}_N = 0$, valid in a measure's sense in the case of point particles.

Theorem 2.6 *Let $\varepsilon > 0$. The conforming* (2.13) *and Conga* (2.30) *discretizations associated with the discrete Gauss laws* (2.52) *defined by the respective operators* (2.57) *and* (2.58) *are charge-conserving in the sense of Definition 2.4 when the discrete sources are defined from* (2.61) *by*

$$\rho_h(t) := P_{V_h^0}\rho_N(t) \in V_h^0 \qquad \textit{and} \qquad \boldsymbol{J}_h(t) := P_{V_h^1}\boldsymbol{J}_N(t) \in V_h^1 \tag{2.62}$$

for the conforming discretization of (2.13)*, and*

$$\rho_h(t) := P_{V_h^0}\rho_N(t) \in V_h^0 \qquad \textit{and} \qquad \boldsymbol{J}_h(t) := (\mathcal{P}_h^1)^*\boldsymbol{J}_N(t) \in \tilde{V}_h^1 \tag{2.63}$$

for the Conga (discontinuous) discretization (2.30)*.*

Here $P_{V_h^0}$ and $P_{V_h^1}$ are the L^2 projections over the H^1 and $H(\mathrm{curl})$-conforming spaces, hence their application requires to solve a global system. By contrast, applying the approximation by $(\mathcal{P}_h^1)^*$ is local to each cell, just like it has been verified on (2.56).

In the article [[49]] we have proposed a high order implementation of similar operators applied to smooth particles, for discretizations of the dual sequence (2.4), and we have verified their numerical stability properties.

To extend these results to the case of point particles, it is convenient to consider a time discretization of the Maxwell solvers. Using an explicit leap-frog scheme for instance, the conforming method (2.13) computes fields $(B_h^{n+1/2}, \boldsymbol{E}_h^n) \in V_h^2 \times V_h^1$ according to

$$\begin{cases} B_h^{n+\frac{1}{2}} - B_h^{n-\frac{1}{2}} + \Delta t \,\mathrm{curl}\, \boldsymbol{E}_h^n = 0 & (\text{in } V_h^2) \\ \langle \boldsymbol{E}_h^{n+1} - \boldsymbol{E}_h^n, \boldsymbol{\varphi}\rangle - c^2 \Delta t \langle B_h^{n+\frac{1}{2}}, \mathrm{curl}\, \boldsymbol{\varphi}\rangle = -\frac{\Delta t}{\varepsilon_0} \langle \boldsymbol{J}_h^{n+\frac{1}{2}}, \boldsymbol{\varphi}\rangle & \boldsymbol{\varphi} \in V_h^1 \end{cases} \tag{2.64}$$

and the Conga method (2.30) computes $(B_h^{n+1/2}, \boldsymbol{E}_h^n) \in V_h^2 \times \tilde{V}_h^1$ according to

$$\begin{cases} B_h^{n+\frac{1}{2}} - B_h^{n-\frac{1}{2}} + \Delta t \,\mathrm{curl}\, \mathcal{P}_h^1 \boldsymbol{E}_h^n = 0 & (\text{in } V_h^2) \\ \langle \boldsymbol{E}_h^{n+1} - \boldsymbol{E}_h^n, \tilde{\boldsymbol{\varphi}}\rangle - c^2 \Delta t \langle B_h^{n+\frac{1}{2}}, \mathrm{curl}\, \mathcal{P}_h^1 \tilde{\boldsymbol{\varphi}}\rangle = -\frac{\Delta t}{\varepsilon_0} \langle \boldsymbol{J}_h^{n+\frac{1}{2}}, \tilde{\boldsymbol{\varphi}}\rangle & \tilde{\boldsymbol{\varphi}} \in \tilde{V}_h^1. \end{cases} \tag{2.65}$$

In [[48]] we have shown that a current $\boldsymbol{J}_h^{n+1/2}$ obtained by an orthogonal projection in the conforming space V_h^1 of the time average of the particle current,

$$\langle \boldsymbol{J}_h^{n+\frac{1}{2}}, \boldsymbol{\varphi}\rangle = \left\langle \int_{t^n}^{t^{n+1}} \boldsymbol{J}_N(\tau) \frac{\mathrm{d}\tau}{\Delta t}, \boldsymbol{\varphi} \right\rangle = \sum_{\kappa=1}^{N} q_\kappa \int_{t^n}^{t^{n+1}} \mathbf{v}_\kappa(\tau) \cdot \boldsymbol{\varphi}(\mathbf{x}_\kappa(\tau)) \frac{\mathrm{d}\tau}{\Delta t}, \qquad \boldsymbol{\varphi} \in V_h^1, \tag{2.66}$$

is well defined, and that it verifies the associated discrete continuity equation,

$$\langle \boldsymbol{J}_h^{n+\frac{1}{2}}, \mathbf{grad}\, \phi\rangle = \frac{1}{\varepsilon_0} \langle \frac{1}{\Delta t}(\rho_h^{n+1} - \rho_h^n), \phi\rangle, \qquad \phi \in V_h^0$$

where $\langle \rho_h^n, \phi\rangle = \langle \rho_N(t^n), \phi\rangle$. Similarly, a discontinuous current $\boldsymbol{J}_h^{n+1/2}$ obtained by the approximation $(\mathcal{P}_h^1)^*$,

$$\langle \boldsymbol{J}_h^{n+\frac{1}{2}}, \tilde{\boldsymbol{\varphi}}\rangle = \left\langle \int_{t^n}^{t^{n+1}} \boldsymbol{J}_N(\tau) \frac{\mathrm{d}\tau}{\Delta t}, \mathcal{P}_h^1 \tilde{\boldsymbol{\varphi}} \right\rangle = \sum_{\kappa=1}^{N} q_\kappa \int_{t^n}^{t^{n+1}} \mathbf{v}_\kappa(\tau) \cdot (\mathcal{P}_h^1 \tilde{\boldsymbol{\varphi}})(\mathbf{x}_\kappa(\tau)) \frac{\mathrm{d}\tau}{\Delta t}, \qquad \tilde{\boldsymbol{\varphi}} \in \tilde{V}_h^1 \tag{2.67}$$

allows to verify the discrete continuity equation (2.55) corresponding to the Conga formulation, i.e.,

$$\langle \boldsymbol{J}_h^{n+\frac{1}{2}}, \mathbf{grad}\, \phi + (I - \mathcal{P}_h^1)\tilde{\boldsymbol{u}}\rangle = \frac{1}{\varepsilon_0} \langle \frac{1}{\Delta t}(\rho_h^{n+1} - \rho_h^n), \phi\rangle, \qquad (\phi, \tilde{\boldsymbol{u}}) \in V_h^0 \times \tilde{V}_h^1.$$

We may specify that the reason why the products (2.66) and (2.67) are well defined (and stable with respect to the particle trajectories) is that the test functions $H(\mathrm{curl})$ have continuous tangential components across the mesh edges. Finally, when the trajectories are piecewise polynomials, it is possible to directly estimate these products by using a few Gauss points in each cell with a current contribution, which is also fully detailed in [[48]].

2.7 Link with a standard DG discretization

We can show that in 2D the Conga discretization described in Section 2.3 coincides with the DG formulation with centered fluxes (not dissipative) studied e.g., in [80]. The argument is simple enough to be reproduced here. We use classical notations ([35]) for the tangential jumps and averages across the interelement edges, i.e.

$$[\![\boldsymbol{u}]\!]_e := (\boldsymbol{n}_e^- \times \boldsymbol{u}|_{T^-} + \boldsymbol{n}_e^+ \times \boldsymbol{u}|_{T^+})|_e \quad \text{and} \quad \{\!\{\boldsymbol{u}\}\!\}_e := \frac{1}{2}(\boldsymbol{u}|_{T^-} + \boldsymbol{u}|_{T^+}))|_e \qquad \text{for } \ e \in \mathcal{E}_h \setminus \mathcal{E}_h^B \tag{2.68}$$

whether e is an interior edge (shared by two cells $T^\pm = T^\pm(e)$ with outgoing normal vectors $\boldsymbol{n}_e^\pm$), or

$$[\![\boldsymbol{u}]\!]_e := (\boldsymbol{n}_e^- \times \boldsymbol{u}|_{T^-})|_e \quad \text{and} \quad \{\!\{\boldsymbol{u}\}\!\}_e := (\boldsymbol{u}|_{T^-})|_e \qquad \text{for } \ e \in \mathcal{E}_h^B. \tag{2.69}$$

whether e is a boundary edge (carried by a single cell $T^- = T^-(e)$, of outgoing normal $\boldsymbol{n}_e^-$). For a scalar field u the definitions are rigorously the same, with the convention that in 2D the product $\boldsymbol{n} \times u$ often denotes the vector $(n_y u, -n_x u)^t$. The curl operators involved in the flux centered DG discretization write then

$$\left\{ \begin{array}{l} \langle \operatorname{curl}_h^{\mathrm{DG}} \boldsymbol{u}, v\rangle = \displaystyle\sum_{T\in\mathcal{T}_h} \langle \boldsymbol{u}, \mathbf{curl}\, v\rangle_T - \sum_{e\in\mathcal{E}_h\setminus\mathcal{E}_h^B} \langle \{\!\{\boldsymbol{u}\}\!\}, [\![v]\!]\rangle_e \\ \langle \mathbf{curl}_h^{\mathrm{DG}} v, \boldsymbol{u}\rangle = \displaystyle\sum_{T\in\mathcal{T}_h} \langle v, \operatorname{curl} \boldsymbol{u}\rangle_T - \sum_{e\in\mathcal{E}_h} \langle \{\!\{v\}\!\}, [\![\boldsymbol{u}]\!]\rangle_e \end{array} \right. \qquad \text{for } \boldsymbol{u} \in \tilde{V}_h^1,\ v \in V_h^2. \tag{2.70}$$

Using the fact that the conforming projection $\mathcal{P}_h^1$ performs a local averaging of the edge degrees of freedom in the Nédélec space, (2.11), we compute

$$\begin{aligned} \langle \operatorname{curl} \mathcal{P}_h^1 \boldsymbol{u}, v\rangle &= \sum_{T\in\mathcal{T}_h} \big(\langle \mathcal{P}_h^1 \boldsymbol{u}, \mathbf{curl}\, v\rangle_T + \langle \boldsymbol{n} \times \mathcal{P}_h^1 \boldsymbol{u}, v\rangle_{\partial T} \big) \\ &= \sum_{T\in\mathcal{T}_h} \big(\langle \boldsymbol{u}, \mathbf{curl}\, v\rangle_T + \langle \boldsymbol{n} \times \{\!\{\boldsymbol{u}\}\!\}, v\rangle_{\partial T\setminus\partial\Omega} \big) \\ &= \sum_{T\in\mathcal{T}_h} \langle \boldsymbol{u}, \mathbf{curl}\, v\rangle_T - \sum_{e\in\mathcal{E}_h\setminus\mathcal{E}_h^B} \langle \{\!\{\boldsymbol{u}\}\!\}, [\![v]\!]\rangle_e \\ &= \langle \operatorname{curl}_h^{\mathrm{DG}} \boldsymbol{u}, v\rangle \end{aligned}$$

and then infer the announced equivalence, i.e., $\operatorname{curl}_h^{\mathrm{DG}} = \operatorname{curl} \mathcal{P}_h^1$ on $\tilde{V}_h^1$. Given that the duality $\mathbf{curl}_h^{\mathrm{DG}} = (\operatorname{curl}_h^{\mathrm{DG}})^*$ is verified with elementary computations based on Green formulas, our analysis thus establishes the spectrally correct nature of the DG discretization with centered fluxes in 2D (2.70), a property numerically observed [89] but not proven yet, at least to our knowledge.

On the other hand, it is possible to see the compatible current approximation (2.63), $\boldsymbol{J}_h = (\mathcal{P}_h^1)^* \boldsymbol{J}_N$, as a local correction of the standard projection

$$\boldsymbol{J}_h^{\mathrm{nc}} = P_{\tilde{V}_h^1} \boldsymbol{J}_N$$

that is usually implemented in discontinuous schemes. Here the exponent "nc" stands for "non-compatible" since this approximation does not verify the Gauss-compatibility criteria, nor the discrete continuity equation established for the nonconforming case.

Indeed, by letting $\boldsymbol{\varphi}_{T,\lambda}$, $\lambda \in \Lambda^1(T)$ denote a basis for the polynomials of $\tilde{V}_h^1$ on each cell T, and by observing that the conforming space V_h^1 is a subspace of $\tilde{V}_h^1$ by construction, we see that it is possible to represent the conforming projection $\mathcal{P}_h^1$ by a matrix $\mathbf{P}$ satisfying

$$\mathcal{P}_h^1 \boldsymbol{\varphi}_{T,\lambda} = \sum_{T' \in \mathcal{T}_h, \gamma \in \Lambda^1(T')} \mathbf{P}_{(T,\lambda),(T',\gamma)} \boldsymbol{\varphi}_{T',\gamma}.$$

The "compatible" moments $m_{T,\lambda}(\boldsymbol{J}_N) := \langle \boldsymbol{J}_N, \mathcal{P}_h^1 \boldsymbol{\varphi}_{T,\gamma} \rangle$ (that determine the current (2.63)) are then easy to compute from the standard (non-compatible) moments $m_{T,\lambda}^{\mathrm{nc}}(\boldsymbol{J}_N) := \langle \boldsymbol{J}_N, \boldsymbol{\varphi}_{T,\gamma} \rangle$, via the local formulas

$$m_{T,\lambda}(\boldsymbol{J}_N) = \sum_{T',\gamma} \mathbf{P}_{(T,\lambda),(T',\gamma)} m_{T',\gamma}^{\mathrm{nc}}(\boldsymbol{J}_N). \tag{2.71}$$

In particular, the vectors $\mathbf{J}$ and $\mathbf{J}^{\mathrm{nc}}$ containing the coefficients of the discontinuous currents $\boldsymbol{J}_h$ and $\boldsymbol{J}_h^{\mathrm{nc}}$ satisfy the relation

$$\mathbf{J} = \mathbf{M}^{-1}\mathbf{P}\mathbf{M}\mathbf{J}^{\mathrm{nc}}$$

where $\mathbf{M}$ represents the mass matrix (block-diagonal) associated to this basis of $\tilde{V}_h^1$. These corrections are then local, moreover their computation is elementary: if the local bases $\boldsymbol{\varphi}_{T,\lambda}$ are defined by a restriction of the bases dual to the edge degrees of freedom, the nonzero coefficients of matrix $\mathbf{P}$ are just $\frac{1}{2}$ for the edge degrees of freedom, and 1 for the interior degrees of freedom [[52]].

Chapter 3

Theoretical and numerical study of some reduced models

Publication list

The material in this chapter is based on the following works:

⟦8⟧ M. Badsi, M. Campos Pinto and B. Després, A minimization formulation of a bi-kinetic sheath, *Kinetic and related models* 9, 2016

⟦70⟧ F. Da Silva, M. Campos Pinto, B. Després and S. Heuraux, Stable explicit coupling of the Yee scheme with a linear current model in fluctuating magnetized plasmas, *Journal of Computational Physics* 295, 2015

⟦90⟧ S. Heuraux, F. da Silva, T. Ribeiro, B. Després, M. Campos Pinto, J. Jacquot, E. Faudot, S. Wengerowsky, L. Colas and L. Lu, Simulation as a tool to improve wave heating in fusion plasmas, *Journal of Plasma Physics* 81, 2015

⟦47⟧ M. Campos Pinto and B. Després, Constructive formulations of resonant Maxwell's equations, ⟨hal-01278860⟩, under revision for SIAM Journal on Mathematical Analysis, 2016

3.1 Kinetic sheaths in an electrostatic plasma

Plasma sheaths are self-regulation phenomena during which the electric potential of an absorbing wall varies in order to balance the fluxes of electrons and ions coming from the plasma. In general this variation is negative and the neutral flux is achieved by accelerating the (positive) ions and slowing down the electrons. Indeed, in a globally neutral plasma at thermal equilibrium, in which the phase space densities are classically assumed maxwellian,

$$f_s(x,v) = \left(\frac{m_s}{2\pi k_B T}\right)^{d/2} \exp\left(-\frac{m_s v^2}{2k_B T}\right), \qquad s = i \text{ or } e,$$

due to their relative low mass the electrons have a characteristic speed $v_e^* = (\frac{k_B T}{m_e})^{1/2}$ much higher to that of the ions, as illustrated in Fig. 3.1. Since the flux of negative charges leaving the plasma

cannot exceed that of the positive charges for a long time, there must be a self-consistent mechanism which equilibrate these fluxes. In practice this mechanism takes the form of a potential drop on the wall associated with an electric field directed towards it. Inside this boundary layer which thickness is about a few Debye lengths (the characteristic distance for screening phenomena in an electrostatic plasma), a positive charge then builds up, as one may expect from the Gauss law.

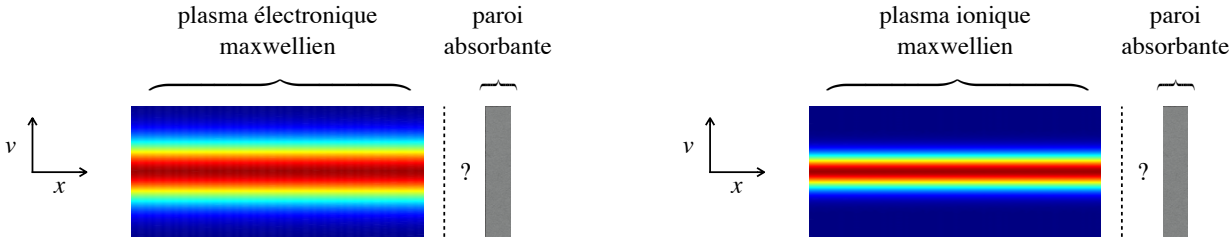

Figure 3.1: Sketch of maxwellian phase space (x, v) densities in a globally neutral plasma at thermal equilibrium, using the same (arbitrary) scale in velocity for both electron and ion densities. In the electron density represented on the left the characteristic speed is higher than that of the ions on the right, due to their lower mass. If such a plasma is in contact with an absorbing wall one sees that the electrons will leave the plasma at a higher rate than the ions. In the absence of self-regulation this would result in a growing positive charge buildup in the plasma, which cannot be stable. The sheath is the thin layer close to the wall in which the plasma is no longer neutral in order to balance the fluxes of outgoing particles.

A property that plays a key role in the classical analysis states that, in a simplified mono-kinetic model, ions must enter the sheath with a speed u_i greater or equal than their characteristic speed

$$u_i \geq v_i^* = \left(\frac{k_B T}{m_i}\right)^{\frac{1}{2}} \tag{3.1}$$

consistent with the self-regulation principle described above. This property is known as the Bohm criterion[58], and there exists a kinetic version of it [120, 126], according to which the velocity distribution of the incoming ions must satisfy the inequality

$$\frac{\int_0^\infty v^{-2} f_i(v)\,\mathrm{d}v}{\int_0^\infty f_i(v)\,\mathrm{d}v} \leq \frac{1}{(v_i^*)^2}. \tag{3.2}$$

In the scope of Mehdi Badsi's PhD [7], advised by Bruno Després and myself, we have proposed ⟦8⟧ a kinetic one-dimensional model that describes most of the key features of this physical phenomenon. Our purpose was to

- specify the role (within this model) of the fluid (3.1) and kinetic (3.2) Bohm criteria,
- determine a simple characterization of the "floating" potential at the wall.

Indeed we believed that these questions had not received fully satisfactory answers yet, despite several works in the mathematical literature [102, 79] and the recent works [83, 84] on a fluid plasma model close to the wall.

In our model, the ion and electron densities are steady state solutions to Vlasov equations in a dimensionless domain $[0, 1] \times \mathbb{R}$, with boundaries $x = 0$ and $x = 1$ representing a point inside the

plasma and the absorbing wall, respectively. Denoting $\mu = m_e/m_i < 1$ the relative electron mass, these equations take the form

$$\begin{cases} v\partial_x f_i - \phi'(x)\partial_v f_i = 0 \\ v\partial_x f_e + \dfrac{1}{\mu}\phi'(x)\partial_v f_e = 0 \end{cases} \tag{3.3}$$

and they are coupled with a Poisson equation that determines the electrostatic potential ϕ,

$$-\varepsilon^2\phi''(x) = \int (f_i + f_e)\,\mathrm{d}v. \tag{3.4}$$

Here $\varepsilon < 1$ represents the Debye length relative to this dimensionless domain, and should characterize the thickness of the boundary layer at the wall position $x = 1$. To model the self-regulation principle we next add to these equations a neutral flux (sometimes called ambipolarity) constraint

$$\int v(f_i + f_e)\,\mathrm{d}v = 0 \tag{3.5}$$

which may be seen as a direct consequence of the Ampère equation in a steady state regime, and a neutrality condition at $x = 0$, expressing the fact that this point is not in the sheath,

$$\int (f_i + f_e)(x = 0)\,\mathrm{d}v = 0. \tag{3.6}$$

This system is then completed by boundary conditions: for the potential we use Dirichlet boundary conditions

$$\phi(0) = 0, \qquad \phi(1) = \phi_w \tag{3.7}$$

where the value at 0 is arbitrary and ϕ_w denotes the potential at the wall. In the physics community it is often referred to as the floating potential: as it should result from the self-regulation mechanism, it is an unknown of the problem. Finally we denote the incoming ion and electron distributions by

$$\begin{cases} f_i(0, v) = f_i^{\mathrm{in}}(v), & v > 0 \\ f_i(1, v) = 0, & v < 0 \\ f_e(0, v) = f_e^{\mathrm{in}}(v) := n_0\sqrt{\mu}\exp\Big(-\dfrac{\mu v^2}{2}\Big), & v > 0 \\ f_e(1, v) = \alpha f_e(1, -v), & v < 0. \end{cases} \tag{3.8}$$

Here $0 \le \alpha < 1$ is a re-emission parameter for the electrons at the wall (which can be set to 0 in a first analysis), and n_0 is a reference density connected to the total number of electrons entering the sheath. The chosen form of the incoming distribution f_e^{in} corresponds to the classical hypothesis of a maxwellian electron distribution in the plasma core, far from the wall. For the moment we do not specify the velocity distribution f_i^{in} of the incoming ions, and instead ask ourselves the following questions:

- can we characterize the wall potential ϕ_w so that it can be computed from the physical parameters μ, ε and α ?
- can we identify conditions on the incoming distribution f_i^{in} such that there exists a non trivial solution ($\phi \not\equiv 0$) to the above problem (3.3)-(3.8)?

To answer these questions we began by considering a given decreasing potential ϕ, so that the values of the densities f_i and f_e could be expressed using the method of characteristics. This method consists of writing $f_i(x,v) = f_i^{\text{in}}(\hat{v}_i(x,v))$ and $f_e(x,v) = f_e^{\text{in}}(\hat{v}_e(x,v))$, where $\hat{v}_i(x,v) \geq 0$ and $\hat{v}_e(x,v) \geq 0$ are the incoming velocities connected to (x,v) by characteristic trajectories solutions to

$$\begin{cases} v_i'(t) = -\phi'(x_i(t)) \\ x_i'(t) = v_i(t) \end{cases} \qquad \text{and} \qquad \begin{cases} v_e'(t) = \dfrac{1}{\mu}\phi'(x_e(t)) \\ x_e'(t) = v_e(t). \end{cases}$$

Using the fact that these trajectories have the respective invariants $\frac{1}{2}v_e^2 - \frac{1}{\mu}\phi(x_e)$ and $\frac{1}{2}v_i^2 + \phi(x_i)$, we find

$$f_i(x,v) = \begin{cases} f_i^{\text{in}}(\sqrt{v^2 + 2\phi(x)}) & \text{if } \ v \geq \sqrt{-2\phi(x)} \\ 0 & \text{otherwise} \end{cases}$$

and

$$f_e(x,v) = \begin{cases} f_e^{\text{in}}(\sqrt{v^2 - \frac{2}{\mu}\phi(x)}) & \text{if } \ v \geq -\sqrt{\frac{2}{\mu}(\phi(x) - \phi_w)} \\ \alpha f_e^{\text{in}}(\sqrt{v^2 - \frac{2}{\mu}\phi(x)}) & \text{otherwise.} \end{cases}$$

From these expressions we infer an explicit form for the macroscopic densities $n_s(x) = \int_{\mathbb{R}} f_s(x,v)\,\mathrm{d}v$, and fluxes $\gamma_s(x) = \int_{\mathbb{R}} v f_s(x,v)\,\mathrm{d}v = \gamma_s(0)$. The constraints (3.5) and (3.6) expressing the neutrality of the fluxes and charges at $x = 0$ then lead to two scalar relations involving f_i^{in}, n_0 and ϕ_w, but not the potential ϕ itself:

$$\begin{cases} \displaystyle\int_0^\infty v f_i^{\text{in}}(v)\,\mathrm{d}v = n_0 \frac{1-\alpha}{\sqrt{\mu}} e^{\phi_w} \\ \displaystyle\int_0^\infty f_i^{\text{in}}(v)\,\mathrm{d}v = n_0\Big(\sqrt{2\pi} - (1-\alpha)\int_{\sqrt{-2\phi_w}}^\infty e^{-\frac{v^2}{2}}\,\mathrm{d}v\Big). \end{cases} \tag{3.9}$$

We then have the following result.

Theorem 3.1 *Under the necessary and sufficient condition*

$$\frac{\int_0^\infty v f_i^{\text{in}}(v)\,\mathrm{d}v}{\int_0^\infty f_i^{\text{in}}(v)\,\mathrm{d}v} < \sqrt{\frac{2}{\pi\mu}}\frac{1-\alpha}{1+\alpha}, \tag{3.10}$$

System (3.9) *has a unique solution* $(n_0, \phi_w) \in \mathbb{R}_+^* \times \mathbb{R}_-^*$.

Thus, the wall potential is well defined by an implicit relation of the form $a(\phi_w) = b$ with a increasing, and it can be computed from the physical parameters α and μ, and the incoming ion distribution f_i^{in} (through the average incoming velocity).

Now that the wall potential is determined, System (3.3)-(3.8) can be expressed as a non-linear Poisson equation

$$-\varepsilon^2\phi''(x) = -\mathcal{U}'(\phi(x))$$

with $\mathcal{U}(\psi) := \int_0^\infty v\sqrt{v^2 - 2\psi}\, f_i^{\text{in}}(v)\,\mathrm{d}v + n_0\big(\sqrt{2\pi}e^\psi - (1-\alpha)\int_{\sqrt{-2\phi_w}}^\infty v\sqrt{v^2+2\psi}\, e^{-\frac{v^2}{2}}\,\mathrm{d}v\big)$ and the boundary conditions (3.7). This equation can be studied using a variational approach which consists of looking for minimizers of the functional

$$J_\varepsilon(\phi) := \int_0^1 \varepsilon^2 \frac{|\phi'(x)|^2}{2} + \mathcal{U}(\phi(x))\,\mathrm{d}x. \tag{3.11}$$

We then prove the following result.

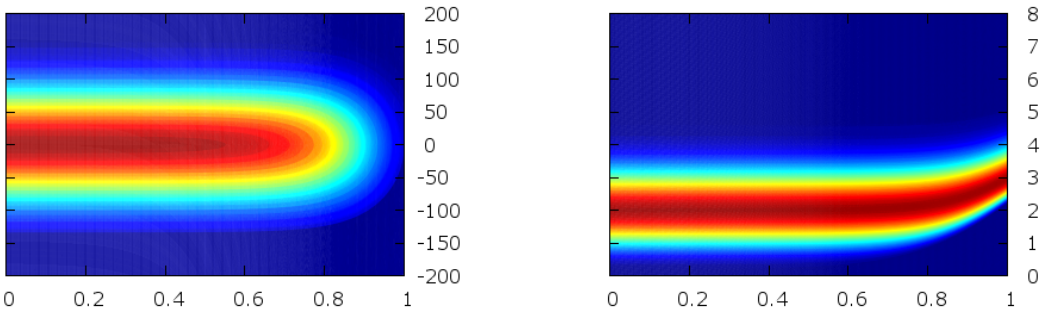

Figure 3.2: Numerical results obtained by Mehdi Badsi: electronic and ionic distributions close to a perfectly absorbing ($\alpha = 0$) wall located at $x = 1$, for a (dimensionless) Debye length $\varepsilon = 0.1$. The difference in the velocity ranges expresses the high relative mobility of the electrons, and in the boundary layer we observe that, as expected, the electrons are repelled and the ions are accelerated.

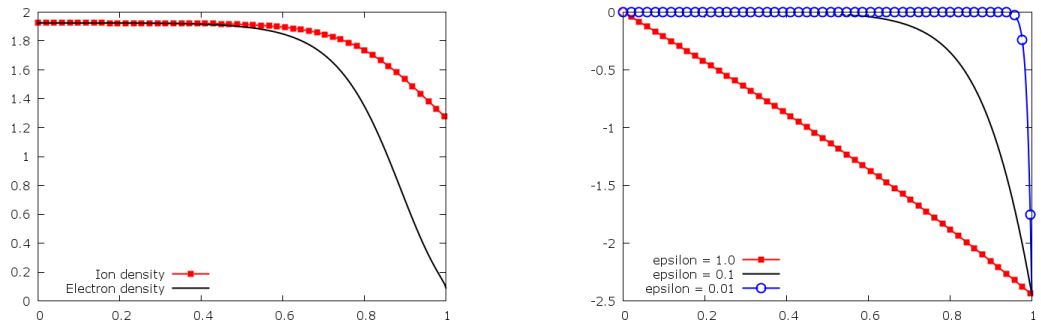

Figure 3.3: Numerical results obtained by Mehdi Badsi: on the left, the macroscopic ion and electron densities correspond to the same parameters than in Figure 3.2. On the right, the different electrostatic potentials correspond to different values of the dimensionless Debye length ε, as indicated.

Theorem 3.2 *If the incoming ion distribution f_i^{in} satisfies the conditions* (3.10) *and*

$$\frac{\int_0^\infty v^{-2} f_i^{\mathrm{in}}(v)\,\mathrm{d}v}{\int_0^\infty f_i^{\mathrm{in}}(v)\,\mathrm{d}v} < \frac{\left(\sqrt{2\pi} + (1-\alpha)\int_{\sqrt{-2\phi_w}}^\infty v^{-2} e^{-\frac{v^2}{2}}\,\mathrm{d}v\right)}{\left(\sqrt{2\pi} - (1-\alpha)\int_{\sqrt{-2\phi_w}}^\infty e^{-\frac{v^2}{2}}\,\mathrm{d}v\right)}, \tag{3.12}$$

then System (3.3)-(3.8) *has a unique solution f_i, f_e, ϕ.*

As the right hand side from (3.12) is larger than 1, we observe that this condition is weaker than the classical kinetic inequality (3.2), indeed in this dimensionless setting the characteristic speed reads $v_i^* = 1$. This solution has the distinctive features of a boundary layer at $x = 1$, and it reproduces the main physical properties of an electrostatic sheath, as described above. The numerical simulations obtained by Mehdi Badsi [7], using a projected gradient method derived from the minimization of the functional (3.11), validate these findings on a quantitative level. Some of these results are shown in Figure 3.2 and 3.3.

3.2 FDTD wave propagation in a magnetized plasma

Reflectometry is a technique where a high frequency ($\sim$ 35 GHz) electromagnetic wave is sent in a plasma and the scattered wave is measured in order to derive a density map of the probed plasma (see Figure 3.4).

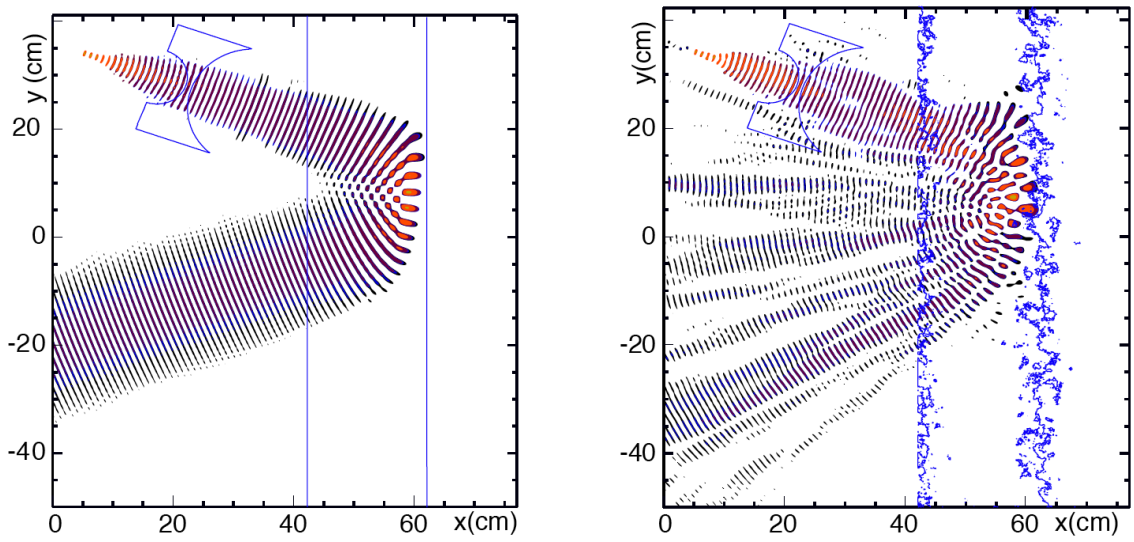

Figure 3.4: Electromagnetic wave emitted by an antenna and reflected by an electronic plasma which macroscopic density is indicated by its isovalues (blue lines). On the left figure the plasma density is a smooth increasing function of x, on the right one it is affected by strong oscillations typical of the turbulences observed in tokamak plasmas.

To perform numerical simulations of such waves in the presence of an intense magnetic field, plasma physicists use a simplified model in which they assume that are given:

- the bulk part B_0 of the magnetic field, stationary and often constant in space,
- the macroscopic electron density $N_e(x)$, considered here to be stationary over the simulation time.

The unknowns being the varying electromagnetic field (E, H) and the electron current density J induced by the displacement of charges within the plasma, we then consider the linearized problem

$$\begin{cases} \varepsilon_0 \partial_t E = \nabla \wedge H - J \\ \mu_0 \partial_t H = -\nabla \wedge E \\ \partial_t J = \varepsilon_0 \omega_p^2 E + \omega_c b \wedge J \end{cases} \tag{3.13}$$

where $\omega_p(\mathbf{x}) := \sqrt{\frac{q_e^2 N_e(\mathbf{x})}{m\varepsilon_0}}$, $\omega_c(\mathbf{x}) := \frac{q_e |B_0(\mathbf{x})|}{m_e}$ and $b(\mathbf{x}) := -\frac{B_0(\mathbf{x})}{|B_0(\mathbf{x})|}$ respectively denote the plasma pulsation, the cyclotron pulsation and the unit vector directed along the background magnetic field.

The standard approach [137] to discretize these equations consists of extending the classical FDTD (Finite Differences Time Domain) scheme designed by Yee [138] for the Maxwell equations in vacuum ($J = 0$). The computational domain being subdivided in regular cubes of diameter h, the x, y and z components of the fields E and H are discretized on staggered grids as represented on Figure 3.5, so

that the different derivatives involved in the curl can be approximated by centered divided differences. The original Yee scheme then writes

$$\begin{cases} \frac{\varepsilon_0}{\Delta t}(E^{n+1} - E^n) = RH^{n+\frac{1}{2}} \\ \frac{\mu_0}{\Delta t}(H^{n+\frac{1}{2}} - H^{n-\frac{1}{2}}) = -R^t E^n \end{cases} \tag{3.14}$$

where R is the matrix representing the curl approximation by finite differences centered on the faces, and R^t the transposed matrix corresponding to finite differences centered on the edges. Here we note

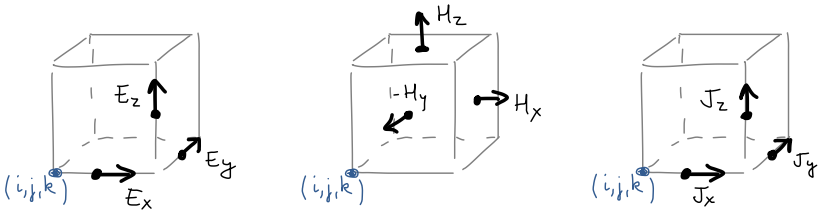

Figure 3.5: The nodes used to discretize the different components of the fields E and H in the staggered grid Yee scheme are pictured on the left and center plots. The right plot shows the nodes used to discretize the current density J in the reflectometry simulations.

that the time discretization is also staggered, in order to approximate the time derivatives by centered finite differences. As is well known this choice allows to preserve exactly a pseudo-energy, namely the quantity $\tilde{\mathcal{E}}^n := \mathcal{E}^n - \Delta t \langle E^n, RH^{n-1/2}\rangle_h$ where $\mathcal{E}^n := \varepsilon_0 \|E^n\|_h^2 + \mu_0 \|H^{n-1/2}\|_h^2$ is the quadratic energy of the discrete solution. By observing that $|\langle E^n, RH^{n-1/2}\rangle| \leq \frac{c}{2}\|R\|_h \mathcal{E}^n$ leads to $\mathcal{E}^n(1 - \frac{c\Delta t}{2}\|R\|_h) \leq \tilde{\mathcal{E}}^n$, we infer from this exact conservation that the scheme is stable as long as

$$c\Delta t < 2/\|R\|_h = h/\sqrt{3}, \tag{3.15}$$

regardless of the treatment of the boundary conditions.

To extend this scheme to the case of a nonzero current density appearing on the right hand side of the first (Ampère) equation in (3.14), a natural option is to discretize the components of J on the same nodes as those of E, and at half integer time steps. This choice leads to discretizing in time the third equation from (3.13) by a finite difference formula centered on the integer time steps, which gives the following scheme

$$\begin{cases} \frac{\varepsilon_0}{\Delta t}(E^{n+1} - E^n) = RH^{n+\frac{1}{2}} - J^{n+\frac{1}{2}} \\ \frac{\mu_0}{\Delta t}(H^{n+\frac{1}{2}} - H^{n-\frac{1}{2}}) = -R^t E^n \\ \frac{1}{\Delta t}(J^{n+\frac{1}{2}} - J^{n-\frac{1}{2}}) = \varepsilon_0 \omega_p^2 E^n + \omega_c b \wedge \frac{1}{2}(J^{n+\frac{1}{2}} + J^{n-\frac{1}{2}}). \end{cases} \tag{3.16}$$

Here the third equation is implicit in $J^{n+\frac{1}{2}}$, but it can be made explicit as follows. Using that b is a unit vector one has

$$(b\wedge)^3 = -(b\wedge), \tag{3.17}$$

which allows to write $(I - \theta b\wedge)^{-1} = I + \frac{\theta}{1+\theta^2}(b\wedge) + \frac{\theta^2}{1+\theta^2}(b\wedge)^2$, with θ a scalar-valued function. The implicit equation on J, put under the form $J^{n+\frac{1}{2}} = W^n + \theta b \wedge J^{n+\frac{1}{2}}$, can then be recast as $J^{n+\frac{1}{2}} = \big(I + \frac{\theta}{1+\theta^2}(b\wedge) + \frac{\theta^2}{1+\theta^2}(b\wedge)^2\big)W^n$.

It is possible to extend the stability analysis sketched above for the Yee scheme to System (3.16), by observing that here the pseudo-energy $\tilde{\mathcal{E}}^n := \mathcal{E}^n - \Delta t \langle E^n, (RH^{n-1/2} - J^{n-1/2})\rangle_h$ is exactly preserved, with $\mathcal{E}^n := \varepsilon_0 \|E^n\|_h^2 + \mu_0 \|H^{n-1/2}\|_h^2 + \frac{1}{\varepsilon_0} \|\frac{J^{n-1/2}}{\omega_p}\|_h^2$ the quadratic energy of the discrete solution. An algebraic argument based on the bound $|\langle E^n, J^{n-1/2}\rangle| \leq \|\omega_p\|_{L^\infty} \|E^n\|_h \|J^{n-1/2}\|_h$ then shows that the scheme (3.16) is stable under the condition

$$\frac{\Delta t}{2} \Big(\frac{12c^2}{h^2} + \|\omega_p\|_{L^\infty}^2\Big)^{\frac{1}{2}} < 1.$$

It is actually possible to improve this condition: by discretizing the current at the integer time steps, we recover the stability condition of the Yee scheme (3.15), which has the advantage that it does not depend on the maximal values of the electronic density.

If this approach may seem satisfactory, it nevertheless suffers from a weakness that eventually appears when the electronic density N_e has strong gradients (as it typically occurs in turbulent plasmas) and when the simulations are very long (of a few thousands, or tens of thousands iterations), under the form of an exponential growth of the numerical solutions. The origin of such an instability is the fact that the formal resolution of the implicit equation on J is only valid if the cross product *effectively used* in the scheme (3.16) satisfies the relation (3.17).

Indeed, the use of staggered grids in the discretization of the components of the current J forbids using the exact (pointwise) cross product in the third equation of (3.16). The common choice consists of using a centered formula to approximate the exact curl, which may be written

$$\begin{aligned}
(b \wedge_h J)_x|_{i+\frac{1}{2},j,k} &:= b_y \{J_z\}_{i+\frac{1}{2},j,k} - b_z \{J_y\}|_{i+\frac{1}{2},j,k} \\
(b \wedge_h J)_y|_{i,j+\frac{1}{2},k} &:= b_z \{J_x\}_{i,j+\frac{1}{2},k} - b_x \{J_z\}_{i,j+\frac{1}{2},k} \\
(b \wedge_h J)_z|_{i,j,k+\frac{1}{2}} &:= b_x \{J_y\}_{i,j,k+\frac{1}{2}} - b_y \{J_x\}_{i,j,k+\frac{1}{2}}
\end{aligned} \tag{3.18}$$

where the curly brackets denote averages on the four neighboring nodes (see the left plot on Figure 3.6), as in $\{J_z\}_{i+1/2,j,k} = \frac{1}{4}\big(J_z|_{i,j,k-1/2} + J_z|_{i,j,k+1/2} + J_z|_{i+1,j,k-1/2} + J_z|_{i+1,j,k+1/2}\big)$. It is then this discrete cross product that is used in the explicit version of the scheme (3.16). The problem resides in the fact that the product (3.18) cannot satisfy the key relation (3.17), indeed its stencil increases with every iteration. In other terms, the explicit (and implemented) version of the scheme (3.16) is not equivalent to its implicit version addressed in the stability analysis. We then understand that numerical instabilities can appear in this scheme, and the more turbulent the density N_e, the sooner these instabilities are likely to be triggered.

To resolve this issue, with Bruno Després we have proposed a new numerical scheme in which the averaged cross product (3.18) is replaced by a *clustered* cross product. Given a pattern $(\alpha, \beta, \gamma) \in \{\pm 1\}^3$, the latter is defined by the relations

$$\begin{aligned}
(b \wedge_h J)_x|_{i+\frac{\alpha}{2},j,k} &:= b_y J_z|_{i,j,k+\frac{\gamma}{2}} - b_z J_y|_{i,j+\frac{\beta}{2},k} \\
(b \wedge_h J)_y|_{i,j+\frac{\beta}{2},k} &:= b_z J_x|_{i+\frac{\alpha}{2},j,k} - b_x J_z|_{i,j,k+\frac{\gamma}{2}} \\
(b \wedge_h J)_z|_{i,j,k+\frac{\gamma}{2}} &:= b_x J_y|_{i,j+\frac{\beta}{2},k} - b_y J_x|_{i+\frac{\alpha}{2},j,k}
\end{aligned} \tag{3.19}$$

(see the right plot on Figure 3.6). This product is indeed local in the sense that the matrix of the operator $J \to b \wedge_h J$ is block diagonal, and it satisfies the key relation (3.17). In particular, the corresponding explicit scheme is equivalent to its implicit version (3.16), so that the stability analysis now applies on the scheme effectively implemented. The actual stability of this new scheme has been observed in a series of numerical simulations implemented by Filipe Da Silva (IST, Lisbonne) and Stéphane Heuraux (IJL, Nancy) ⟦70, 90⟧, using very turbulent density profiles and simulations of about a million time steps, see Figure 3.7.

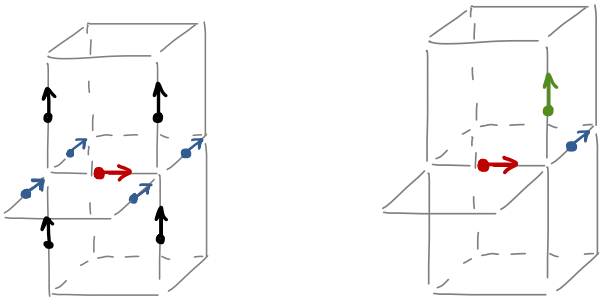

Figure 3.6: Stencils (nodes of J) used for the x component of the cross product $b \wedge_h J$ when computed with the averaged formula (3.18) (on the left) or with the clustered formula (3.19) (on the right), here with a pattern $(\alpha, \beta, \gamma) = (-1, 1, 1)$. For the clustered cross product the same stencil is used to compute the three components, so that the matrix of the operator $J \to b \wedge_h J$ is block-diagonal.

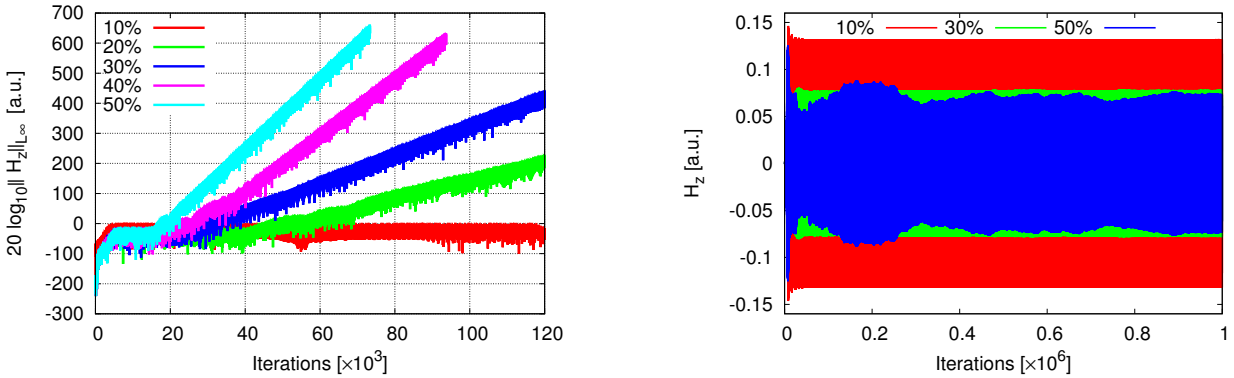

Figure 3.7: Amplitude of the numerical H field computed by the standard scheme (on the left) and by the new scheme (on the right). The colors of the curves correspond to different turbulence levels on the electronic density, as indicated. We note that on the left figure the amplitudes are plotted using a logarithmic scale, and that the higher the turbulence level, the sooner and the stronger the instabilities. On the right figure the long time stability is evidenced by the linear scale and the fact that the simulations run over a period about ten times longer.

3.3 Hybrid resonances in magnetized plasmas

In addition to the probing function described in the previous section, electromagnetic waves play an important role in the heating of fusion plasmas. Resonance phenomena, in particular, are used to transfer energy from the fields to the particles. Starting from the linearized system (3.13) one may write a simplified model to describe such resonances, which correspond to the interaction of the wave with an electronic plasma (again the ions are assumed frozen at first order) in the presence of a strong magnetic field B_0. Assuming that the time varying field oscillates with a pulsation ω imposed by an antenna ($X(t, \mathbf{x}) = e^{-i\omega t} X(\mathbf{x})$), and using the second equation to eliminate the H field, the system becomes

$$\begin{cases} \dfrac{1}{i\omega\mu_0} \nabla \wedge \nabla \wedge E + i\omega\varepsilon_0 E = J \\ -i\omega J - \omega_c b \wedge J = \varepsilon_0 \omega_p^2 E \end{cases} \tag{3.20}$$

where we remind that the plasma pulsation $\omega_p = \omega_p(\mathbf{x})$ and the cyclotron pulsation $\omega_c = \omega_c(\mathbf{x})$ characterize the electron density and the bulk background magnetic field, respectively. As above, it is possible to invert the operator $(i\omega I + \omega_c b\wedge)$ and to express J as a function of E. Using the classical simplification where the background field has a constant orientation, $b = e_z$, we arrive at

$$\nabla \wedge \nabla \wedge E - \left(\frac{\omega}{c}\right)^2 \underline{\underline{\varepsilon_\omega}}\, E = 0,$$

where $\underline{\underline{\varepsilon_\omega}} = \underline{\underline{\varepsilon_\omega}}(\mathbf{x})$ denotes the dielectric tensor of the cold plasma [136, 81],

$$\underline{\underline{\varepsilon_\omega}}(\mathbf{x}) = \begin{pmatrix} 1 - \frac{\omega_p^2}{\omega^2-\omega_c^2} & i\frac{\omega_c\omega_p^2}{\omega(\omega^2-\omega_c^2)} & 0 \\ -i\frac{\omega_c\omega_p^2}{\omega(\omega^2-\omega_c^2)} & 1 - \frac{\omega_p^2}{\omega^2-\omega_c^2} & 0 \\ 0 & 0 & 1 - \frac{\omega_p^2}{\omega^2} \end{pmatrix}. \tag{3.21}$$

If one assumes in addition that the different parameters only depend on x, the propagation direction of the wave, we may look for solutions depending only on this variable. We then obtain two decoupled problems on the interval $\Omega =]-1, 1[$. First, one scalar equation for the the field component E_z parallel to B_0, often referred to as the *ordinary* wave (O mode) in the physics community,

$$(\partial_x)^2 E_z + \frac{\omega^2 - \omega_p^2}{c^2} E_z = 0. \tag{3.22}$$

For this component, the plasma is a propagative medium in the regions where $\omega_p^2(x) = \frac{q_e^2}{m_e\varepsilon_0} N_e(x) < \omega^2$. The curve $\omega_p^2(x) = \omega^2$ is called *cut-off* [128, 76] and the Airy equation $u'' - xu = 0$ can be used as a prototype for a fine study of the transition between the propagative region and the evanescent one.

Second, a system involving the orthogonal components E_x, E_y referred to as the *extraordinary* wave (X mode), corresponding to the upper left block of the dielectric tensor (3.21),

$$\begin{pmatrix} 0 \\ -(\partial_x)^2 E_y \end{pmatrix} - \begin{pmatrix} \alpha(x) & i\delta(x) \\ -i\delta(x) & \alpha(x) \end{pmatrix} \begin{pmatrix} E_x \\ E_y \end{pmatrix} = 0 \qquad \text{with} \quad \begin{cases} \alpha = \left(\frac{\omega}{c}\right)^2 \left(1 - \frac{\omega_p^2}{\omega^2-\omega_c^2}\right) \\ \delta = \left(\frac{\omega}{c}\right)^2 \left(\frac{\omega_c\omega_p^2}{\omega(\omega^2-\omega_c^2)}\right). \end{cases} \tag{3.23}$$

By a formal elimination of the first component this system leads to the Budden equation [33, 136]

$$-(\partial_x)^2 E_y + \left(\frac{\delta^2}{\alpha} - \alpha\right) E_y = 0 \tag{3.24}$$

that is associated with two kinds of resonances. The *cyclotron* resonance $\omega = \omega_c(x)$ corresponding to the poles of the coefficients α and δ, and the *hybrid* resonance $\omega^2 = \omega_c^2(x) + \omega_p^2(x)$ corresponding to the zeros of the coefficient α. In the configuration considered here (and in others, see [74]) the poles $\omega = \omega_c$ do not pose any problem. A simple computation gives indeed

$$\frac{\delta^2}{\alpha} - \alpha = \frac{\omega^2\omega_c^2 - (\omega^2 - \omega_p^2)^2}{c^2(\omega^2 - \omega_c^2 - \omega_p^2)}$$

so that cyclotron resonances do not represent true singularities. In contrast, the presence of hybrid resonances raises a few issues. By using as a prototype the Whittaker equation $u'' + \left(\frac{1}{x} - \frac{1}{4}\right)u = 0$ for which we have explicit exact solutions, one can indeed show [75] that in the neighborhood of a zero of α the equation (3.24), endowed with standard boundary conditions of the form $E_y'(\pm 1) \mp i\lambda E_y(\pm 1) = f_\pm$,

has at least two distinct solutions. Moreover, as these solutions do not necessarily vanish at this point we see that $E_x = -i\frac{\delta}{\alpha}E_y$ contains a nonintegrable, $\frac{1}{x}$ singularity.

One way to better understand the nature of the hybrid resonances is to take into account the small friction between the electrons and the ions (that have been assumed frozen up to now), by adding a dissipative term in the system (3.13) where the third equation becomes

$$\partial_t J = \varepsilon_0 \omega_p^2 E + \omega_c b \wedge J - \nu J.$$

Here the small parameter ν describes the collisionality between the electrons and the background ion bath. For physical reasons ν must be positive, but negative values can also be considered in the mathematical analysis. Inserting this term in the computations one obtains a modified version of System (3.23) in which the plasma coefficients read

$$\alpha^\nu = \Big(\frac{\omega}{c}\Big)^2 \left(1 - \frac{\tilde{\omega}\omega_p^2}{\omega(\tilde{\omega}^2 - \omega_c^2)}\right) \qquad \text{and} \qquad \delta^\nu = \Big(\frac{\omega}{c}\Big)^2 \left(\frac{\omega_c \omega_p^2}{\omega(\tilde{\omega}^2 - \omega_c^2)}\right), \qquad \tilde{\omega} = \omega + i\nu.$$

In particular, α^ν does not vanish anymore for real values of ω and the equation (3.24) becomes well-posed [6]. Consistent with the limit absorption principle [123] the resonant problem can then be seen as a singular limit $\nu \to 0^+$ of the dissipative case, which is conveniently recast as a first order problem by reintroducing the magnetic field,

$$\begin{cases} i\omega B_z - \partial_x E_y = 0 \\ -\alpha^\nu E_x - i\delta^\nu E_y = 0 \\ -i\omega \partial_x B_z + i\delta^\nu E_x - \alpha^\nu E_y = 0. \end{cases} \tag{3.25}$$

This approach is followed in [75], where the authors have considered simplified coefficients

$$\alpha^\nu = \alpha + i\nu \qquad \text{and} \qquad \delta^\nu = \delta \tag{3.26}$$

and the generic case where the function α had an isolated zero at $x = 0 \in \Omega$. They have then justified the limit absorption principle and finely quantified the singularity of the solutions $E^+ := \lim_{\nu\to 0^+} E^\nu \notin L^1_{\text{loc}}$ and $B^+ := \lim_{\nu\to 0^+} B^\nu$. Moreover they have shown that the energy transferred to the ions by a resonant wave was positive,

$$\mathcal{Q}(E^+) = \lim_{\nu\to 0^+} \nu \int_\Omega |E^\nu|^2 = \lim_{\nu\to 0^+} \nu \int_\Omega |E_x^\nu|^2 > 0.$$

In the article ⟦47⟧ we have studied several characterizations of the resonant solutions of (3.24) which seem well suited for the derivation of numerical methods. In particular, our formulations allow us to complement (3.24) into well-posed problems, which all contain the information of the one-sided limit $\nu \to 0^+$ without involving the dissipative solutions themselves.

The basic idea of this work is due to Bruno Després who drew his inspiration from a comparison principle used in the theory of hyperbolic equations to establish entropy conditions on discontinuous solutions. In the framework of the cold plasma system (3.25), this principle led him to look for pseudo-solutions built in a similar way than the *manufactured solutions* used in the validation of some numerical methods. Here, they are explicit solutions $F_x^\nu, F_y^\nu, C_z^\nu$ of the modified system

$$\begin{cases} i\omega C_z^\nu - \partial_x F_y^\nu = q^\nu \\ -\alpha^\nu F_x^\nu - i\delta^\nu F_y^\nu = 0 \\ -i\omega \partial_x C_z^\nu + i\delta^\nu F_x^\nu - \alpha^\nu F_y^\nu = g^\nu \end{cases} \tag{3.27}$$

involving the simplified coefficients (3.26) and right hand sides chosen in such a way that the limits $F_y^\nu \to F_y^+$ and $C_z^\nu \to C_z^+$, as well as $q^\nu \to q^+$ and $g^\nu \to g^+$, for $\nu \to 0^+$, hold in L^2 and are straightforward to compute. In dimension 1, we essentially found two kinds of such solutions, which main features reproduce those of the solutions to (3.24):

- *smooth* manufactured solutions, for which the C_z field is continuous and does not vanish at 0,
- *singular* manufactured solutions, for which the F_y field does not vanish at 0,

From (3.27) we see that solutions of the first kind have a component F_x that is a priori integrable. This will not be the case for the solutions of the second kind, for which the C_z component will be a priori discontinuous at 0. Thus, we can consider as a typical singular manufactured solution a function of the form

$$F_y^\nu := \frac{i}{\delta} = F_y^+, \tag{3.28}$$

which leads to

$$F_x^\nu := -\frac{1}{\alpha + i\nu} \quad \to \quad F_x^+ = -\frac{1}{\alpha}, \tag{3.29}$$

the convergence holding in an (almost everywhere) pointwise sense in Ω. To verify the third equation in (3.27) with a function g^ν satisfying a L^2 bound uniformly in ν, we have then set

$$C_z^\nu := \frac{\delta(0)}{\omega r}\left(\frac{1}{2}\log\left(r^2x^2+\nu^2\right) - i\arctan\left(\frac{rx}{\nu}\right)\right) \quad \to \quad C_z^+ = \frac{\delta(0)}{\omega r}\left(\log\left(|rx|\right) - i\frac{\pi}{2}\mathrm{sign}(rx)\right) \tag{3.30}$$

with $r := \alpha'(0) \neq 0$. The convergence now holds in $L^2(\Omega)$, and we observe that the sign of the imaginary part of C_z^+ keeps track of the one-sided limit $\nu \to 0^+$. The comparison principle mentioned above leads then to evaluate the energy dissipated by the difference between the exact and manufactured solutions, via the Poynting vector $\Pi^\nu := \Re\big((E^\nu - F^\nu) \wedge (\overline{B^\nu - C^\nu})\big)$ which divergence satisfies

$$\nabla\cdot\Pi^\nu - \Re\Big(q^\nu(\overline{B^\nu - C^\nu})_z - (E^\nu - F^\nu)_y\overline{\Big(\frac{g^\nu}{i\omega}\Big)}\Big) = -\frac{\nu}{\omega}|E^\nu - F^\nu|^2 \leq 0. \tag{3.31}$$

By using the fact that smooth solutions E_y^ν and B_z^ν possess L^2-convergent subsequences we infer that the inequality pass to the limit, which leads a dissipative relation of the form

$$\mathcal{J} := \int_\Omega \Re\big((E_y^+ - kF_y^+)(\overline{B_z^+ - kC_z^+})\big)\varphi' + \int_\Omega \Re\Big(kq^+(\overline{B^+ - kC^+})_z - (E^+ - kF^+)_y\overline{\Big(\frac{kg^+}{i\omega}\Big)}\Big)\varphi \geq 0$$

where $k \in \mathbb{C}$ is a complex degree of freedom and $\varphi \geq 0$ a nonnegative test function. It is then natural to write the Euler-Lagrange equations for the functional $\mathcal{J} = \mathcal{J}(E^+, B^+, k)$ associated with constraints corresponding to the equation (3.24). In ⟦47⟧ we have shown that these relations fully characterize the resonant (one-sided limit) solution, under the form of a linear system of 5 equations, one of which is scalar. The unique solution of this system contains, through the value of k, the intensity of the resonant heating $\mathcal{Q}(E^+)$.

Interestingly, it is possible to derive a second formulation by using an alternate characterization of the limit solutions. This formulation is simpler as it only involves 3 equations (one of which being scalar). Again the basic idea is to compare the dissipative and manufactured solutions, but instead of (3.31) we now compute

$$\nabla\cdot(E^\nu \wedge C^\nu - F^\nu \wedge B^\nu) = (E_x^\nu C_z^\nu - F_y^\nu B_z^\nu)' = \Big(q^\nu B_z^\nu - \frac{g^\nu}{i\omega}E_y^\nu\Big).$$

Although the physical meaning of this term is not obvious, the convergence properties of the different solution components allow us to pass to the limit in an integral formulation

$$\int_\Omega (E_y^+ C_z^+ - F_y^+ B_z^+)\varphi' \,\mathrm{d}x = \int_\Omega \Big(q^+ B_z^+ - \frac{g^+}{i\omega} E_y^+\Big)\varphi \,\mathrm{d}x \tag{3.32}$$

where φ is an arbitrary smooth function. We infer the following problem, where we again assume that α has an isolated zero at $x = 0$, inside the interval $\Omega =]-1, 1[$ (if $\alpha'(0) = 0$ then the singularity is an even stronger one and the problem is still open).

Problem 3.1 *Find* $(E_y, B_z) \in L^2(\Omega) \times L^2(\Omega)$ *satisfying:*

i) *the limit problem* (3.24) *in a weak sense,*

$$\begin{cases} \displaystyle\int_\Omega (i\omega B_z \varphi_1 + E_y \varphi_1')dx = 0, & \forall \varphi_1 \in H_0^1(\Omega), \\ \displaystyle\int_\Omega \left(i\omega B_z \varphi_2' + \left(\frac{\delta^2}{\alpha} - \alpha\right) E_y \varphi_2\right) dx = 0, & \forall \varphi_2 \in H_0^1(\Omega), \quad \varphi_2(0) = 0, \end{cases}$$

ii) *boundary conditions corresponding to an antenna*

$$i\omega B_z(-1) + i\lambda E_y(-1) = f_- \qquad \text{and} \qquad i\omega B_z(1) - i\lambda E_y(1) = f_+,$$

in a distribution sense,

iii) *an integral relation* (3.32) *associated with a smooth manufactured solution such as* (3.28)-(3.30)*, and a test function* $\varphi \in H_0^1(\Omega)$ *such that* $\varphi(0) \neq 0$*.*

Here the restriction of the second variational equation to the test functions vanishing at $x = 0$ is necessary for the product $\frac{1}{\alpha} E_y \varphi_2$ to be integrable, and thanks to Hardy's inequality it is also sufficient. We then observe that if E_y and φ_2 are approximated by $\mathbb{P}_1$ finite elements, the absence of the test function associated with the node $x = 0$ will a priori prevent the discrete system to be square, a defect that clearly reminds the lack of uniqueness for the equation (3.24). In this context, the role of the integral relation (3.32) is obvious, and it is natural to think that its introduction allows to recover the missing uniqueness. And indeed the following result holds.

Theorem 3.3 ([47]) *For any* $(f_-, f_+) \in \mathbb{C}^2$*, there exists a unique solution* (E_y, B_z) *to Problem 3.1, and it coincides with the limit* $(E_y^+, B_z^+) = \lim_{\nu \to 0^+} (E_y^\nu, B_z^\nu)$ *of the dissipative solutions to* (3.25)*.*

In dimension 2 we have extended this study by constructing manufactured solutions which form seems to be compatible with (i) the singularities known in the 1D case, and (ii) singular solutions observed in meta-materials [23]. Under natural assumptions on the singularity of the exact solutions these functions allow us to write new formulations for the limit problem, which well-posedness remains an open problem.

These works have been pursued during the master thesis of Anouk Nicolopoulos [116], who proved that Problem 3.1, reformulated using a decomposition of the solution in a smooth part (to be determined) and a singular part (proportional to the singular manufactured solution), would involve a Fredholm operator of index 0. Anouk Nicolopoulos also implemented two numerical schemes. One directly based on the formulation proposed in Problem 3.1, and another one involving the decomposition into a smooth part and a singular part. In both cases, the quality of her results has demonstrated the validity of this approach (see Figure 3.8), as well as its relevance for numerical applications.

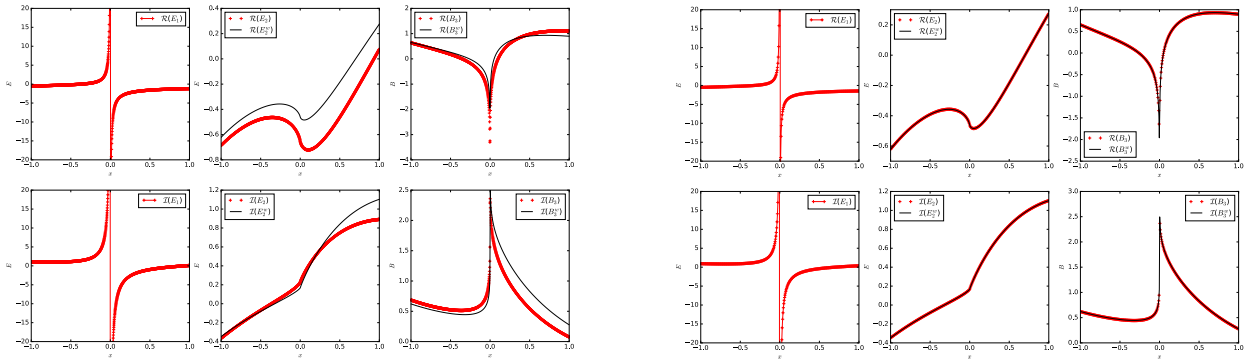

Figure 3.8: Numerical approximation of the Budden equation (3.24) in 1D performed by Anouk Nicolopoulos, for the coefficients $\alpha(x) = -x$ and $\delta(x) = \sqrt{1 - x/4 + x^2}$ (corresponding to Whittaker's equation) for which an exact solution is known (black line) with a singularity at $x = 0$. On the left, the approximation involves a naive technique to locally smooth out the singularity so that the scheme does not crash (using a small parameter which value does not seem to be appropriate here), and on the right the numerical scheme discretizes the new formulation of Problem 3.1, which is well-posed.

Some prospects

As my research is at the interface between mathematics and plasma physics, the natural developments to the work presented here may be divided into three groups: a first one consisting of objectives not fully realized yet, a second one where some of the tools developped here would be extended to related problems, and a third one fed by new physics problems where the viewpoint of numerical analysis is likely to bring an illuminating perspective.

Improving the accuracy of particle codes falls into the first group. As we have seen, methods such as PIC (Particle-In-Cell) are among the most popular in plasma physics, notably because of their efficiency in high dimensions compared to that of grid-based methods (eulerian or semi-lagrangian). However they suffer from an important level of "numerical noise" that is characterized by strong oscillations on the transported densities. Within this framework, the methods presented in this memoir such as LTPIC (Linearly-Transformed PIC) and FBL (Forward-Backward Lagrangian) seem to provide a convenient setting to improve the quality of these densities via a local exploitation of the data computed by the particle solver. Now that the accuracy of these approximation methods has been validated on simple problems, the natural sequel is to study their efficiency in the denoising of larger particle simulations. These works have started already, within a EuroFusion project carried out on the software platform Selalib to which I regularly contribute. Developped jointly by CEA, INRIA, the IPP (Institute for Plasma Physics) in Garching (Germany), the IRMA in Strasbourg, the IRMAR in Rennes and the LJLL in Paris, this platform is a convenient framework where mathematicians, physicists and computer scientists can implement and share numerical methods relevant in the lagrangian and semi-lagrangian simulation of plasmas, as well as test cases and diagnostic tools.

In parallel, it seems to me that compatible nonconforming discretization methods should be extended to new problems. Now that my results have allowed to identify new schemes of discontinuous Galerkin type that preserve the structure of Maxwell's equations, thus coming with good stability and conservation properties, I want to extend their application to other problems such as fluid ones and MHD. Further studies of the numerical properties of these schemes are also planned, and with physicists from the Max Planck-IPP in Garching we would like to use these compatible discontinuous discretization methods to the numerical modeling of plasma reflectometers, aimed at probing the density of tokamak plasmas.

Finally, I intend to pursue my works on the modeling of electromagnetic waves started with Bruno Després within the framework of the ANR Chrome project, with the purpose to improve the simulation

of resonant heating in tokamak plasmas. This project will naturally involve further collaborations with plasma physicists, and there is no doubt that new problems will appear during these exchanges, raising new interesting questions. It also fits into the PhD of Anouk Nicolopoulos which is now starting on new constructive models for resonant waves in magnetized plasmas.

Bibliography

[1] J.-C. Adam, A. Gourdin Serveniere, J.-C. Nédélec, and P.-A. Raviart. Study of an implicit scheme for integrating Maxwell's equations. *Computer Methods in Applied Mechanics and Engineering*, 22:327–346, 1980.

[2] D.N. Arnold, R.S. Falk, and R. Winther. Finite element exterior calculus, homological techniques, and applications. *Acta Numerica*, 15:1–155, 2006.

[3] D.N. Arnold, R.S. Falk, and R. Winther. Finite element exterior calculus: from Hodge theory to numerical stability. *Bull. Amer. Math. Soc.(NS)*, 47(2):281–354, 2010.

[4] F. Assous and P. Ciarlet, Jr. Quelques résultats sur la régularité en temps des équations de Maxwell instationnaires. *Comptes Rendus de l'Académie des Sciences - Series I - Mathematics*, 327(8):719–724, 1998.

[5] F. Assous, P. Ciarlet, Jr, and E. Sonnendrücker. Resolution of the Maxwell equations in a domain with reentrant corners. *M2AN. Mathematical Modelling and Numerical Analysis*, 32(3):359–389, 1998.

[6] A. Back, T. Hattori, S. Labrunie, J.R. Roche, and P. Bertrand. Electromagnetic wave propagation and absorption in magnetised plasmas: variational formulations and domain decomposition. *M2AN. Mathematical Modelling and Numerical Analysis*, 49(5):1239–1260, 2015.

[7] M. Badsi. *Etude mathématique et simulations numériques de modèles de gaines bi-cinétiques (in french).* PhD thesis, UPMC - Université Paris 6 Pierre et Marie Curie, 2016.

[8] M. Badsi, M. Campos Pinto, and B. Després. A minimization formulation of a bi-kinetic sheath. *Kinetic and related models*, 9(4):621–656, 2016.

[9] R. Barthelmé, P. Ciarlet, Jr, and E. Sonnendrücker. Generalized formulations of Maxwell's equations for numerical Vlasov-Maxwell simulations. *Mathematical Models & Methods in Applied Sciences*, 17(5):657–680, 2007.

[10] J.T. Beale. On the accuracy of vortex methods at large times. In *Computational fluid dynamics and reacting gas flows (Minneapolis, MN, 1986)*, pages 19–32. Springer, New York, 1988.

[11] J.T. Beale and A. Majda. Vortex methods. II. Higher order accuracy in two and three dimensions. *Mathematics of Computation*, 39(159):29–52, 1982.

[12] M. Bergdorf, G.-H. Cottet, and P. Koumoutsakos. Multilevel adaptive particle methods for convection-diffusion equations. *Multiscale Modeling & Simulation*, 4(1):328–357, 2005.

[13] M. Bergdorf and P. Koumoutsakos. A Lagrangian particle-wavelet method. *Multiscale Modeling & Simulation*, 5(3):980–995, 2006.

[14] N. Besse, F. Filbet, M. Gutnic, I. Paun, and E. Sonnendrücker. An adaptive numerical method for the Vlasov equation based on a multiresolution analysis. In *Numerical Mathematics and Advanced Applications. ENUMATH 2001*, pages 437–446, 2003.

[15] D. Boffi. Fortin operator and discrete compactness for edge elements. *Numerische Mathematik*, 87(2):229–246, 2000.

[16] D. Boffi. Compatible Discretizations for Eigenvalue Problems. In *Compatible Spatial Discretizations*, volume 142 of *IMA Vol. Math. Appl.*, pages 121–142. Springer New York, 2006.

[17] D. Boffi. Finite element approximation of eigenvalue problems. *Acta Numerica*, 19:1–120, 2010.

[18] D. Boffi, F. Brezzi, and M. Fortin. *Mixed finite element methods and applications*, volume 44 of *Springer Series in Computational Mathematics*. Springer, 2013.

[19] D. Boffi, F. Brezzi, and L. Gastaldi. On the convergence of eigenvalues for mixed formulations. *Annali della Scuola Normale Superiore di Pisa. Classe di Scienze. Serie IV*, 25(1-2):131–154 (1998), 1997.

[20] D. Boffi, F. Brezzi, and L. Gastaldi. On the problem of spurious eigenvalues in the approximation of linear elliptic problems in mixed form. *Mathematics of Computation*, 69:121–140, 2000.

[21] D. Boffi, A. Buffa, and L. Gastaldi. Convergence analysis for hyperbolic evolution problems in mixed form. *Numerical Linear Algebra with Applications*, 20(4):541–556, 2013.

[22] D. Boffi, P. Fernandes, L. Gastaldi, and I. Perugia. Computational Models of Electromagnetic Resonators: Analysis of Edge Element Approximation. *SIAM Journal on Numerical Analysis*, 36(4):1264–1290, 1999.

[23] A.-S. Bonnet-Ben Dhia, L. Chesnel, and X. Claeys. Radiation condition for a non-smooth interface between a dielectric and a metamaterial. *Mathematical Models & Methods in Applied Sciences*, 23(9):1629–1662, 2013.

[24] J.P. Boris. Relativistic plasma simulation-optimization of a hybrid code. In *Fourth Conf Num Sim Plasmas, 1970*. Proc. Fourth Conf. Num. Sim. Plasmas, 1971.

[25] A. Bossavit. Whitney forms: a class of finite elements for three-dimensional computations in electromagnetism. In *Physical Science, Measurement and Instrumentation, Management and Education - Reviews, IEE Proceedings A*, pages 493–500, 1988.

[26] A. Bossavit. Solving Maxwell equations in a closed cavity, and the question of 'spurious modes'. *IEEE Transactions on Magnetics*, 26(2):702–705, 1990.

[27] A. Bossavit. *Computational electromagnetism: variational formulations, complementarity, edge elements*. Academic Press, 1998.

[28] A. Bottino and E. Sonnendrücker. Monte Carlo particle-in-cell methods for the simulation of the Vlasov-Maxwell gyrokinetic equations. *Journal of Plasma Physics*, 81:435810501, 2015.

[29] S.C. Brenner, F. Li, and L.Y. Sung. Nonconforming Maxwell eigensolvers. *Journal of Scientific Computing*, 40(1-3):51–85, 2009.

[30] H. Brezis. *Functional analysis, Sobolev spaces and partial differential equations*. Springer, 2010.

[31] K. Brix, M. Campos Pinto, and W. Dahmen. A multilevel preconditioner for the interior penalty discontinuous Galerkin method. *SIAM Journal on Numerical Analysis*, 46(5):2742–2768, 2008.

[32] K. Brix, M. Campos Pinto, W. Dahmen, and R. Massjung. Multilevel preconditioners for the interior penalty discontinuous Galerkin method. II. Quantitative studies. *Communications in Computational Physics*, 5(2-4):296–325, 2009.

[33] K.G. Budden. *Radio Waves in the Ionosphere*. Cambridge University Press, 1966.

[34] A. Buffa, P. Houston, and I. Perugia. Discontinuous Galerkin computation of the Maxwell eigenvalues on simplicial meshes. *Journal of Computational and Applied Mathematics*, 204(2):317–333, 2007.

[35] A. Buffa and I. Perugia. Discontinuous Galerkin Approximation of the Maxwell Eigenproblem. *SIAM Journal on Numerical Analysis*, 44(5):2198–2226, 2006.

[36] A. Buffa, G. Sangalli, and R. Vázquez. Isogeometric analysis in electromagnetics: B-splines approximation. *Computer Methods in Applied Mechanics and Engineering*, 199(17):1143–1152, 2010.

[37] O. Buneman and G. Kooyers. Computer Simulation of the Electron Mixing Mechanism in Ion Propulsion. *AIAA Journal*, 1:2525–2528, 1963.

[38] M. Campos Pinto. *Développement et analyse de schémas adaptatifs pour les équations de transport*. PhD thesis, Université Pierre et Marie Curie - Paris VI, 2005.

[39] M. Campos Pinto. Adaptive semi-Lagrangian schemes for Vlasov equations. In Etienne Emmrich and Petra Wittbold, editors, *Analytical and Numerical Aspects of Partial Differential Equations*, pages 69–114. Walter de Gruyter, 2009.

[40] M. Campos Pinto. How to predict accurate wavelet grids in adaptive semi-Lagrangian schemes? *ESAIM: Proceedings*, 29:43–57, 2009.

[41] M. Campos Pinto. Towards smooth particle methods without smoothing. *Journal of Scientific Computing*, 65:54–82, 2015.

[42] M. Campos Pinto. Constructing exact sequences on non-conforming discrete spaces. *Comptes Rendus Mathematique*, 354(7):691–696, 2016.

[43] M. Campos Pinto. Structure-preserving conforming and nonconforming discretizations of mixed problems. ⟨hal-01471295⟩, 2017.

[44] M. Campos Pinto, J.A. Carrillo, F. Charles, and Y.P. Choi. Convergence of a linearly transformed particle method for aggregation equations. ⟨arXiv:1507.07405⟩, 2015.

[45] M. Campos Pinto and F. Charles. From particle methods to hybrid semi-Lagrangian schemes. ⟨hal-01385676⟩, 2016.

[46] M. Campos Pinto and F. Charles. Uniform Convergence of a Linearly Transformed Particle Method for the Vlasov–Poisson System. *SIAM Journal on Numerical Analysis*, 54(1):137–160, 2016.

[47] M. Campos Pinto and B. Després. Constructive formulations of resonant Maxwell's equations. ⟨hal-01278860⟩, 2016.

[48] M. Campos Pinto, S. Jund, S. Salmon, and E. Sonnendrücker. Charge conserving fem-pic schemes on general grids. *C.R. Mecanique*, 342(10-11):570–582, 2014.

[49] M. Campos Pinto, M. Lutz, and M. Mounier. Electromagnetic PIC simulations with smooth particles: a numerical study. *ESAIM: Proc.*, 53:133–148, 2016.

[50] M. Campos Pinto and M. Mehrenberger. Convergence of an adaptive semi-Lagrangian scheme for the Vlasov-Poisson system. *Numerische Mathematik*, 108(3):407–444, 2008.

[51] M. Campos Pinto, M. Mounier, and E. Sonnendrücker. Handling the divergence constraints in Maxwell and Vlasov–Maxwell simulations. *Applied Mathematics and Computation*, 272:403–419, 2016.

[52] M. Campos Pinto and E. Sonnendrücker. Compatible Maxwell solvers with particles I: conforming and non-conforming 2D schemes with a strong Ampere law. ⟨hal-01303852⟩, 2016.

[53] M. Campos Pinto and E. Sonnendrücker. Compatible Maxwell solvers with particles II: conforming and non-conforming 2D schemes with a strong Faraday law. ⟨hal-01303861⟩, 2016.

[54] M. Campos Pinto and E. Sonnendrücker. Gauss-compatible Galerkin schemes for time-dependent Maxwell equations. *Mathematics of Computation*, 85:2651–2685, 2016.

[55] M. Campos Pinto, E. Sonnendrücker, A. Friedman, D.P. Grote, and S.M. Lund. Noiseless Vlasov–Poisson simulations with linearly transformed particles. *Journal of Computational Physics*, 275(C):236–256, 2014.

[56] S. Caorsi, P. Fernandes, and M. Raffetto. On the convergence of Galerkin finite element approximations of electromagnetic eigenproblems. *SIAM Journal on Numerical Analysis*, 38(2):580–607 (electronic), 2000.

[57] M. Cessenat. *Mathematical methods in electromagnetism*, volume 41 of *Series on Advances in Mathematics for Applied Sciences*. World Scientific Publishing Co., Inc., River Edge, NJ, 1996.

[58] F. Chen. *Introduction to Plasma Physics and Controlled Fusion*. Volume 1: Plasma Physics. Plenum Press, New York and London, second edition edition, 1984.

[59] A.J. Chorin. Numerical study of slightly viscous flow. *J. Fluid Mech.*, 57(4):785–796, 1973.

[60] S.H. Christiansen and R. Winther. Smoothed projections in finite element exterior calculus. *Mathematics of Computation*, 77:813–829, 2008.

[61] P. Ciarlet, Jr and S. Labrunie. Numerical analysis of the generalized Maxwell equations (with an elliptic correction) for charged particle simulations. *Mathematical Models & Methods in Applied Sciences*, 19(11):1959–1994, 2009.

[62] A. Cohen. *Numerical analysis of wavelet methods*, volume 32 of *Studies in Mathematics and its Applications*. North-Holland Publishing Co., Amsterdam, 2003.

[63] A. Cohen and B. Perthame. Optimal Approximations of Transport Equations by Particle and Pseudoparticle Methods. *SIAM Journal on Mathematical Analysis*, 32(3):616–636, 2000.

[64] S. Colombi and C. Alard. A "metric" semi-Lagrangian Vlasov-Poisson solver. Submitted, 2016.

[65] C.J. Cotter, J. Frank, and S. Reich. The remapped particle-mesh semi-Lagrangian advection scheme. *Quarterly Journal of the Royal Meteorological Society*, 133(622):251–260, 2007.

[66] G.-H. Cottet. Artificial Viscosity Models for Vortex and Particle Methods. *Journal of Computational Physics*, 127:299–308, 1996.

[67] G.-H. Cottet and P.-A. Raviart. Particle methods for the one-dimensional Vlasov-Poisson equations. *SIAM Journal on Numerical Analysis*, pages 52–76, 1984.

[68] G.H. Cottet and P. Koumoutsakos. *Vortex Methods: Theory and Practice*. Cambridge University Press, Cambridge, 2000.

[69] N. Crouseilles, T. Respaud, and E. Sonnendrücker. A forward semi-Lagrangian method for the numerical solution of the Vlasov equation. *Computer Physics Communications*, 180(10):1730–1745, 2009.

[70] F. Da Silva, M. Campos Pinto, B. Després, and S. Heuraux. Stable explicit coupling of the Yee scheme with a linear current model in fluctuating magnetized plasmas. *Journal of Computational Physics*, 295:24–45, 2015.

[71] I. Daubechies. *Ten lectures on wavelets*, volume 61 of *CBMS-NSF Regional Conference Series in Applied Mathematics*. Society for Industrial and Applied Mathematics (SIAM), Philadelphia, PA, 1992.

[72] J. Dawson. One-Dimensional Plasma Model. *Physics of Fluids*, 5(4):445–459, 1962.

[73] J. Denavit. Numerical Simulation of Plasmas with Periodic Smoothing in Phase Space. *Journal of Computational Physics*, 9:75–98, 1972.

[74] B. Després, L.-M. Imbert-Gérard, and O. Lafitte. Singular solutions for the plasma at the resonance. ⟨hal-01097364⟩, 2014.

[75] B. Després, L.-M. Imbert-Gérard, and R. Weder. Hybrid resonance of Maxwell's equations in slab geometry. *Journal de Mathématiques Pures et Appliquées*, 101(5):623–659, 2014.

[76] R. Dumont. Waves in plasmas. In *M2 lecture notes*, pages 1–117. CEA, IRFM F-13108 Saint-Paul-lez-Durance, France., 2011.

[77] A. Ern and J.-L. Guermond. Finite Element Quasi-Interpolation and Best Approximation . ⟨hal-01155412v2⟩, 2015.

[78] M.W. Evans, F.H. Harlow, and E. Bromberg. The Particle-in-Cell Method for Hydrodynamic Calculations. Technical Report LAMS-2139, Los Alamos Laboratory, 1957.

[79] M. Feldman, S.-Y. Ha, and M. Slemrod. A Geometric Level-Set Formulation of a Plasma-Sheath Interface. *Archive for Rational Mechanics and Analysis*, 178(1):81–123, 2005.

[80] L. Fezoui, S. Lanteri, S. Lohrengel, and S. Piperno. Convergence and stability of a discontinuous Galerkin time-domain method for the 3D heterogeneous Maxwell equations on unstructured meshes. *ESAIM: Mathematical Modelling and Numerical Analysis*, 39(6):1149–1176, 2005.

[81] J.P. Freidberg. *Plasma physics and fusion energy*. Cambridge : Cambridge University Press, 2007.

[82] X. Garbet, Y. Idomura, L. Villard, and T.H. Watanabe. TOPICAL REVIEW: Gyrokinetic simulations of turbulent transport. *Nuclear Fusion*, 50(4):043002, 2010.

[83] D. Gérard-Varet, D. Han-Kwan, and F. Rousset. Quasineutral limit of the Euler-Poisson system for ions in a domain with boundaries. *Indiana University Mathematics Journal*, 62(2):359–402, 2013.

[84] D. Gérard-Varet, D. Han-Kwan, and F. Rousset. Quasineutral limit of the Euler-Poisson system for ions in a domain with boundaries II. *Journal de l'École Polytechnique. Mathématiques*, 1:343–386, 2014.

[85] V. Girault and P.-A. Raviart. *Finite Element Methods for Navier-Stokes Equations – Theory and Algorithms*. Springer Series in Computational Mathematics. Springer-Verlag, Berlin, 1986.

[86] V. Grandgirard, Y. Sarazin, X. Garbet, G. Dif-Pradalier, Ph. Ghendrih, N. Crouseilles, G. Latu, E. Sonnendrücker, N. Besse, and P. Bertrand. GYSELA, a full-f global gyrokinetic Semi-Lagrangian code for ITG turbulence simulations. In *Theory of Fusion Plasmas: Joint Varenna-Lausanne International Workshop. Proceedings held at Varenna*, pages 100–111. Association Euratom-CEA, CEA/DSM/DRFC CEA-Cadarache, France, 2006.

[87] V. Grandgirard, Y. Sarazin, X. Garbet, G. Dif-Pradalier, Ph. Ghendrih, N. Crouseilles, G. Latu, E. Sonnendrücker, N. Besse, and P. Bertrand. Computing ITG turbulence with a full-f semi-Lagrangian code. *Communications in Nonlinear Science and Numerical Simulation*, 13:81–87, 2008.

[88] J.S. Hesthaven and T. Warburton. Nodal High-Order Methods on Unstructured Grids. *Journal of Computational Physics*, 181(1):186–221, 2002.

[89] J.S. Hesthaven and T. Warburton. High-order nodal discontinuous Galerkin methods for the Maxwell eigenvalue problem. *Philosophical Transactions of the Royal Society A: Mathematical, Physical and Engineering Sciences*, 362(1816):493–524, 2004.

[90] S. Heuraux, F. da Silva, T. Ribeiro, B. Després, M. Campos Pinto, J. Jacquot, E. Faudot, S. Wengerowsky, L. Colas, and L. Lu. Simulation as a tool to improve wave heating in fusion plasmas. *Journal of Plasma Physics*, 81(05):435810503, 2015.

[91] R. Hiptmair. Nonconforming mixed discretization of second order elliptic problems. Report TUM M9404, 1994.

[92] R. Hiptmair. Canonical construction of finite elements. *Mathematics of Computation*, 68(228):1325–1346, 1999.

[93] R. Hiptmair. Finite elements in computational electromagnetism. *Acta Numerica*, 11:237–339, 2002.

[94] R. Hiptmair. Maxwell's Equations: Continuous and Discrete. In A Bermúdez de Castro and A Valli, editors, *Computational Electromagnetism, Lecture Notes in Math., Vol. 2148*, pages 1–58. Springer International Publishing, Switzerland, 2015.

[95] R.W. Hockney and J.W. Eastwood. *Computer simulation using particles*. Taylor & Francis, Inc, Bristol, PA, USA, 1988.

[96] G.B. Jacobs and J.S. Hesthaven. High-order nodal discontinuous Galerkin particle-in-cell method on unstructured grids. *Journal of Computational Physics*, 214(1):96–121, 2006.

[97] G.B. Jacobs and J.S. Hesthaven. Implicit–explicit time integration of a high-order particle-in-cell method with hyperbolic divergence cleaning. *Computer Physics Communications*, 180(10):1760–1767, 2009.

[98] P. Koumoutsakos. Inviscid Axisymmetrization of an Elliptical Vortex. *Journal of Computational Physics*, 138:821–857, 1997.

[99] A.B. Langdon and C.K. Birdsall. *Plasma Physics via Computer Simulation*. Taylor & Francis, New York, 2005.

[100] A. Leonard. Vortex methods for flow simulation. *Journal of Computational Physics*, 37:289–335, 1980.

[101] A. Magni and G.-H. Cottet. Accurate, non-oscillatory, remeshing schemes for particle methods. *Journal of Computational Physics*, 231(1):152–172, 2012.

[102] P.-H. Maire. *Etablissement et comparaison de modèles fluides pour un plasma faiblement ionisé quasi-neutre. Détermination des conditions aux limites à la paroi.* PhD thesis, Université Pierre et Marie Curie - Paris VI, 1996.

[103] C.G. Makridakis and P. Monk. Time-discrete finite element schemes for Maxwell's equations. *RAIRO Modél Math Anal Numér*, 29(2):171–197, 1995.

[104] P.J. Mardahl and J.P. Verboncoeur. Charge conservation in electromagnetic PIC codes; spectral comparison of Boris/DADI and Langdon-Marder methods. *Computer Physics Communications*, 106(3):219–229, 1997.

[105] B. Marder. A method for incorporating Gauss' law into electromagnetic PIC codes. *Journal of Computational Physics*, 68(1):48–55, 1987.

[106] P. Monk. A mixed method for approximating Maxwell's equations. *SIAM Journal on Numerical Analysis*, pages 1610–1634, 1991.

[107] P. Monk. Analysis of a Finite Element Method for Maxwell's Equations. *SIAM Journal on Numerical Analysis*, 29(3):714–729, 1992.

[108] P. Monk. An analysis of Nédélec's method for the spatial discretization of Maxwell's equations. *Journal of Computational and Applied Mathematics*, 47(1):101–121, 1993.

[109] P. Monk. *Finite Element Methods for Maxwell's Equations*. Numerical Mathematics and Scientific Computation. Oxford University Press, New York, University of Delaware, Newark, 2003.

[110] P. Monk and L Demkowicz. Discrete compactness and the approximation of Maxwell's equations in $\mathbb{R}^3$. *Mathematics of Computation*, 70:507–523, 2001.

[111] C.-D. Munz, P. Omnes, R. Schneider, E. Sonnendrücker, and U. Voß. Divergence Correction Techniques for Maxwell Solvers Based on a Hyperbolic Model. *Journal of Computational Physics*, 161(2):484–511, 2000.

[112] C.-D. Munz, R. Schneider, E. Sonnendrücker, and U. Voss. Maxwell's equations when the charge conservation is not satisfied. *Comptes Rendus de l'Académie des Sciences-Series I-Mathematics*, 328(5):431–436, 1999.

[113] R.D. Nair, J.S. Scroggs, and F.H.M. Semazzi. A forward-trajectory global semi-Lagrangian transport scheme. *Journal of Computational Physics*, 190(1):275–294, 2003.

[114] J.-C. Nédélec. Mixed finite elements in $\mathbb{R}^3$. *Numerische Mathematik*, 35(3):315–341, 1980.

[115] J.-C. Nédélec. A new family of mixed finite elements in $\mathbb{R}^3$. *Numerische Mathematik*, 50(1):57–81, 1986.

[116] A. Nicolopoulos. Formulations Variationnelles des Equations de Maxwell (in french). Master's thesis, UPMC - Université Paris 6 Pierre et Marie Curie, 2016.

[117] A. Pazy. *Semigroups of linear operators and applications to partial differential equations*. Springer-Verlag, New York, 1983.

[118] P.-A. Raviart. An analysis of particle methods. In *Numerical methods in fluid dynamics (Como, 1983)*, pages 243–324. Lecture Notes in Mathematics, Berlin, 1985.

[119] P.-A. Raviart and J.-M. Thomas. A mixed finite element method for 2nd order elliptic problems. In *Mathematical aspects of finite element methods, Lecture Notes in Math., Vol. 606*, pages 292–315. Springer, Berlin, 1977.

[120] K.U. Riemann. The Bohm criterion and sheath formation. *Journal of Physics D: Applied Physics*, 24:493–518, 1991.

[121] A. Robert. A stable numerical integration scheme for the primitive meteorological equations. *Atmosphere-Ocean*, 19(1):35–46, 1981.

[122] J.S. Sawyer. A Semi-Lagrangian Method of Solving the Vorticity Advection Equation. *Tellus*, 15(4):336–342, 1963.

[123] J.R. Schulenberger and C.H. Wilcox. The limiting absorption principle and spectral theory for steady-state wave propagation in inhomogeneous anisotropic media. *Archive for Rational Mechanics and Analysis*, 41:46–65, 1971.

[124] Selalib. Semi-Lagrangian Library. http://selalib.gforge.inria.fr/.

[125] E. Sonnendrücker, J.R. Roche, P. Bertrand, and A. Ghizzo. The semi-Lagrangian method for the numerical resolution of the Vlasov equation. *Journal of Computational Physics*, 149(2):201–220, 1999.

[126] P.C. Stangeby. *The Plasma Boundary of Magnetic Fusion Devices*. Institute of Physics Publishing, Bristol and Philadelphia, 2000.

[127] A. Staniforth and J. Côté. Semi-Lagrangian integration schemes for atmospheric models-a review. *Monthly weather review*, 119:2206–2223, 1991.

[128] T.H. Stix. *The theory of plasma waves*. McGraw-Hill Book Co., Inc., New York-Toronto-London, 1962.

[129] A. Stock, J. Neudorfer, R. Schneider, C. Altmann, and C.-D. Munz. Investigation of the Purely Hyperbolic Maxwell System for Divergence Cleaning in Discontinuous Galerkin based Particle-In-Cell Methods. In *COUPLED PROBLEMS 2011 IV International Conference on Computational Methods for Coupled Problems in Science and Engineering*, 2011.

[130] M.L. Stowell and D.A. White. Discretizing Transient Current Densities in the Maxwell Equations. In *ICAP 2009*, 2009.

[131] J. Strain. 2D Vortex Methods and Singular Quadrature Rules. *Journal of Computational Physics*, 124(1):131–145, 1996.

[132] J. Villasenor and O. Buneman. Rigorous charge conservation for local electromagnetic field solvers. *Computer Physics Communications*, 69(2-3):306–316, 1992.

[133] B. Wang, G.H. Miller, and P. Colella. A Particle-In-Cell method with adaptive phase-space remapping for kinetic plasmas. *SIAM Journal on Scientific Computing*, 33:3509–3537, 2011.

[134] T. Warburton and M. Embree. The role of the penalty in the local discontinuous Galerkin method for Maxwell's eigenvalue problem. *Computer Methods in Applied Mechanics and Engineering*, 195(25-28):3205–3223, 2006.

[135] D.A. White, J.M. Koning, and R.N. Rieben. Development and application of compatible discretizations of Maxwell's equations. In *Compatible Spatial Discretizations*, pages 209–234. Springer, New York, 2006.

[136] R.B. White and F.F. Chen. Amplification and absorption of electromagnetic waves in overdense plasmas. *Plasma Physics*, 16:565–587, 1974.

[137] L. Xu and N. Yuan. FDTD Formulations for Scattering From 3-D Anisotropic Magnetized Plasma Objects. *IEEE Antennas and Wireless Propagation Letters*, 5(1):335–338, 2006.

[138] K.S. Yee. Numerical solution of initial boundary value problems involving Maxwell's equations in isotropic media. *IEEE Transactions on Antennas and Propagation*, 14(3):302–307, 1966.

[139] K. Yosida. *Functional analysis*, volume 123 of *Classics in Mathematics*. Springer-Verlag, Berlin, sixth edition, 1995.

[140] S. Zaglmayr. *High order finite element methods for electromagnetic field computation*. PhD thesis, Universität Linz, Diss, 2006.